COAL ENERGY CONVERSION INTEGRATED WITH
DEEP SALINE AQUIFER CARBON STORAGE
VIA COMBUSTION IN SUPERCRITICAL WATER

A DISSERTATION
SUBMITTED TO THE DEPARTMENT OF
MECHANICAL ENGINEERING
AND THE COMMITTEE ON GRADUATE STUDIES
OF STANFORD UNIVERSITY
IN PARTIAL FULFILLMENT OF THE REQUIREMENTS
FOR THE DEGREE OF
DOCTOR OF PHILOSOPHY

John Russell Heberle
August 2011

This dissertation is online at: http://purl.stanford.edu/tk857jm1866

I certify that I have read this dissertation and that, in my opinion, it is fully adequate in scope and quality as a dissertation for the degree of Doctor of Philosophy.

Christopher Edwards, Primary Adviser

I certify that I have read this dissertation and that, in my opinion, it is fully adequate in scope and quality as a dissertation for the degree of Doctor of Philosophy.

Mark Cappelli

I certify that I have read this dissertation and that, in my opinion, it is fully adequate in scope and quality as a dissertation for the degree of Doctor of Philosophy.

Reginald Mitchell

Approved for the Stanford University Committee on Graduate Studies.

Patricia J. Gumport, Vice Provost Graduate Education

This signature page was generated electronically upon submission of this dissertation in electronic format. An original signed hard copy of the signature page is on file in University Archives.

In Memory of George R. Hague
Master Teaching Chair of Chemistry
St. Mark's School of Texas

Abstract

Carbon capture and sequestration (CCS) technologies aim to allow the continued use of fossil fuels by outputting carbon in a form other than atmospheric CO_2. Several types of geologic reservoirs are considered as alternatives; of these, deep saline aquifers have the largest potential storage capacity worldwide. Unfortunately, neat CO_2 injected into an aquifer is less dense than the native brine. The resulting buoyancy presents a potential for leakage from the storage formation, and, ultimately, to the atmosphere.

This work describes a method for using coal to produce electricity that creates a pre-equilibrated brine/CO_2 solution for injection into a saline aquifer. Such solutions are more dense than the original brine, and present no potential for buoyancy-driven leakage. A concept is introduced in which coal is oxidized in high-pressure, high-temperature water drawn from a saline aquifer in a process known as supercritical water oxidation (SCWO). Combustion in supercritical water and subsequent aquifer storage of all coal-derived fluid effluent removes the need for CO_2 separation and compression steps common in other coal-fired designs with CCS. The properties of supercritical water ($T > 647$ K, $P > 221$ bar) are described that make it a suitable combustion medium—in contrast to water at ambient conditions.

A conceptual plant is developed that includes systems to manage brine and coal (a solid, complex fuel). The system uses a heat engine for work extraction from hot combustion products, and so may be called a supercritical water oxidation, indirectly-fired combined cycle, or SCWO/IFCC. Next, a thermodynamic model is developed to evaluate the performance of this plant and compare it to other coal-fired designs with CCS.

Next, a laboratory-scale combustor, constructed to study flames in supercritical

water, is described. This apparatus follows from previous supercritical water reactors that were built to study the destruction of hazardous wastes, but is targeted toward the development of a combustor suitable for use in a power plant. Challenges encountered operating systems that are simultaneously high-pressure and high-temperature are discussed, including the use of several types of metal seals. Autoignition results from initial combustion experiments are presented and compared to previous work.

Acknowledgements

I arrived at Stanford in the fall of 2004 with interests in air-breathing propulsion and the electric power sector. Though not well-defined, these leanings were adequate to steer me towards the energy systems course series, where I would meet my advisor, Chris Edwards. I desired to work on a new project, starting at the idea stage, figuring it would be more instructive than resuming where a prior student had left off. Chris presented me with such an opportunity, and I accepted his offer of a research assistantship just before spring break. This dissertation details the work that followed. It was funded by the Global Climate & Energy Project, to whom we are grateful. A sister project in the group of Prof. Reggie Mitchell was covered by the same grant, and he was the principal investigator of the overall effort. He also served on my reading committee and taught entertaining courses in combustion and radiation heat transfer. Thanks also to Prof. Mark Cappelli for reading this thesis.

Despite a long awareness of the adage, "If you knew what you were doing, it wouldn't be called research," I have benefitted from reassurance of the same from Chris on multiple occasions. He has provided valuable guidance ranging from the meaning of an engineering Ph.D., to uncannily prophetic advice on laboratory hardware, to tips for managing one's path and resources (mental, time, and otherwise) within a large organization. As useful as all of that is, it takes more than an advisor to make a productive research group. Thanks to Robin Bell for the initial implementation of some details in the modeling part of the project. Thanks to summer undergrads Sage Wright and Will Smith. Chief among my co-workers I thank Paul Mobley. Whereas my natural tendency during the build phase was to be paralyzed by uncertainty, Paul was able to move the project forward in a judicious manner. Without him,

I would still be counting how many tube fittings to buy. He also makes eastern North Carolina pork barbecue, which, despite my being from Texas, garners my approval. Ken Hencken did the detailed design work on the combustor, drawing on his experience with optically-accessible pressure vessels. We would be nowhere (or worse?) without our lab technician Scott Sutton. I have probably learned more about hands-on, practical engineering from Scott than from anyone else at a university. When Scott does a job, the result is as reliable as one can ask for in a research setting, and is, without a doubt, *safe*. Also, thanks to our department machinist Lakhbir for his assistance. I thank all of the other Engine Lab students through the years for their friendship and support, including—but not limited to—Kwee-Yan, Shannon, Matt, and Sankaran. And, more recently, "the kids": Adelaide, Rebecca, Julie, Greg, Ben, and BJ.

Before working with those listed above, I had to get to Stanford. The farthest back I can trace my formal developement as an engineer is to fourth grade, with Ms. Melinda Zeares and Mr. Trimble at Arthur L. Kramer Elementary in Dallas. I have a clear snapshot in my mind of the day Ms. Zeares taught us how to find the area of a circle, a skill I use frequently to this day.

In the sixth grade, at the urging of admissions head Ed Young, I entered the St. Mark's School of Texas. The mission of St. Mark's is to educate the "whole boy", and in this regard it did not disappoint. On a campus with fewer than ninety boys per class, a surprisingly large fraction of the faculty and staff are involved directly or indirectly with the education (in the broadest sense) of each student. Accordingly, I must refer the reader to old copies of the school phone directory for an unabridged list of teachers, coaches, administrators, and even IT, custodial, and cafeteria staff who are deserving of praise. Of particular relevance for me personally, the preparation for a technical education that I received at 10600 Preston Road left nothing to be desired. From the mathematics department, I thank Mark Mrozek, John Cocharo, Dr. Michael Keyton, Jon Searles, J.T. Sutcliffe, and John Stutsman. In addition to their standard obligations, Mr. Cocharo and Dr. Keyton coached the math teams, which means they spent many weekends chauffeuring us up and down I-35 and I-45. From the science department: John Mead, Dan Northcut, Stephanie Barta, and Dr. Stephen

Balog. Also, Richard Abbondanzio (just "Abbo") and Doug Rummel for coaching the robotics team. Outside of those departments, I was privileged to take five English and history courses from Dr. Henry Ploegstra, tying the record.

I have reserved one teacher for special mention. George Hague taught chemistry and AP chemistry with legendary enthusiasm. It was in his classroom that I first learned to think microscopically. Unfortunately, he passed away before I completed my undergraduate work at Caltech, an Institute he maintained I was not weird enough to attend. While this work alone is not an adequate tribute to his passion and skill for clarifying the invisible, I think he would agree that is it worthy of at least two "violas".[1]

From middle school through graduate school, a few friends stood out. Max, who taught me a lot of what I know about computers (and everything I know about microwave communication systems). Ben, who was a classmate every day for five and a half years and was on almost every type of team I was on, and without whom those teams surely wouldn't have been as successful. Due to Caltech's reputation at St. Mark's (see above), I wouldn't have gone there if he hadn't. Will, who I didn't know well during undergrad, but who became a fantastic roommate in grad school, is a true gentleman and scholar.

Finally, my family. Most importantly, my mom, who—among many other feats—spent entirely too much time waiting to pick me up from track practice. Her practicality, preparedness, and diplomacy makes her a favorite among many groups. After she visited for commencement, I received more than one comment from my friends about how great she is. I suppose I have been fortunate that she has always been this way, with the side effect that I don't fully appreciate what I have. Chris Barker was key at times when, as a young lad, I was too much for her to handle. My dad is a source of real-world advice. I have saved the final words for my grandmother, who at age 100 was my most ardent supporter as I completed my degree.

<div align="right">J.R.H.</div>

---

[1] A corruption of *voilà*, pronounced VIE-oh-la.

Contents

List of Tables

List of Figures

Chapter 1

Motivation

Coal has been a key energy resource since the dawn of the industrial age. Long in use to provide thermal energy, Newcomen's steam engine allowed coal to produce work. This engine facilitated the mining of ever more coal. With Watt's improvements, the steam engine spread into wide use in mills and factories. Coal-fueled work production soon went mobile, as boilers found a home on the rails. The discovery of petroleum began a long decline and finally cessation of coal use as a transportation fuel, due to the ease of use of liquid fuels on small and mobile platforms. However, electrification resulted in new demand for coal. Due to its low price and reliable supplies, coal has remained an important energy resource into the 21st century.

On more than one occasion since coal burning began on an industrial scale, concern has arisen over the non-monetary costs of coal use. These have ranged from the obvious—visible soot from smokestacks—to the less immediate but still apparent effects of acid rain, formed when sulfur-containing emissions interact with the environment. More recently, the release of carbon dioxide to the atmosphere has been scrutinized [1]. Reducing CO_2 emissions will require different types of solutions than reducing other pollutants. Unlike soot, CO_2 cannot be eliminated as a reaction product through better engineering of the combustion process; it is the major product of carbon oxidation. Unlike sulfur and mercury, carbon is not a trace component of the fuel.

There are several responses with the potential to reduce CO_2 emissions from

coal. These options can be divided into four classes, distinguished by the chemical state of the carbon atoms as they are left in the environment by an energy system. One class involves substituting coal with other primary energy resources, such as renewables, large hydropower, or nuclear. In these cases, coal and its carbon is simply left undisturbed in the lithosphere. Even if the alternative resource employed was another fossil fuel, CO_2 emission rates would be reduced since petroleum and, in particular, natural gas, have lower carbon-to-hydrogen ratios and lower carbon per unit of exergy than coals of any rank. The second class is to continue using coal, but to leave the carbon in a reduced form. An example is sooty plasma reforming [2]. But here again, natural gas would be a better fuel because of its lower carbon content. A third class, related to the second, is to leave the carbon in a higher oxidation state than in CO_2 by forming carbonates [3]. Such reactions are thermodynamically favored at environmental temperatures, but are kinetically limited. While this option is chemically the opposite of the second (oxidation vs. reduction), it is similar in that it places the output carbon into a solid phase. The fourth class is to continue producing CO_2, but to discharge it to some place other than the atmosphere. The last three classes are strategies known as carbon capture and sequestration, or CCS.[1]

While coal combustion is not the only source of CO_2 emissions, it is an important one with regards to emissions reduction options because of the scale and nature of its use. The sources of U.S. CO_2 emissions are shown in Fig. 1.1, categorized by fuel and broad economic sector. Coal-fired electric power plants accounted for 33.5% of total U.S. CO_2 emissions in 2008. The only other source classification with a contribution anywhere near this high is the petroleum-fueled transportation sector. Since vehicles do not readily lend themselves to CCS implementation at the point of primary energy conversion, the coal-fired electric sector is strategically the most opportune place to deploy CCS technologies. This development would also reduce emissions from the transportation sector, since electric vehicles shift part of the transportation emissions to the electric sector.

Coal is predominantly carbon by mass. As a result, the volume required for the storage of product forms of carbon is as important a consideration for selecting a

---

[1]Alternatively, carbon capture and storage.
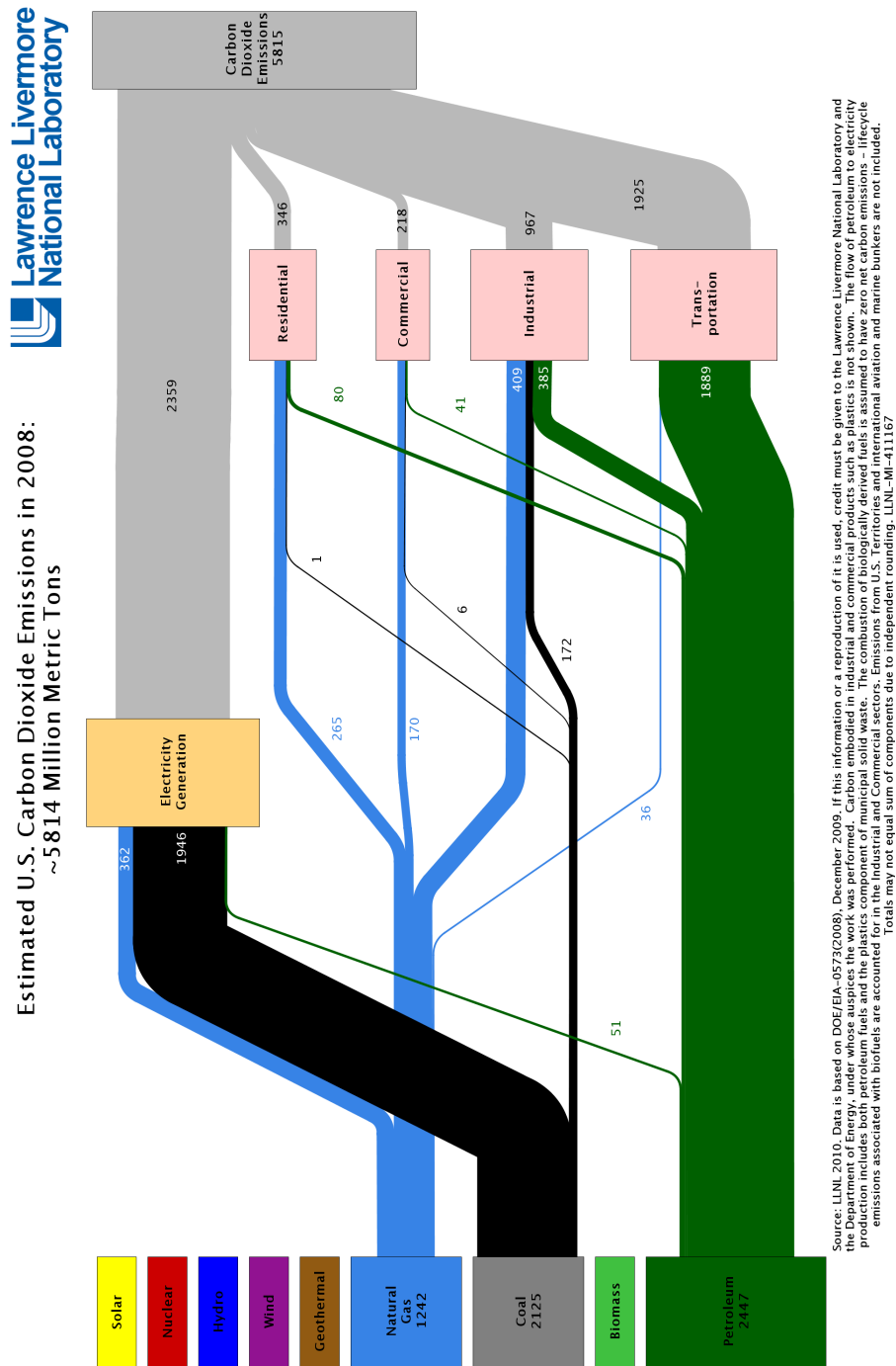
Figure 1.1: Chart of 2008 U.S. carbon emissions by energy resource and sector of energy use [4]. Coal-fired electric power plants accounted for 33.5% of domestic atmospheric CO_2 release in that year.

storage mode as other factors, such as the quality of containment. Since coal comes from geologic reservoirs, geologic reservoirs are sought as storage options with sufficient capacity.

1.1   Deep Saline Aquifer Storage

There are several types of geologic formations that are candidates for CO_2 storage. These include depleted oil and gas reservoirs, unminable coal beds, and deep saline aquifers. This last group is of interest because it has the largest worldwide storage capacity, likely exceeding 1000 $GtCO_2$ [5]. Deep saline aquifers are porous, sedimentary layers whose pore spaces are filled with brine. They are common in sedimentary basins, which coincide geographically with many major coal-producing and consuming regions of the world, including the central United States and Canada as well as China. Due to their high salinity, they are not used as potable supplies or for agriculture. In the future, saline aquifers may be used with desalination plants as water supplies in some inland, arid areas. However, in most locations there is no foreseen use of the brine in these formations.

According to most visions of deep saline aquifer sequestration, CO_2 is first separated from plant exhaust (as with a pulverized-coal-fired steam plant) or from an intermediate stream (as in an integrated gasifier combined cycle, or IGCC, plant). Then, it is compressed, sent through pipelines to a storage site, and injected into an aquifer, as illustrated in Fig. 1.2. In the target formation, the CO_2 displaces native brine, creating a pocket of neat CO_2 in the vicinity of the injection wells.[2] (One well is depicted in the figure, but in practice many would be required to handle the flow rate from a utility-scale plant [6].)

A concern with deep saline aquifer storage by neat injection is that the CO_2 is initially in a non-equilibrium state with potential for leakage. Neat CO_2 is less dense than native brine at most aquifer conditions (temperatures, pressures, and brine compositions). The resulting buoyant force pushes the CO_2 towards the surface until it

---

[2]The stream is *neat* in the sense that it has not been intentionally mixed with another substance. The term *pure* is not used to avoid the implication that the stream has been purified.
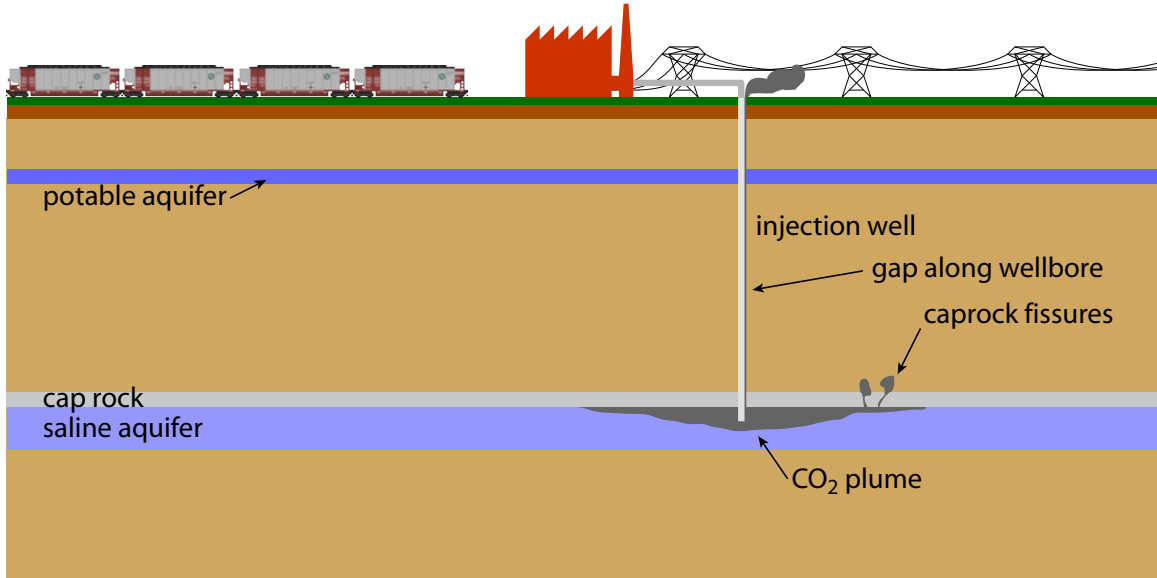
Figure 1.2: Neat CO_2 storage in a deep saline aquifer. Saline aquifers are distinct from potable groundwater sources, and are typically deeper.

reaches an impermeable layer, such as a cap rock. Sequestration sites must be chosen carefully since the CO_2 will be forced out of the aquifer and towards the surface if a permeable path is available. Even if an appropriate type of rock overlies the aquifer, it may harbor leakage paths that are difficult to detect. Potential paths include undetected fissures in formation cap rock or poorly-cemented or deteriorated well bores, both depicted in Fig. 1.2. With reasonable engineering effort, the possibility of leaks at new injection wells can be reduced. Unfortunately, the same cannot be said for known or unknown abandoned well bores in the area, nor can it be guaranteed that a presently-sound cap rock will remain intact after future seismic events.

Fortunately, a buoyant plume of CO_2 will not persist indefinitely. Neat CO_2 in an aquifer is not in thermodynamic equilibrium with its environment. Rather, it will dissolve in the brine, creating an aqueous solution that is denser than the original brine [7]. Depending on the composition of the aquifer and host rock, further interactions may leave the carbon chemically trapped in the form of solid carbonates, resulting in truly permanent storage. Figure 1.3a qualitatively shows the contributions of these trapping mechanisms as time passes. On the order of a century after injection,

most CO_2 will be contained by solubility or residual trapping. The reliance on structural trapping at a site continually decreases after the injection period ends.
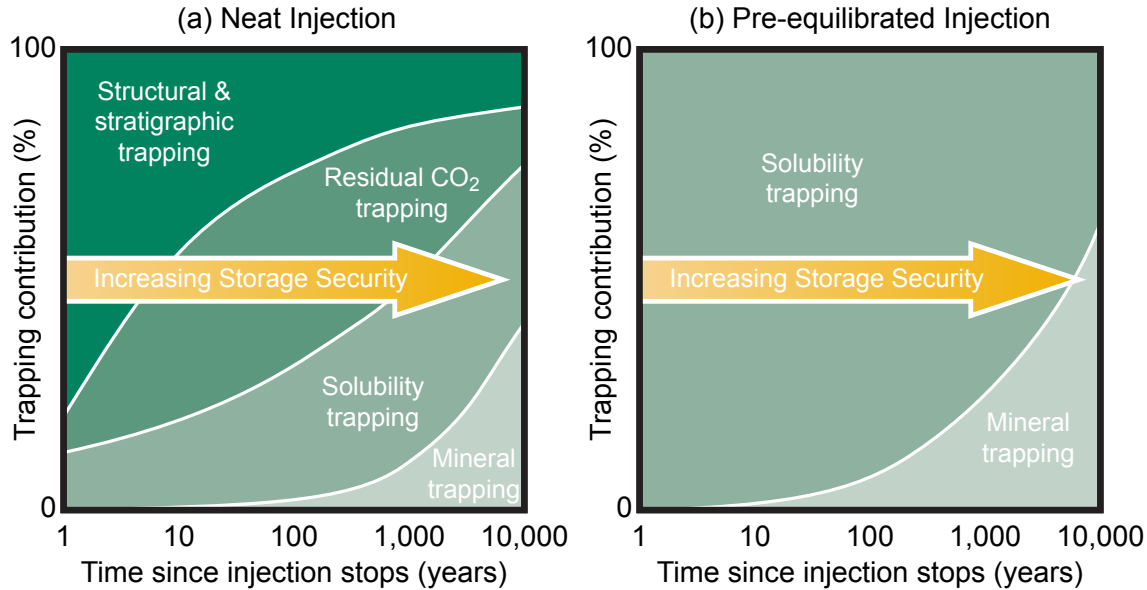
Figure 1.3: Qualitative contribution of storage mechanisms versus time after injection of (a) neat CO_2 and (b) pre-equilibrated brine/CO_2 solution. Adapted from [5].

1.2   Surface Dissolution

It is encouraging that aquifer sequestration naturally becomes more secure over time. Still, injected plumes of CO_2 should be monitored to verify the integrity of structural traps. Such monitoring may be necessary to gain public acceptance of sequestration in potentially mobile phases. Since the kinetics leading to enhanced trapping are slow, monitoring of a plume must continue at least until it stops migrating [5]. A process to speed the equilibration is desired in order to reduce the risk of leakage and the amount of monitoring required. In the best of such cases, the CO_2 would be pre-equilibrated with brine prior to injection. The contributions of trapping mechanisms versus time in that scenario are shown in Fig. 1.3b. The lack of a buoyant phase containing CO_2

removes the need for a reliable structural trap. Monitoring requirements would be minimal.

One method involving pre-equilibration has been explored by Burton and Bryant [6]. Called surface dissolution, it is shown schematically in Fig. 1.4. Brine is extracted from an aquifer—typically the same one used for storage, though in principle it could be another. CO_2 is dissolved in brine in a pressurized mixing tank, and the pre-equilibrated solution is injected in the target aquifer.
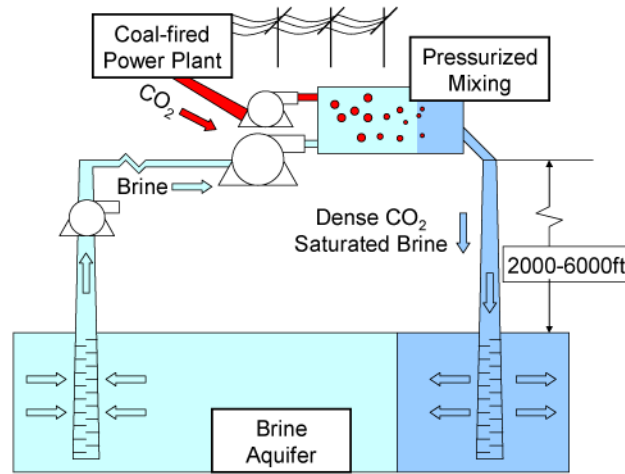
Figure 1.4: Schematic of surface dissolution from Burton and Bryant [6]. CO_2 separated from a fossil fuel power plant is mixed with brine drawn from a saline aquifer. The pre-equilibrated solution—a non-buoyant phase—is injected back into the aquifer.

Feasibility of this idea depends, among other criteria, on the amount of aquifer water that must be circulated for total dissolution. Figure 1.5 is a contour plot of the water required by a typical plant for varying aquifer conditions. Flow rates are given in thousands of kilograms per second (10^3 kg/s) for a 500 MW$_e$ coal plant like the one that will be introduced and studied in this work. An aquifer salinity of 20,000 ppm w/w as sodium chloride is assumed. For reference, the amount of cooling water required by a traditional plant is ~12,000–13,000 kg/s [8]. (About the same amount is required for the plant introduced below.) Figure 1.5 shows that less water is required for dissolution than is needed for cooling. The amount needed is nearly an order of magnitude less with some aquifers. Although cooling and dissolution

are completely separate processes in this scheme, and the water for them comes
from different sources, this comparison shows that the amount of water that must be
handled is not unusual.
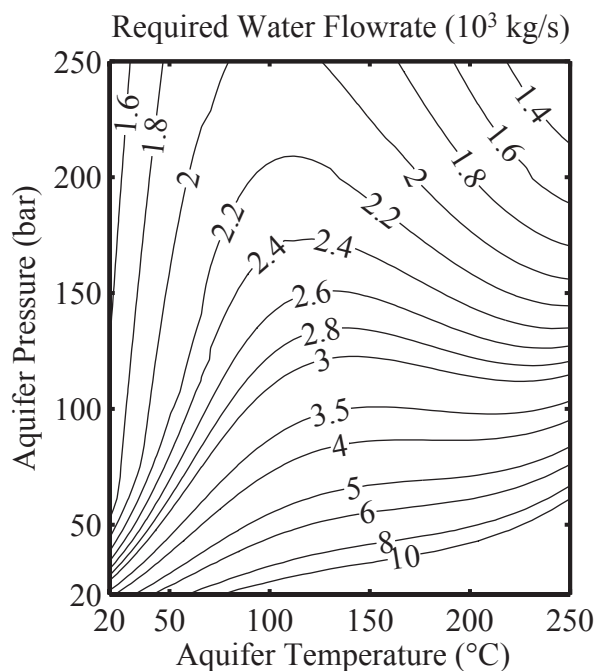
Figure 1.5: Carbon dioxide dissolution water requirement as a function of aquifer
temperature and pressure. Salinity is 20,000 ppm w/w as NaCl. Water flow rates are
shown for a 500 MW$_e$ plant in thousands of kilograms per second.

Burton and Bryant's discussion of surface dissolution presupposes an input of neat
CO_2 produced by a separation process. Their mechanism could be useful as part of a
post-combustion separation system for retrofitting to an existing plant, or at a plant
where CO_2 is produced by a chemical process, such as ammonia synthesis. However,
surface dissolution with neat CO_2 is not ideal for use with new generating station
construction for two reasons. First, a conceptual problem with this setup and with
many other carbon sequestration plans for use with electric power production is that
a large amount of energy and capital are used to separate carbon dioxide when the
real goal of the system is to keep carbon out of the atmosphere. The production
of concentrated carbon dioxide is an intermediate step which reduces efficiency and

is, in general, not necessary. Surface dissolution highlights the improvidence of this separation since the carbon dioxide flows from a *separator* to a *mixer*. The second concern is the way carbon is pressurized. CO_2 must be pressurized for injection or, in this case, for effective dissolution on the path to injection. In coal-fired plants the carbon enters the system in a solid form. Pressurizing the carbon while in a solid requires much less energy than pressurizing carbon dioxide gas. What is sought is a more tightly integrated process that will allow for increased efficiency while providing the robustness of sequestration inherent to surface dissolution.

1.3 An Integrated, Pre-equilibrated Method

This work examines a new concept for obtaining work from carbon-containing fuels and sequestering the carbon dioxide that is produced. Figure 1.6 shows the essential idea, where combustion is carried out at high pressure in fluid drawn from a saline aquifer. This scheme allows the carbon to be pressurized for injection before combustion, while it is still in a solid phase. It is a CCS system with inherent pre-equilibration, since the oxidation of carbon occurs in water.

As shown in Fig. 1.6, water from a saline aquifer is pumped to the surface where it is used as a processing medium for the reaction of coal and oxygen in a supercritical water oxidation (SCWO) system. The outputs of the SCWO system are solid mineral matter (ash), heat that is used to drive a heat engine, and a single-phase, pre-equilibrated effluent that is injected into the aquifer. No fluid from the combustion process is released to the atmosphere; all combustion products are directed to the lithosphere. A heat engine is used for work production. Work production by expansion of the products in a turbine is not possible because the products must be kept at high pressure for reinjection. Since the product carbon dioxide must be thoroughly mixed with aquifer water before re-injection into the aquifer, the combustion can be done at high pressure in supercritical water.

In the next chapter, the properties of supercritical water (SCW) are described. These will show why it is a suitable medium for combustion in contrast to ambient water. Previous work on oxidation and combustion in supercritical water is reviewed.
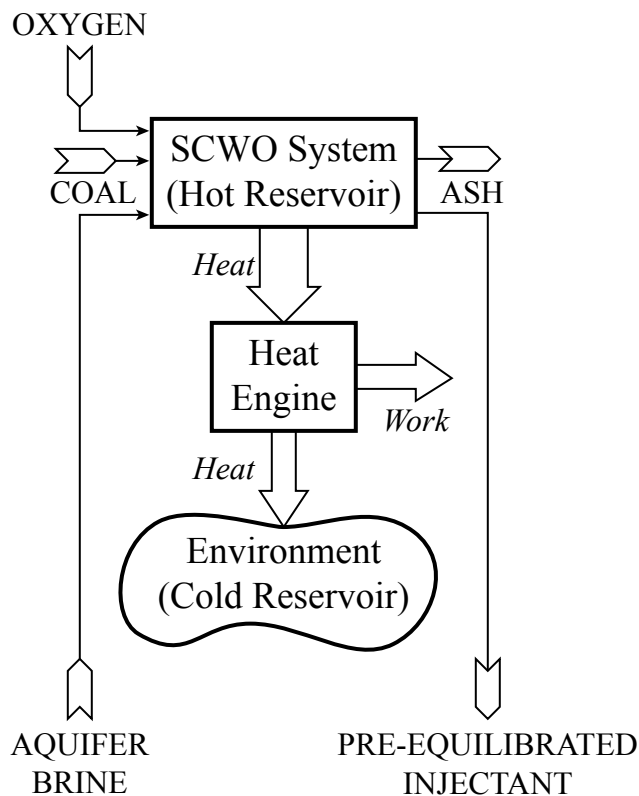
Figure 1.6: Concept of an energy system with integrated, pre-equilibrated CCS. Coal is burned at high pressure in supercritical water. A heat engine is used for work extraction so that the combustion products can remain at high pressure for sequestration.

Chapter 3 presents an initial vision of a supercritical-water-combustion electric power plant. The design addresses several practicalities of using coal as a fuel and of using aquifer brine. Then, a thermodynamic model of the plant is described. Initial performance calculations are reported that indicate that pre-equilibration via supercritical water combustion could be competitive with other coal-fired electricity generation technologies.

Several components of the plant of Ch. 3 will require research in order make such a plant feasible. A key component is the combustor. A lab-scale combustor and associated systems were designed and constructed as part of this work; they are

detailed in Ch. 4. Chapter 5 is a discussion of experience to date commissioning and operating the combustor. Difficulties operating with SCW are covered, as are the results of initial combustion experiments.

Chapter 2

Prior Work With Supercritical Water Oxidation

The reaction of fuel and oxidizer in water is the central enabling concept of the proposed pre-equilibrated CCS system. This chapter considers the existing technologies that aim to use water as a medium for oxidation reactions. These fall into two classes: systems that employ supercritical water oxidation, with modest-temperature, homogeneous reaction zones, and those that are supercritical water combustors, featuring localized flames similar to those in gas-phase combustors. First, as bulk phases of water are typically considered impediments to combustion, the enabling physics of supercritical water are described.

2.1   Properties of Supercritical Water

The phase diagram of water in P-T space is shown in Fig. 2.1. Moving up in temperature and pressure along the liquid-gas saturation curve, the latent heat of vaporization (Δh_{fg}) decreases. The point at which it reaches zero is known as the *critical point*. The fluid properties at that point are the critical properties, including the *critical temperature* (T_c) and *critical pressure* (P_c). For water, these are 647 K (374°C) and 221 bar. In the space beyond the critical point, there is no combination of T and P at which distinct liquid and gas phases coexist; there is only one phase

known as a *supercritical fluid.* While a supercritical fluid by convention has both $T > T_c$ and $P > P_c$, the boundaries of the supercritical region do not have physical meaning; there is no discontinuity of properties (e.g., density) between the liquid and supercritical phases or between the gas and supercritical phases.

While enthalpy is continuous across the liquid and supercritical regions above P_c, it does have an inflection point. Since the specific heat is a maximum at the inflection point, this state is called the *pseudocritical point.* The temperature of a pseudocritical point is the *pseudocritical temperature.* As this temperature is derived from the values of enthalpy at a particular pressure, it is a function of pressure. These points will be of more than just mathematical interest later in this work due to the rapid property variations in their neighborhoods.
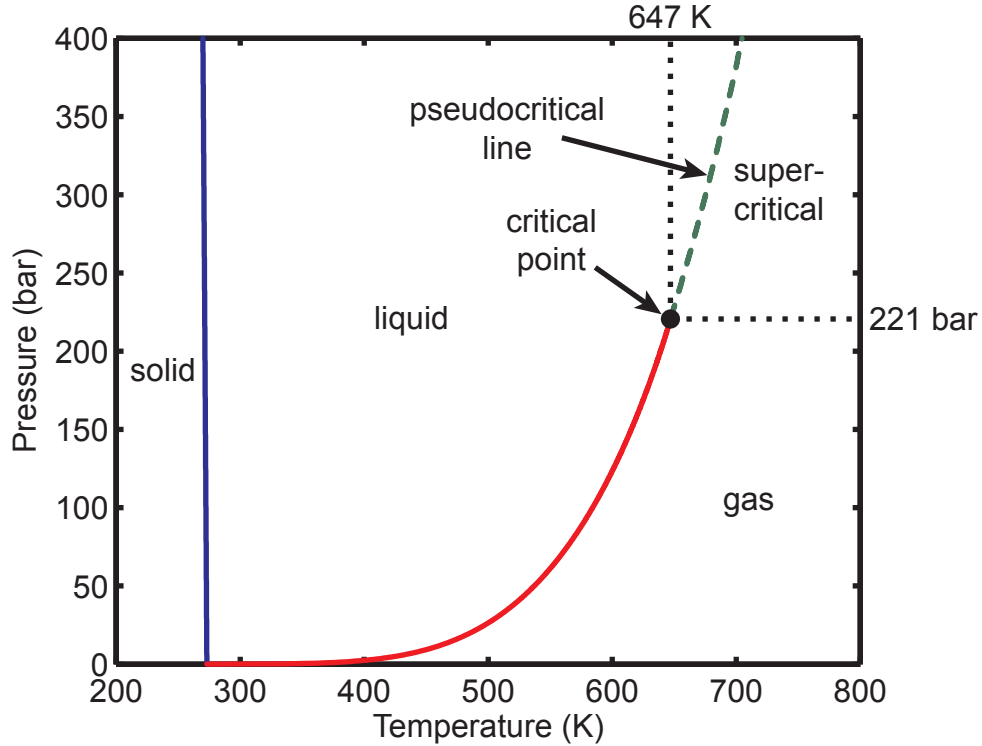
Figure 2.1: Phase diagram of water, showing the supercritical region.

While all supercritical fluids have a lack of phase distinctions, supercritical water behaves differently than water at ambient pressure in other ways as well. The

unusually high polarity of water at ambient conditions is responsible for much of its behavior, such as high boiling point and ready solvation of many ionic species. The dielectric constant is an indicator of the degree of polar behavior, and the dissociation constant (K_w) indicates the ability of water to ionize other compounds (as well as itself). The value of these properties as a function of temperature at 250 bar are plotted in Fig. 2.2. The dielectric constant decreases as temperature increases, falling especially quickly around the pseudocritical point. Further, Raman spectroscopy shows that little hydrogen bonding occurs in supercritical water [9]. Meanwhile, the dissociation constant drops dramatically near the pseudocritical point. These property variations indicate that water loses its polar character beyond the critical point. In fact, supercritical water behaves as a dense, non-polar gas, exhibiting miscibility with gases and many non-polar compounds [9]. The drop in dissociation constant indicates that SCW is not as effective at ionizing other species. The solubilities of ionic salts are orders of magnitude lower than in liquid water.

While polarity gives water its versatile role in many geological and biological processes, it is precisely the diminished expression of this property beyond the critical point that allows supercritical water to serve as a combustion medium. Since non-polar organic molecules are highly soluble in supercritical water, and gases are completely miscible, hydrocarbon fuels and oxidizer can meet in supercritical water, allowing reaction to occur.

2.2   Supercritical Water Oxidation

Supercritical water oxidation has been of interest for hazardous waste destruction since around 1980 [9, 12]. Unlike gas-phase incinerators, SCWO reactors have a dense effluent that can be contained and tested to ensure that a sufficiently low amount of inlet hazardous species remain. This capability suits them for processing wastes that must not be allowed into the environment, such as chemical munitions, rocket propellants, and mixed (simultaneously toxic and radioactive) wastes. Additionally, many wastes are dilute, aqueous solutions, which are difficult to incinerate well. Processing in water is a natural method for such wastes.
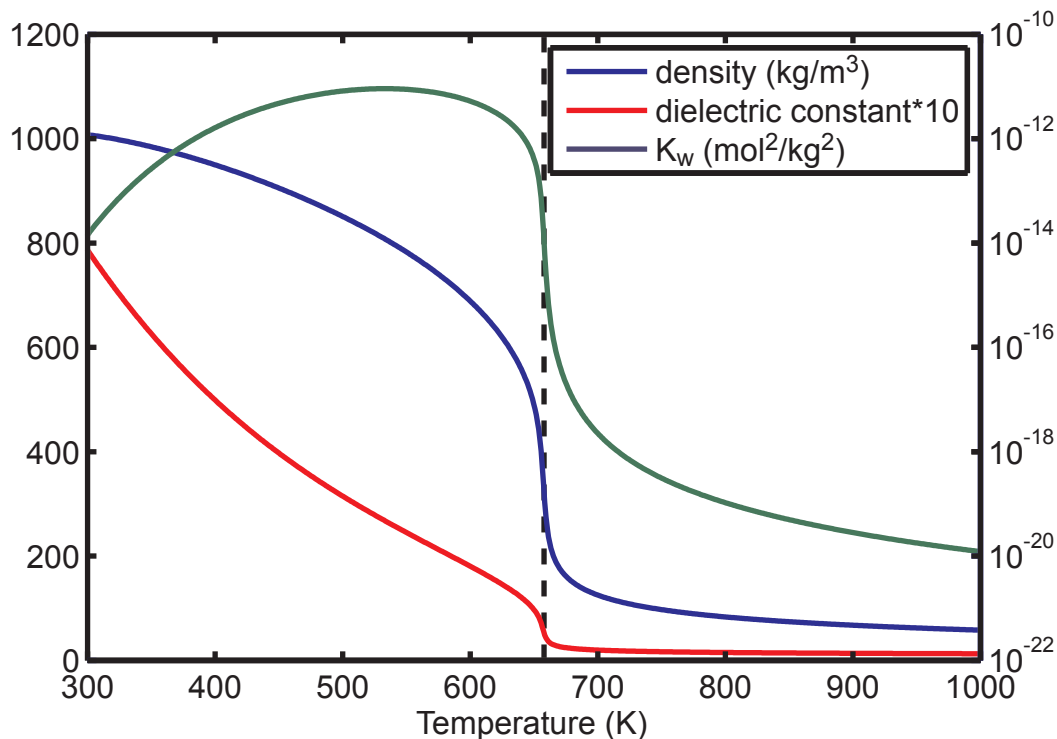
Figure 2.2: The density, dielectric constant, and self-dissociation constant of water at 250 bar [10, 11]. The pseudocritical temperature at this pressure (658 K) is marked by the dashed line.

The schematic of a generalized SCWO system is shown in Fig. 2.3. To enable oxidation, waste must be pressurized and preheated to supercritical conditions. Oxygen (or another oxidizer, such as hydrogen peroxide) is added in the reactor, where the waste is consumed. The effluent from the reactor is cooled and depressurized. Returning to ambient conditions, gaseous species separate from the liquid.

Destruction efficiency (the fraction of inlet species consumed) is typically very high in SCWO systems. Carbon atoms oxidize to CO_2 and hydrogen to water. Halogen atoms become monatomic ions (e.g., Cl^-, F^-), and other atoms form their respective acid anions (e.g., SO_4^{2-}, PO_4^{3-}) [13]. Because the reactions occur in a homogenous flow at relatively low temperatures without flames, little NO_x is formed.

Two considerable difficulties with the development and deployment of SCWO are corrosion and salt plugging. Many wastes contain ionic species that precipitate from
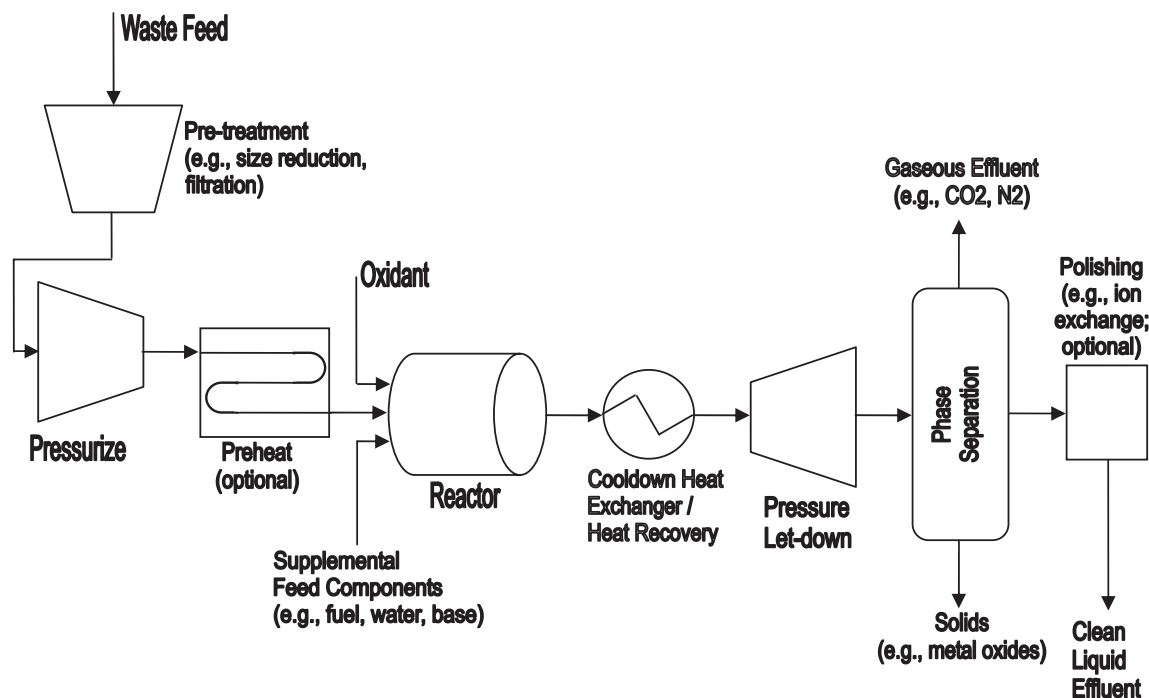
Figure 2.3: Schematic of a generic SCWO process [13].

the waste stream once it has passed the critical temperature. Product anions can also precipitate if sufficient cations (other than H^+) are present.

2.3   Supercritical Water Combustion

2.3.1   Inverse Laminar Diffusion Flames

The first studies of supercritical water combustion, or SCWC, were conducted by the group of Franck at Universität Karlsruhe. The first published photograph of a hydrothermal flame (Fig. 2.4) appeared in a paper discussing several aspects of high-pressure, high-temperature fluids [14]. Little discussion accompanied that photograph, since it was a proof-of-concept, but Schilling and Franck soon devoted a paper to the topic [15], detailing their apparatus and methods. A drawing of their combustor is reproduced in Fig. 2.5. This setup is typical of early SCW combustors. The body

(labeled 1) is an 80 mm OD, 30 mm ID nickel-alloy cylinder. Ports (5 and 6) for cone-and-thread fittings allow for insertion of a coaxial burner nozzle and thermocouple. Optical access is provided by two opposed sapphire windows (4). These are mounted to the inside of two sealing cones (2), which, with matching collars (3), function like large cone-and-thread fittings. The internal volume of the reactor when assembled is approximately 30 mL. Although the construction of the feed system and burner allow for the simultaneous injection of fuel and oxidizer, the usual procedure was to prepare the cell with a supercritical mixture of water and fuel, then inject neat oxygen into the quiescent fuel mixture. If the temperature was sufficiently high, autoignition occured. Images of the backlit flames were recorded through a microscope. Although a Schlieren arrangement was not used, Schlieren effects are visible since the variation of density (and thus refractive index) with temperature is large in supercritical water. This effect is responsible for the dark band above the luminous flame in Fig. 2.4.
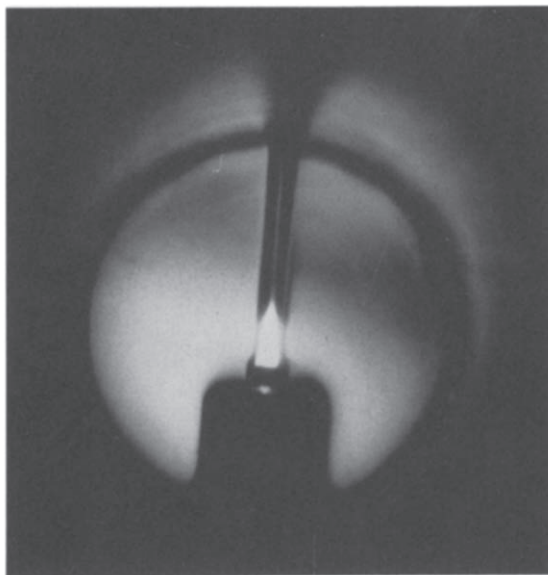
Figure 2.4: First published picture of a hydrothermal flame [14]. Oxygen was injected at 3 mm^3/s (2.4 mg/s) into a cell filled with 30 mole-% CH_4 at 450°C and 1000 bar, producing a laminar inverse-diffusion flame 3 mm long and 0.5 mm wide at the base.

With the flow rates, conditions, and geometry used, the injected oxygen jet is laminar. Flame heights were measured at pressures from 300 to 2000 bar; the behavior
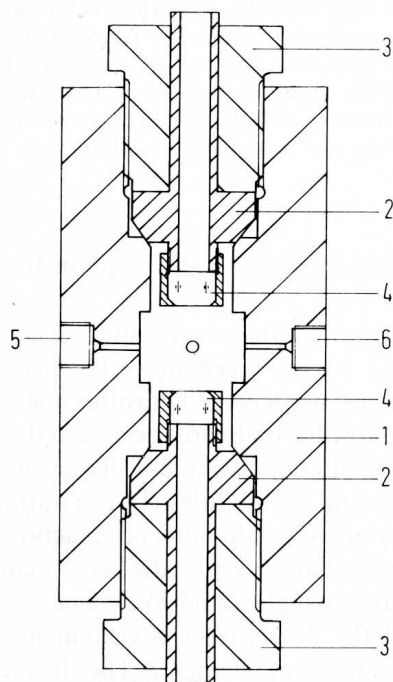
Figure 2.5: Reactor used for first hydrothermal flame studies. "1: Cylindrical body with 80 mm o.d. and 30 mm i.d. 2: Sealing cones. 3: Threaded screws. 4: Sapphire windows. 5: Opening for the introduction of a burner. 6: Openings for a sheathed thermocouple and two capillaries" [15].

corresponds with that of laminar diffusion flames in air at more conventional conditions. This result showed that despite the unusual conditions, the behavior of hydrothermal flames is largely in accordance with that of other flames. The rotational temperature of the flame was estimated as 3100 K using ultraviolet spectra of OH chemiluminescence.

Steeper and colleagues at Sandia National Laboratory in Livermore constructed a combustion cell similar to Franck's [16]. The chief difference was the addition of a third window with a viewing axis normal to the axis of the other two (Fig. 2.6). This window was included to allow the use of Raman spectroscopy. With this reactor, Steeper made measurements of flame heights, flame temperatures, and ignition and extinction temperatures, extending the work of Schilling and Franck. Raman spectroscopy allowed for kinetics studies of methane in sub- and supercritical water, as well as in argon.
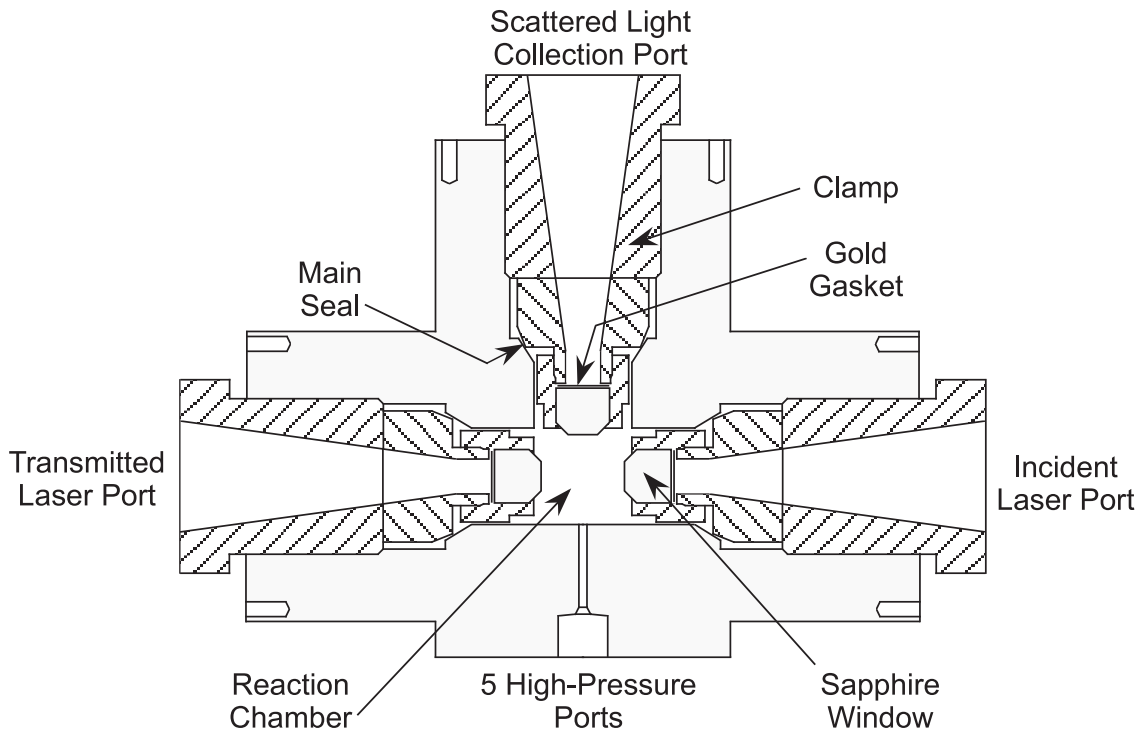
Figure 2.6: Strirred optical cell from Sandia Livermore [17].

2.3.2 Turbulent Diffusion Flames

While the foregoing experiments established the possibility and relatively normal behavior of combustion in supercritical water, they did not address the practical problems encountered in the SCWO work. The group of von Rohr at ETH Zurich set out to apply hydrothermal flames to solve the problems of corrosion and plugging. By using a flame to localize the reaction zone, problematic fluids could be kept away from surfaces with a layer of subcritical, neat water [18]. Whereas an externally heated plug-flow reactor must have supercritical water in contact with tube walls, in a SCW combustor, the necessary enthalpy is provided chemically at low temperature, or by recirculation.

The resulting vessel is shown in Fig. 2.7. As with the reaction cells above, optical access is provided by opposed sapphire windows at the level of the nozzle. Unlike those reactors, this one is designed for continuous flow. At the bottom are two coaxial

nozzles for the injection of preheated (400°C) oxygen and fuel. (Note that the fuel is the central flow, so this is not an inverse flame.) The fuel stream, a mixture of methane and water, is termed artificial wastewater in reference to the objectives of this research. In the annular space between the outer nozzle and the pressure vessel, a flow of ambient temperature (25°C) water is injected. This cooling water flow segregates the reaction zone from the walls. With cooling flow that could be more than seven times the mass flow of the fuel and oxygen streams combined, the temperature of the pressure vessel walls was kept below 200°C, even when temperatures exceeded 1200°C in the core of the flow.

With knowledge gained from the WCHB-1, a second generation reactor was built, termed the WCHB-2. As seen in Fig. 2.8, this reactor has a burner (labeled 1) similar to the WCHB-1, but the tempered glass windows (4) and glass tube (3) for confining the flow have been elongated. The notable addition is a quartz tube (2) separating the reacting part of the flow from the annular cooling water flow until a distance of 15 diameters downstream.

Figure 2.9 is a photograph of a flame in the WCHB-2. The fuel mixture is 25% w/w methanol in water injected around 100°C. The flame is confined to the quartz tube, but since there is no seal at the bottom of this tube, oxygen leaks into the cooling flow. As the outer flow is subcritical, the oxygen forms gas-phase bubbles.

The pair of WCHBs demonstrated that by using a hydrothermal flame, organics can be oxidized in a supercritical zone within a reactor without supercritical fluids contacting vessel walls. For organic waste mixtures with sufficiently high heating values, a design like the WCHBs would be adequate. However, many wastes are too dilute to sustain combustion by recirculation zones when the inlet temperature is subcritical. Furthermore, it is inefficient to introduce all of the cooling flow at one axial location, since only a small, subcritical boundary layer is required to protect the surfaces. The next generation experiment at ETH sought to address these problems by means of a self-sustaining hydrothermal flame to provide the exothermicity required for the incoming waste water stream to react.

The transpiring wall reactor (TWR) (Fig. 2.10) was designed for this purpose. Similar to WCHB-2, fuel and oxygen are injected in the central and next-innermost
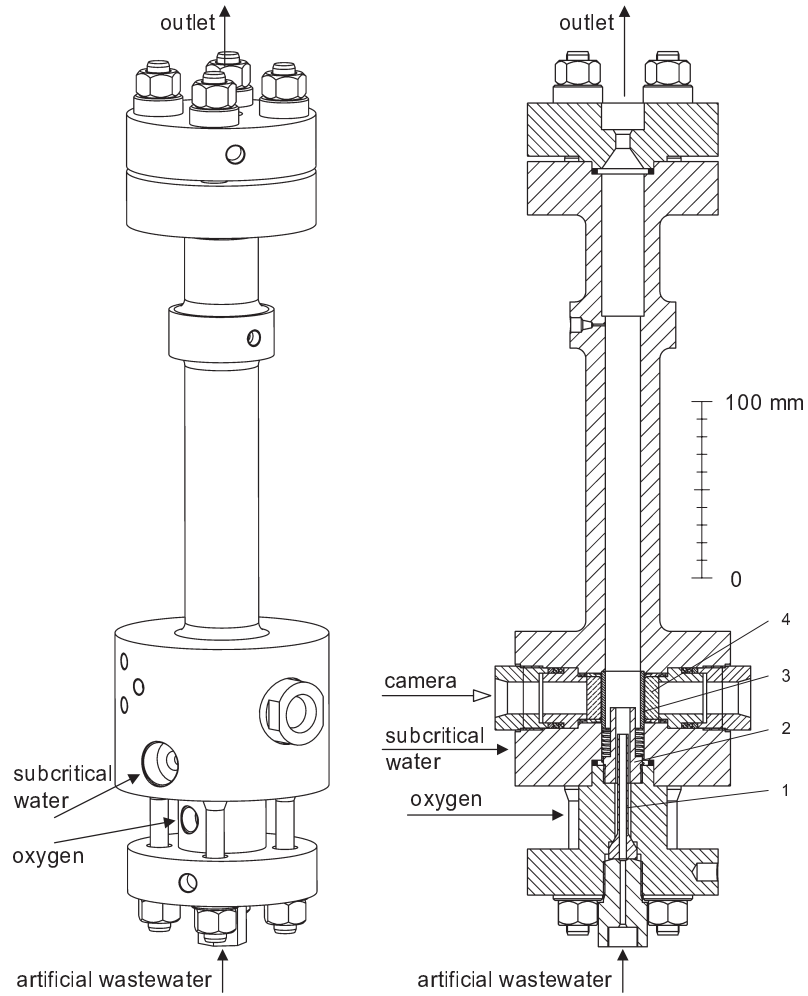
Figure 2.7: Wall-cooled hydrothermal burner 1 (WCHB-1) at ETH Zurich [19]. "1: core tube of the burner, 2: coaxial tube, 3: cylindrical glass tube (keeps cross section constant), 4: sapphire windows." [19] Operation described in detail in [18].

flows, respectively. They are segregated from the third flow by a metal tube instead of quartz. Furthermore, the third flow is simulated waste water. The hydrothermal flame preheats the waste water by conduction through the metal tube. Unlike the WCHB-2, there is a fourth coaxial flow; this flow is oxygen to react with the waste water, and is initially segregated from the waste water by a second metal tube. Both tubes end at approximately the same axial location. At that point hot products of the pilot flame mix with the waste water, further raising the temperature of the latter, and the
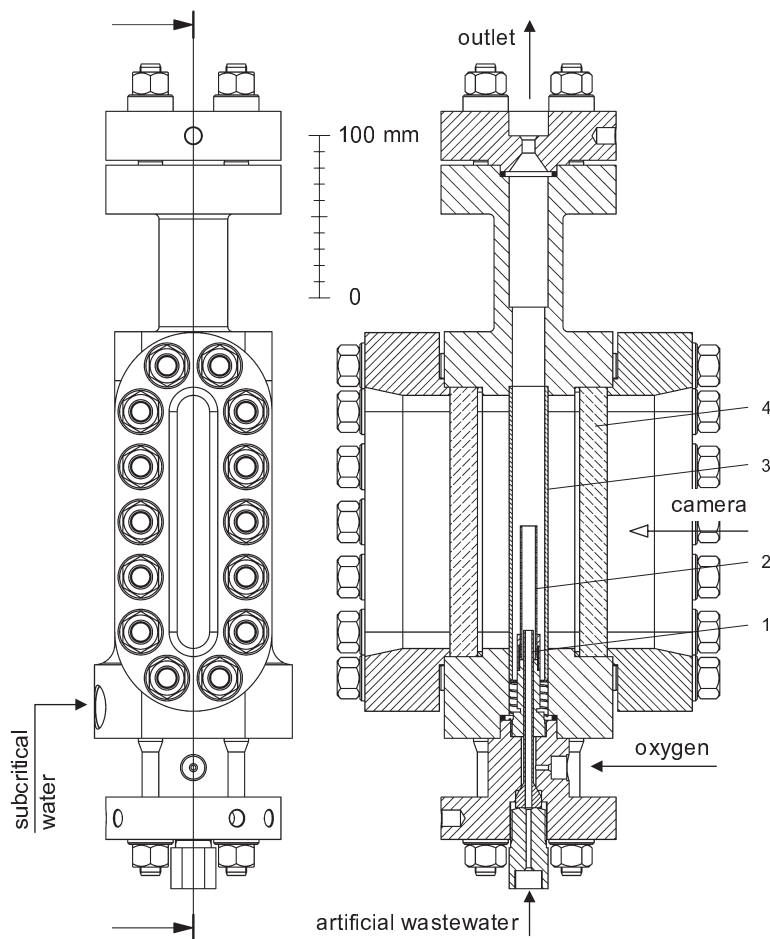
Figure 2.8: Wall-cooled hydrothermal burner 2 (WCHB-2) at ETH Zurich [19]. "1: core tube of the burner, 2: coaxial quartz glass tube, 3: cylindrical glass tube (keeps cross section constant), 4: high-pressure windows (tempered glass)." [19]

waste water mixes with the second oxygen flow and begins to oxidize. If the design continued with the philosophy of the earlier WCHBs, there would be a fifth, annular flow of subcritical water to shield the walls and lower the outlet temperature. However, the introduction of such a flow in sufficient volume to accomplish those purposes at one early axial location is not desirable for one of two reasons. If the flow was not preheated, mixing with the waste water flow would quench the reactions; with a residence time limited thusly, waste destruction efficiency would be reduced, defeating the purpose of operating the reactor. If the flow were preheated to a temperature
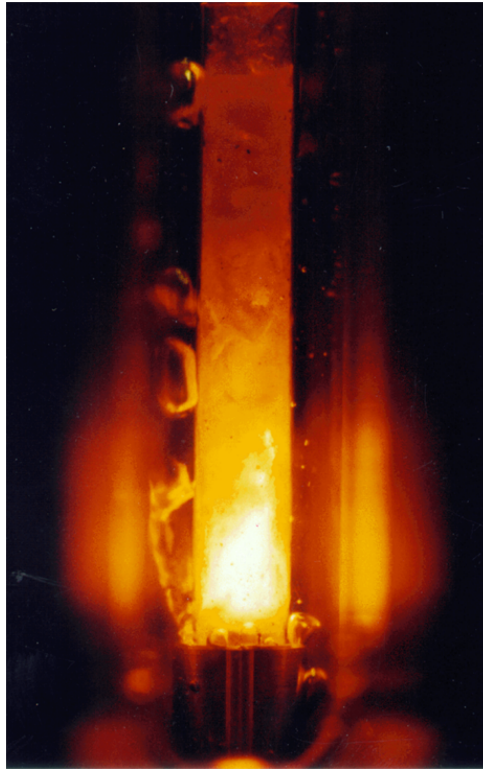
Figure 2.9: Photograph of a flame in the WCHB-2 at ETH Zurich [19].

high enough to not shorten residence time in the reaction zone (but still subcritical to preserve the functions of this stream), the energy requirement to operate the reactor would increase. The cost of the additional preheating could make such a reactor an uneconomical mode of waste disposal. A response to this problem is to spatially distribute the introduction of cooling water. Along the length of the reactor, cooling water is only required to form a boundary layer on the walls, which can be done with many small injections. Wellig chose to achieve this flow using a sintered metal liner as a transpiring wall; this feature lends the reactor its name. The liner is divided into four sections, each fed by an independent stream. The first three are transpiring water (TW1–TW3) flows to form the boundary layer. The last is cooling water (CW), a bulk flow to reduce the mean outlet temperature.

Experiments conducted by Wellig using methanol fuel and methanol as waste water simulant show that conversion of simulated waste driven by a pilot flame works as
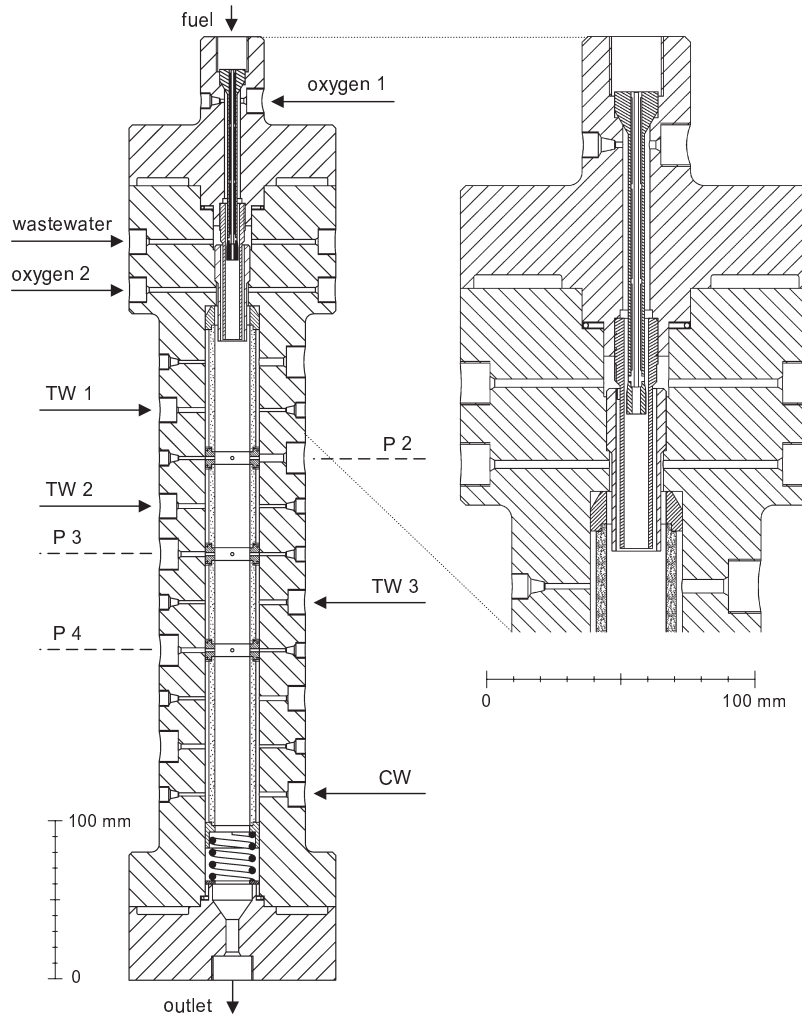
Figure 2.10: Transpiring-wall reactor at ETH Zurich [19].

intended in the TWR [19]. Príokpský extended the studies to include 1–3% w/w NaCl or Na_2SO_4 in the fuel stream [20]. Salt deposition was not observed on the transpiring wall.

These studies demonstrate that SCWC processes can be managed in an engineered system. The ranges of firing rates used in these and other investigations are listed in Table 2.1. With a maximum of ∼20 kW, further study of SCWC will be required to scale-up the process for implementation in a production plant. In addition, many

other aspects of a pre-equilibrated CCS system based on SCWC must be developed. The beginning analysis of a complete system is the subject of the next chapter.

Study	Firing Rate (W)	Ref.
Schilling & Franck	15–30	[15]
Steeper	77	[16]
La Roche (WCHB-1)	2,100–15,000	[18, 19]
Weber (WCHB-1)	2,200–11,000	[19]
Wellig (WCHB-2)	17,000–20,000	[19]
Wellig (TWR)	1,900–9,500	[19]

Table 2.1: Firing rate (LHV basis) ranges used in some previous supercritical water combustors.

Chapter 3

System Concept & Analysis

In this chapter, a schematic for a complete plant is described that includes all major subsystems. Then, a thermodynamic model is developed that gives the flow conditions that will be present in different components of the plant. Most importantly, the calculated efficiency will present a key comparison between the present concept and other coal-fired energy systems with CCS.

3.1 System Concept

A proposed a block diagram for a coal-fired SCWO plant is shown in Fig. 3.1. The defining characteristic of this system is the use of aquifer water as a processing medium, so the path of water is followed through the plant. A sufficient amount of aquifer brine to dissolve all of the carbon dioxide enters the plant from production wells (see Fig. 1.5). If all of this water passed through the SCWO system, its outlet temperature would be low, leading to poor heat engine efficiency. Hence, the flow rate of water through the SCWO system is determined by its desired outlet temperature. Figure 3.2 shows the SCWO system outlet temperature as a function of the fraction of total dissolution water directed through it. The remainder of the water bypasses the SCWO system and heat engine.

The water that will be used for fuel processing must be preheated to near-critical conditions. Preheating improves the kinetics of fuel oxidation in the SCWO system.
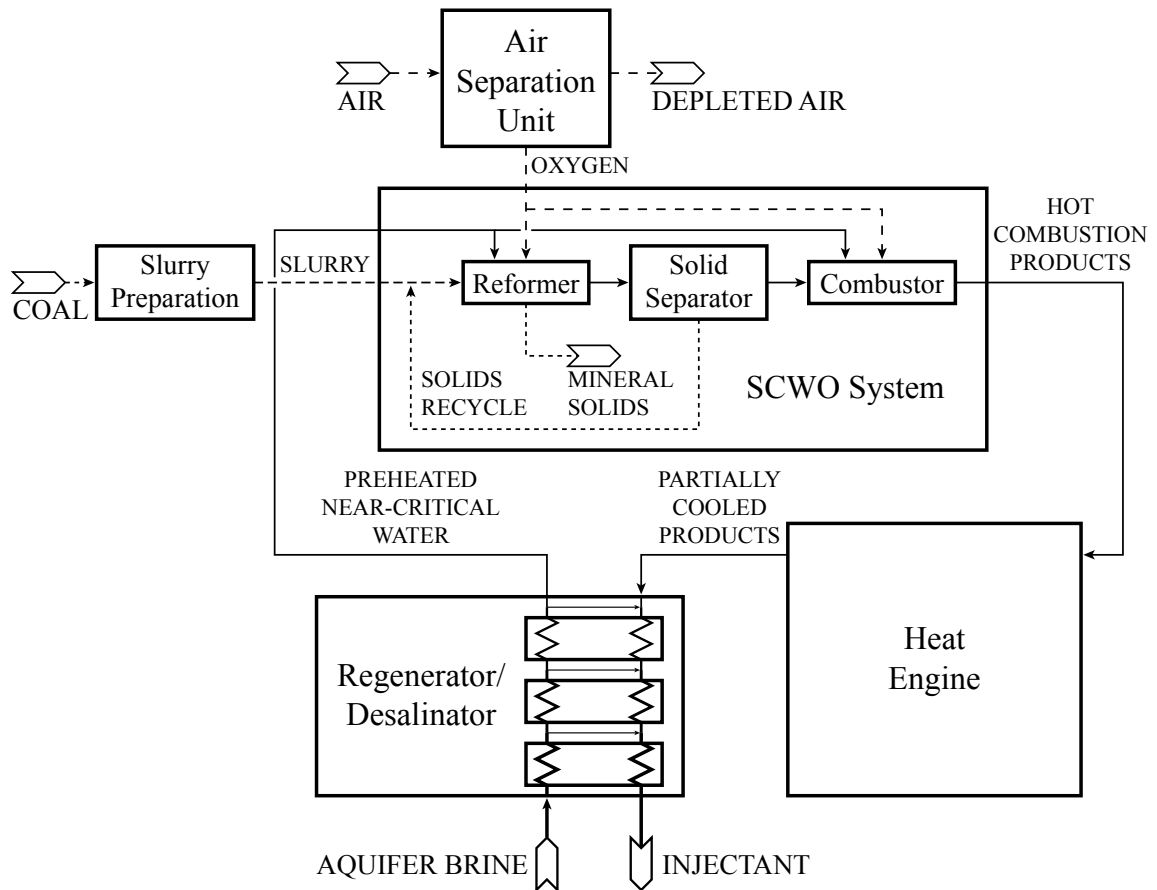
Figure 3.1: Diagram of a SCWO-based power plant. A regenerator is used for desalination and to improve thermal efficiency. Multiple stages prevent formation of a gas phase in the product stream. (Three stages are shown for illustration.) Oxygen from an ASU is used instead of air since nitrogen is much less water soluble than carbon dioxide. Coal processing is divided into reformer and combustor sections to facilitate mineral matter removal and protection of vessel walls. The choice of heat engine is left open at this stage.
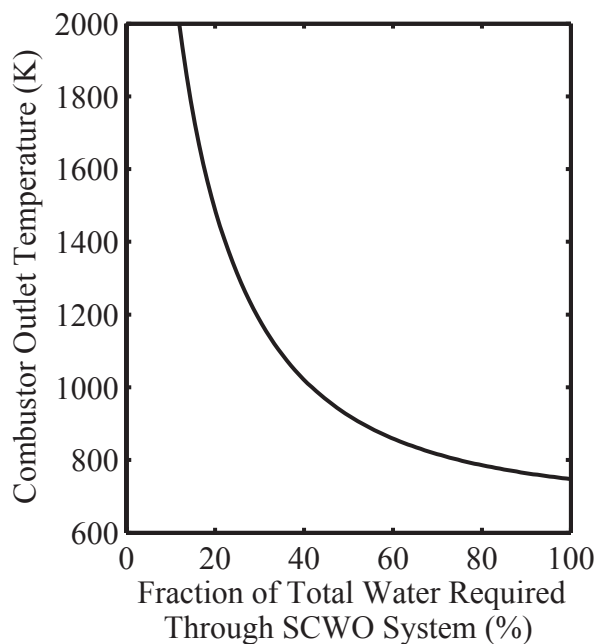
Figure 3.2: More water is required for dissolution of carbon dioxide in the aquifer than for moderation of combustion. The fraction of aquifer water required to achieve various adiabatic flame temperatures at the SCWO system outlet is shown.

Faster reactions lead to lower residence times and smaller reaction vessels. Preheating in a regenerator with heat transfer from the warm outlet stream improves the efficiency of the system, since it raises the average temperature of heat addition to the heat engine. Note that while this regenerator is not part of a power cycle, its purpose is similar. A side effect of heating the inlet brine to near the critical temperature is the precipitation of salts; while organics and gases become highly soluble in water above the critical point, ionic materials have low solubilities in supercritical water. Salt removal at this stage is desirable since it precludes precipitation in the combustor and high-temperature heat exchangers where it would be more difficult to manage than in a moderate-temperature regenerator. Taking advantage of the behavior of SCW, desalination is accomplished by temperature driven precipitation in a combination regenerator/desalinator unit. Separation could be by mechanical means [21], or by redissolving the precipitated salts in a subcritical zone of the vessel. The latter option

is related to the boundary layer in the TWR, except in the present case the salt-enriched subcritical stream would leave the vessel through a different outlet than the heated stream. After preheating, low-salinity, near-critical water leaves the regenerator. The small amount of impurities remaining may be removed by sorption or filtration. Desalinated water passes into the SCWO system to moderate the reaction process.

The other inputs to the SCWO system are coal-water slurry and an oxidizer. Air was used for the oxidizer in Fig. 1.6, but oxygen from an air separation unit (ASU) is used in Fig. 3.1. Since nitrogen is much less soluble in water than carbon dioxide, nitrogen from air would separate into a gas phase in the cooled effluent leaving the plant. Oxygen is used to ensure that the products will be a single-phase solution that can be securely stored in an aquifer. An alternative is to use air and circulate enough aquifer water to dissolve all of the nitrogen, but this would require a prohibitive amount of water. Although the proposed system does not avoid a separation and attendant energy cost, the trade-off of carbon separation for air separation is advantageous since it comes with the ability to sequester all fluid coal combustion products, including sulfur and metals, in addition to carbon dioxide.

Since coal is a complex, solid fuel, processing in the SCWO system is divided into reformer and combustor sections so that mineral matter (ash) can be removed. Mineral matter should be removed early to prevent deposition in downstream components where it would be more difficult to manage. In the reformer, near-critical water heats the coal particles, causing them to devolatilize. Oxygen from the ASU is used to assist with char burnout. These decomposition processes separate the carbonaceous fuel from the mineral matter so that it can be removed. Atoms other than hydrogen and carbon, such as sulfur and metals, may form salts that precipitate and can be removed. The addition of a base can help precipitate acid anions [13]. The temperature rise through the reformer should be relatively low so that the process stream remains easy to handle in the solid separator. From here, any solids are recycled to the reformer so that they have sufficient residence time to achieve the required degree of carbon extraction.

The fluid output from the solid separator is a single-phase synthesis fuel solution of water, hydrocarbons evolved from coal, and products of reaction. This synfuel

and the remainder of the oxygen (which is the majority) from the ASU meet in the combustor, where oxidation is completed. Since the fuel is a fluid and no heat exchange is desired within this component, the combustor can be similar to modern gas turbine combustors. These combustors feature intense, localized flames that are stabilized by fluid flow. Perforated liners allow cooling flows to protect surfaces from the destructive heat and oxidation of the flame zone. In gas turbine engines, stabilization and cooling flows use compressed air. In the proposed combustor, desalinated, preheated aquifer water is used. This concept has been already been demonstrated with supercritical water in the transpiring wall reactor at ETH (see Sec. 2.3.2).

The stream exiting the combustor is a single-phase, supercritical solution of hot combustion products suitable for driving the heat engine. The choice of heat engine is immaterial with regard to the CCS strategy of the plant; an appropriate type will be introduced in the next section to develop a performance model. The products pass through a heat exchanger, transferring energy to the heat engine working fluid. A chief difficulty with design of heat engines is heat exchangers that can withstand very high temperatures, since this limitation affects the upper bound of cycle efficiency. To make the construction of this heat exchanger feasible, the pressure of the working fluid should equal the pressure of the combustion products. The heat exchange surfaces must operate at very high temperatures, but by pressure matching the streams these surfaces do not have to withstand significant mechanical stress. With this design choice, stability and corrosion are the key material limitations instead of high-temperature creep strength.

After cooling to near the critical temperature, the product stream flows through the hot side of the regenerator/desalinator where it heats the incoming aquifer brine. To prevent the formation of a gas phase in the regenerator, the cooling is done in stages, with partially heated aquifer water (drawn from the inlet side) added between each stage. If the product stream were cooled completely without the addition of more water, it would become two-phase in the regenerator, since carbon dioxide is miscible in supercritical water but has a limited solubility below the critical temperature. (Recall that only a portion of the dissolution water went through the SCWO system and is present in the products stream. See Fig. 3.2.) Staged cooling ensures that the product

stream at any location contains enough water to dissolve all of the carbon dioxide. Finally, the salts removed by the desalinator are reintroduced. This mixing could be done in stages with the aquifer water, or all at once after the product stream is completely cooled. The salts that were removed from the inlet brine are reintroduced, rather than sold as a co-product of electricity, in order to maintain solution density, since the objective of pre-equilibration of CO_2 is to inject a stream that is denser than the original brine. The result after mixing is a pre-equilibrated, single-phase solution of carbon dioxide and other fluid coal combustion products ready for injection into the aquifer.

3.2 System Analysis

3.2.1 Thermodynamic Model

Next, a thermodynamic analysis is used to see if this type of plant is efficient enough to merit further study. The modeled system is shown in Fig. 3.3. There are three major differences from the block diagram of Fig. 3.1. First, the multi-stage regenerator/ desalinator is replaced by a single-stage regenerator that preheats both the water and the oxygen. Precipitation of salts by reduction of solubility is a consequence of this heating. Physical removal of salts is not energetically significant and is therefore not modeled. Second, the process details and kinetics of the SCWO system are not included.

From a thermodynamic perspective, only its inlet and outlet states are relevant. Finally, and in contrast to the SCWO system, the details of the heat engine must be specified in order to obtain a realistic projection of plant performance. A combined cycle with a closed helium Brayton topping cycle and a steam Rankine bottoming cycle was chosen. This arrangement is similar to combined cycle systems presently in use, except that the Brayton cycle is closed.[1] A combined cycle where energy is input to the topping cycle through a heat exchanger instead of from combustion within the cycle is known as an indirectly fired combined cycle, or IFCC. Thus, the complete

---

[1]Closed Brayton cycles have been discussed for nuclear applications [22].

system presented here may be described as a supercritical water oxidation, indirectly fired combined cycle, or SCWO/IFCC.

Figure 3.3: The SCWO/IFCC system as implemented in the thermodynamic model. Details of the SCWO system do not affect this efficiency analysis, but the specifics of the heat engine are required. A closed combined cycle is used.

Since the main heat exchanger should be pressure matched to ease materials limitations (as discussed in Sec. 3.1), the pressure at the Brayton compressor outlet (station B2 in Fig. 3.3) is set at the pressure of the SCWO system outlet (P1). Cooling of the first four turbine blade rows is included in the analysis using the methods and parameters of Horlock [23]. The Rankine cycle is conventional, with an operating pressure that satisfies other requirements of the system (it is not constrained to be sub- or supercritical; the pressure is determined through optimization of the whole system). For simplicity, further refinements to increase combined cycle efficiency, such as intercooling, are not considered in this analysis; there is no conceptual reason for their exclusion.

Instead of modeling a complete ASU, a work requirement (energy per unit mass of oxygen produced) is taken from the literature [24]. This value assumes the production of low-pressure oxygen, so the model explicitly includes a high-pressure liquid oxygen pump within the ASU. The model fuel is moisture-and-ash-free (MAF) coal, with composition based on a Powder River Basin sub-bituminous coal [25]. Mineral matter is not considered; the removal of sensible enthalpy with hot ash would cause only a small decrease in performance. Only carbon, hydrogen, oxygen, and nitrogen atoms are included in the model since usable real fluid data were readily available for major products involving these elements. The excluded trace elements are not energetically important since they are present in relatively small amounts. Water, oxygen, carbon dioxide, and nitrogen are modeled as real fluids using the formulations of Reynolds [26]. The combustion products stream (found at stations beginning with P) is treated as an ideal solution of these real fluids, with property data computed using a linear mixing rule. The Brayton cycle helium is modeled as an ideal gas with variable specific heat. Aquifer conditions and pressure losses in the wells used to calculate the work requirements of the three aquifer water pumps are taken from the surface dissolution study by Burton and Bryant [6]. These parameters and all other assumed component performance ratings are listed in Appendix A.

The model is solved as follows: For a fixed flow rate of MAF coal, the flow rate of aquifer water at W1 for dissolution is calculated for specified aquifer conditions. Carbon dioxide solubility is obtained from relations reported by Hangx [27]. The oxygen flow rate for stoichiometric combustion is computed from the coal composition. Next, the temperature at the SCWO system outlet (P1) is chosen. An adiabatic flame temperature calculation at this station gives the flow rate at W2 of aquifer water required in the SCWO system loop. (The major-products combustion model is used in this calculation.) The enthalpy balance of the main heat exchanger determines the Brayton cycle helium mass flow rate. The Rankine cycle pressure ratio is set to achieve a specified steam quality at the turbine outlet (R4). The pinch point temperature difference in the HRSG fixes the Rankine cycle mass flow rate. Temperatures in the Rankine cycle are calculated starting at the condenser outlet (R5) saturation temperature and moving around the loop. The temperatures in the Brayton cycle and

the SCWO system loop are not prescribed at any station except P1. Starting with temperature guesses at B1 and O4/W4, these loops are iterated until temperatures converge to a physical solution. Using this procedure, the only remaining free parameter of the model is the Brayton cycle compressor inlet pressure at station B1. For a chosen SCWO system outlet temperature, this parameter is varied to optimize the efficiency of the system.

3.2.2   Model Results

Efficiency Trends

Overall efficiency is defined as the net power output divided by the mass flow rate of MAF coal times its lower heating value:

$$\eta_{ov} = \frac{\dot{W}_{Brayton} + \dot{W}_{Rankine} - \dot{W}_{ASU} - \dot{W}_{pumps}}{\dot{m}_{MAF} \cdot L\dot{H}V_{MAF}}.$$

Figure 3.4 shows plots of overall efficiency versus Brayton compressor inlet pressure for five SCWO system outlet temperatures. As expected, the overall efficiency increases with SCWO system outlet temperature since the product stream is the hot reservoir for the combined cycle. For each outlet temperature, the overall efficiency increases with Brayton inlet pressure over most of the range shown. At certain inlet pressures, the combination of conditions in the SCWO system loop causes decreased efficiency. The net output of the combined cycle dominates the overall efficiency. This work output is the product of combined cycle efficiency and the amount of energy input from the product stream that passes through the main heat exchanger into the heat engine. Combined cycle efficiency increases with Brayton inlet pressure, but not enough to account for the trend in overall efficiency. The increasing cycle efficiency also fails to explain the marked decrease in overall efficiency seen over a small range of pressures. But Brayton inlet pressure also affects the amount of energy input. This effect strengthens the increasing trend and accounts for the decrease in overall efficiency.

Energy input to the combined cycle generally increases with Brayton inlet pressure
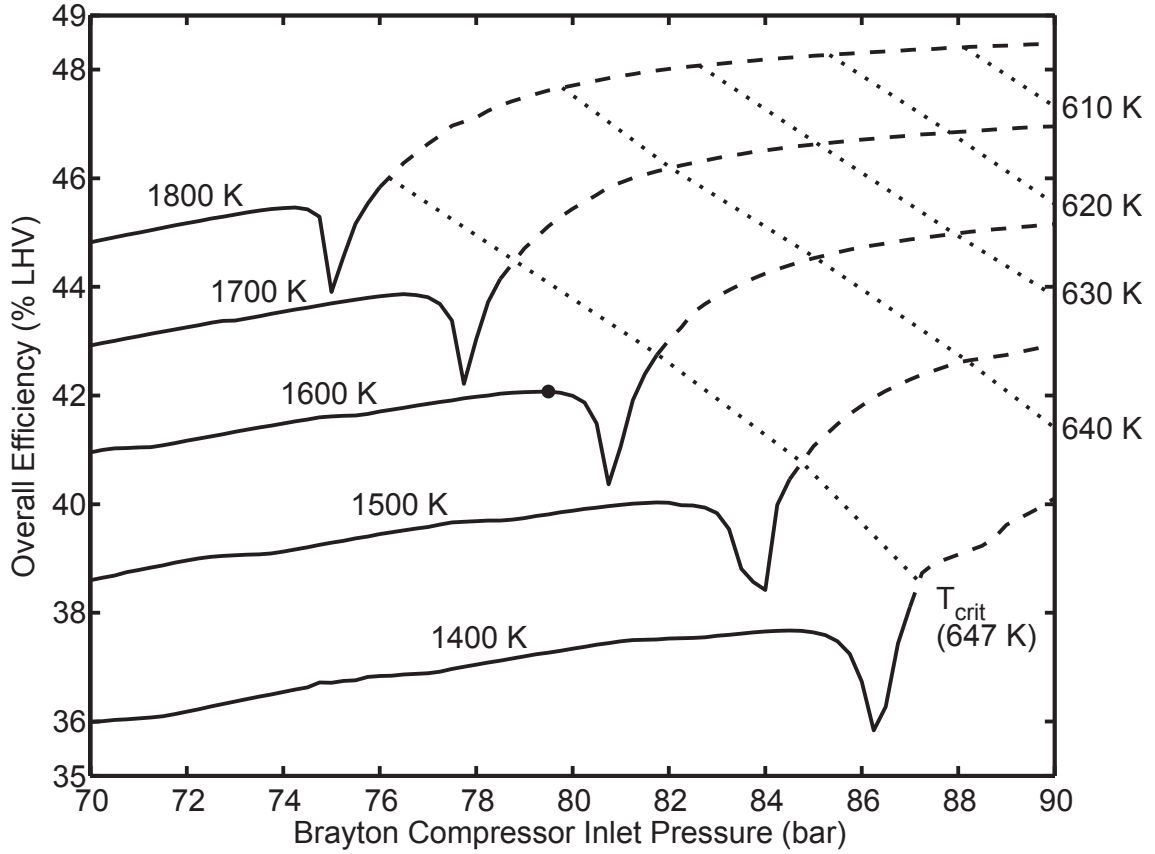
Figure 3.4: Overall efficiency versus Brayton compressor inlet pressure for five SCWO system outlet temperatures from 1400–1800 K. Solid portions are operating conditions with supercritical SCWO system inlet temperatures; dashed portions are those with subcritical inlet temperatures. Dotted lines are contours of equal inlet temperature. The point marked denotes the 1600 K, 79.5 bar conservative optimum condition.

for the following reasons. The Rankine cycle condenser operates at a specified pressure, so the states at the condenser outlet (R5) and storage tank (R1) are fixed. The feed pump between stations R1 and R2 operates at different pressure ratios for different plant conditions, but since it pumps a liquid (viz. water), the temperature at station R2 is nearly independent of the pressure ratio. Cooling of the Brayton cycle working fluid in the HRSG is limited by the pinch point. Still, since the temperature at R2 is roughly constant, the temperature at B1 is approximately independent of Rankine pressure ratio and Brayton inlet pressure. As Brayton inlet pressure increases, the

pressure ratio across the Brayton cycle compressor decreases, and the temperature at the compressor outlet (B2) decreases. Since the main heat exchanger cools the product stream at P2 to near the temperature at B2 (limited by its effectiveness), the temperature at P2 also decreases. Similarly, the temperatures of the SCWO system inlet oxygen (O4) and water (W4) decrease. Since the flow rate of SCWO system water is chosen to regulate the SCWO system outlet temperature, the water requirement decreases as this inlet water gets cooler. With less inlet water, the flow rate of the product stream drops. At any operating condition, the mass flow rate of products is greater than the mass flow rate of incoming water and oxygen (since coal is added in the SCWO system). Due to this mismatch, the products at P3 are not fully cooled, and there is available energy leaving the plant. Since increasing Brayton inlet pressure causes the product flow rate to drop, the enthalpy flux leaving with the products also drops. More energy is transferred to the heat engine instead, and the overall plant efficiency increases.

Effect of Near-pseudocritical Operation on the Regenerator

With ideal heat exchangers, the trend in overall efficiency would be strictly increasing over the Brayton inlet pressure range shown for the reasons cited above. With realistic heat exchangers, there is an operating regime (apparent in Fig. 3.4) with diminished efficiency. This decrease is caused by a capacity mismatch when the streams at the hot end of the regenerator are near-pseudocritical.

Figure 3.5 shows the semi-extensive enthalpies of the reactants and products flowing through the regenerator as a function of temperature for two different operating conditions. These are enthalpy flow rates ($\dot{m}h$) normalized by the flow rate of water at W3. Here, "reactants" means water and oxygen only, since coal does not flow through the regenerator. The enthalpy reference states for the reactants are the regenerator inlet states at stations O3 and W3, which have the same temperature and pressure as each other. The reference state for the products stream has the same composition and pressure as the regenerator outlet (P3), but the temperature of O3 and W3. With these references, the curves show the relative sensible enthalpy capacities of the two streams as functions of temperature. The curves are isobars at the pressures present

at the hot end of the regenerator (O4/W4 and P2). The products have higher capacity that the reactants due to the addition of matter (coal) in the SCWO system. The steepest point on each isobar is the pseudocritical point for the corresponding stream. The pressure of the reactants is higher than that of the products, so the reactant stream has a slightly higher pseudocritical temperature.
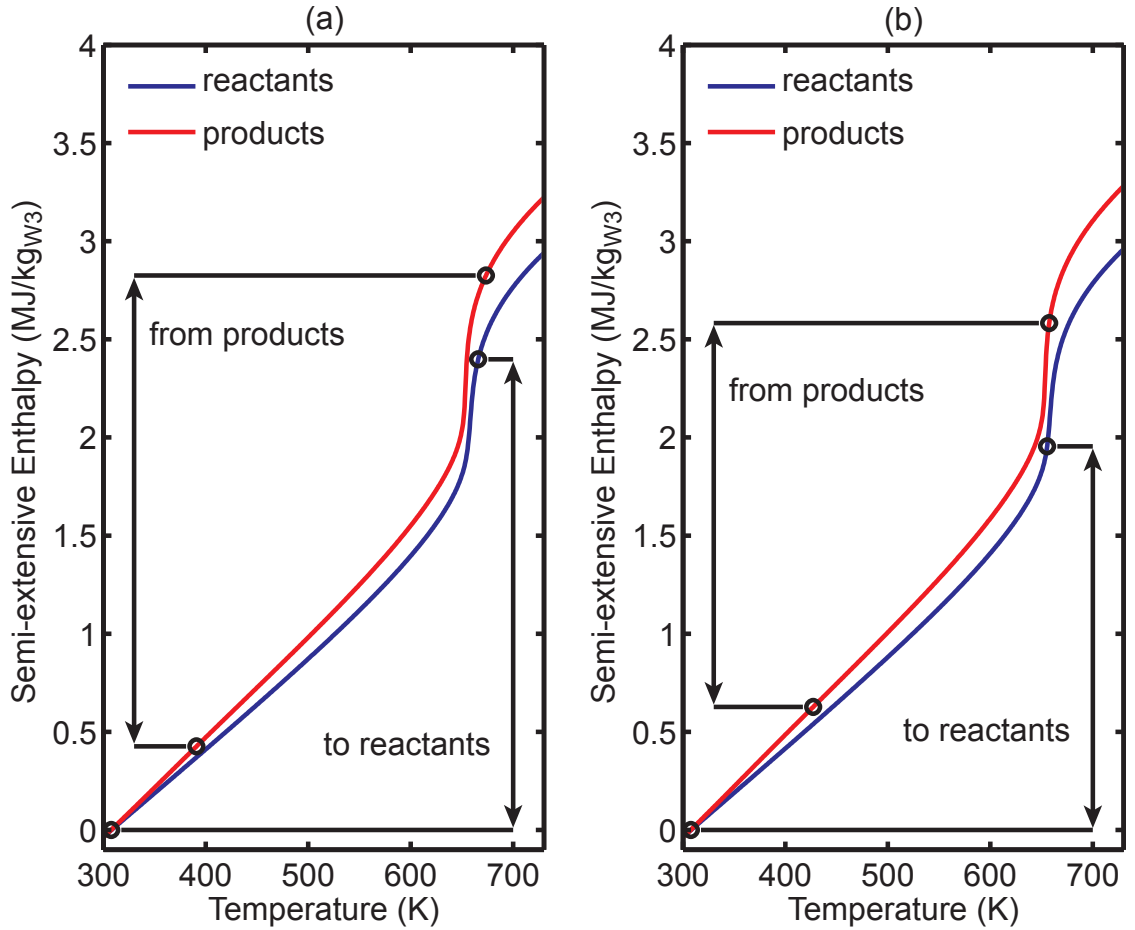
Figure 3.5: Semi-extensive enthalpies versus temperature in the regenerator. Pressure losses and heat exchanger ineffectiveness result in a rise in product outlet temperature and drop in overall efficiency at specific operating conditions.

Figure 3.5a corresponds to the optimized case with 1600 K SCWO system outlet temperature and 79.5 bar Brayton compressor inlet pressure. In addition to the capacity isobars, the actual inlet and outlet states are marked. The regenerator is

taken as adiabatic, so the heat transfer from the products equals the heat transfer to the reactants. This transfer is shown by the the arrows marking equal vertical distances between the inlet and outlet state of each stream. Since the reactant stream does not have enough capacity to absorb all of the available sensible enthalpy of the products, an amount of enthalpy equal to the capacity mismatch remains with the product stream instead of being returned through the regenerator. The remaining enthalpy is lost as it exits the plant.

At certain plant conditions (Fig. 3.5b) the temperature of the products is just above the pseudocritical point of the products, while the temperature of the reactants is just below the pseudocritical point of the reactants. At such conditions, the capacity mismatch increases, and the temperature and enthalpy of the products leaving the regenerator increases. Since waste enthalpy is increased, less enthalpy is available for the heat engine, and overall efficiency drops. Figure 3.5b corresponds to the worst-case Brayton inlet pressure of 80.75 bar at 1600 K SCWO system outlet (the local minimum in Fig. 3.4). At slightly higher or lower hot-side temperatures (as in Fig. 3.5a), the reactant and product states are either both above or both below their respective pseudocritical points, and overall efficiency follows the usual increasing trend.

The width and severity of the efficiency dip depends on the pressure drops in the regenerator and main heat exchanger since the difference in pressure between the reactants and products is responsible for their unequal pseudocritical temperatures. The other contributing characteristic is the regenerator effectiveness; since the regenerator is less than 100% effective, the outlet temperature of the products is higher that the inlet temperature of the reactants. Smaller pressure drops and a higher effectiveness reduce the size of the efficiency dip until it disappears completely in a system with ideal devices.

Implications for Reformer Inlet Temperature

As discussed above, as Brayton inlet pressure increases, the regenerator outlet temperature of the reactants decreases (W4, O4). In the present model, this temperature is also the SCWO system inlet temperature, as the SCWO system is directly downstream

of the regenerator. The operation of the supercritical water oxidation system depends on its contents being supercritical, so its inlet temperature should be near, if not above, the critical temperature. In Fig. 3.4, the solid parts of each efficiency curve are for plant conditions with supercritical SCWO system inlet temperature, and the dashed parts correspond to operation with subcritical inlet temperature. For any SCWO system outlet temperature in the range shown, the requirement of supercritical inlet temperature is a significant handicap. Overall efficiency could be more than two percentage points higher if the fuel oxidation system could accommodate slightly subcritical inlet temperatures. The dotted contours connect operating points accessible when various subcritical inlet temperatures are acceptable. Another way to make the system function with subcritical reformer outlet temperatures is to raise the temperature of the reactants after leaving the reformer. Conditions similar to these may be reachable in the model by including a second stage of reactant preheating by heat transfer from the SCWO system. The corresponding change to the plant of Fig. 3.2 is preheating by heat transfer from the regenerator. This change would allow the regenerator outlet temperature to be lower than the SCWO system inlet temperature. In this case, the higher overall efficiencies shown to the right on Fig. 3.4 could be achieved without a subcritical reformer section. As an added benefit, this heat transfer would help limit the temperatures in the reformer.

Choice of Optimum Operating Condition

The key parameter affecting overall efficiency is the SCWO system outlet temperature. Since work extraction is done with a heat engine, the Carnot limit applies, and the highest temperature that can be withstood by the materials of construction is desired. Referring to Fig. 3.4, about 2% efficiency is gained for each 100 K increase. Presently, nickel superalloy turbine blades can operate at material temperatures around 1400 K [28]. Titanium-zirconium-molybdenum alloy (TZM) retains a significant fraction of its ambient-temperature tensile strength at even higher temperatures (Fig. 3.6). Heat exchange surfaces in the pressure-matched main heat exchanger would not be subject to the stresses found in turbine blades, and so could operate close to their melting temperatures. A cautiously optimistic value of 1600 K is assumed for

the SCWO system outlet temperature for the purpose of comparing the SCWO/IFCC system to other designs.
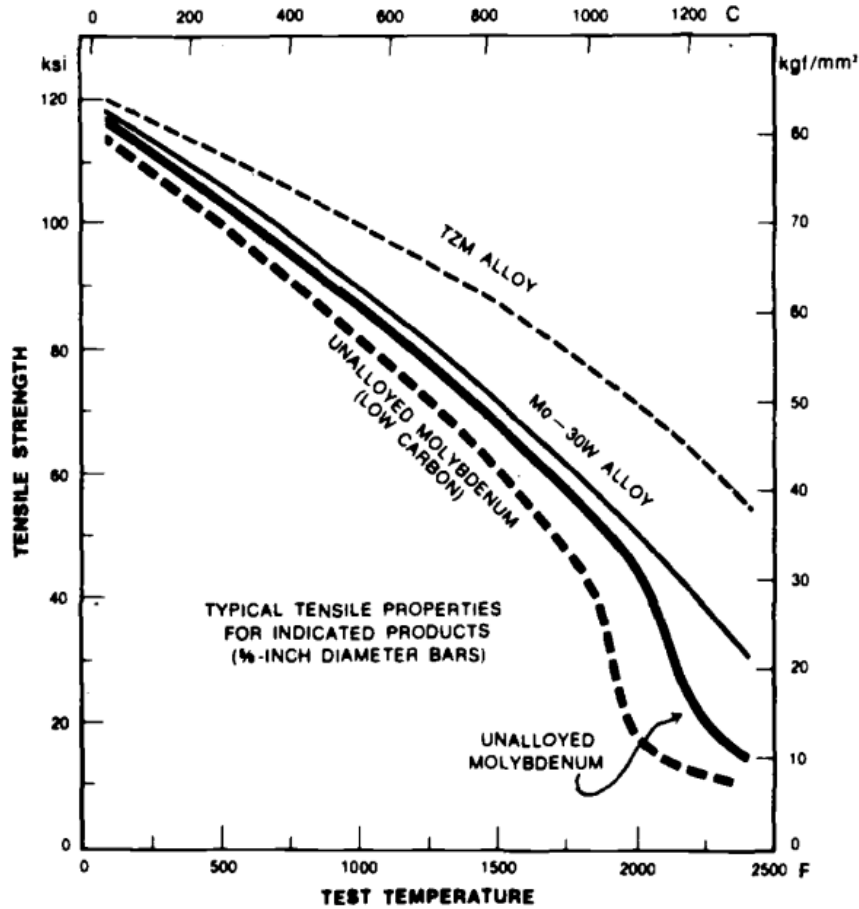
Figure 3.6: High-temperature tensile strength of molybdenum and its alloys [29]. Titanium-zirconium-molybdenum (TZM) has a strength above 340 MPa (35 kgf/mm^2) at 1573 K (1300°C).

With the design as shown in Fig. 3.1, a good choice of Brayton inlet pressure is the pressure that gives maximum efficiency but is to the left of the efficiency dip. Slightly higher efficiencies with supercritical inlet temperatures can be found to the right, but the local maximum on the left is a conservative choice that relies less on assumptions of process controllability, and avoids operating regions near the critical temperature where fluid properties vary rapidly with temperature. For a SCWO system outlet temperature of 1600 K, the optimum value is about 79.5 bar. Table 3.1

Component	Power (MW)
Brayton cycle	
Compressor	-390.1
Turbine	661.9
Net	271.8
Rankine cycle	
Condensate Pump	-0.026
Feed pump	-2.27
Turbine	332.5
Net	330.2
ASU	-74.2
Water pumps	-27.8
Overall plant	500.0
Fuel heat rate (LHV)	1203.0
Efficiency (% LHV)	41.6

Table 3.1: Power balance for a plant operating at a SCWO system outlet temperature of 1600 K. The model plant has been optimized by adjusting the Brayton compressor inlet pressure to 79.5 bar.

gives the power balance for a 500 MW plant operating at these conditions. Overall efficiency, after energy penalties for oxygen separation, carbon sequestration, and non-ideal components, is 41.6% on a lower heating value basis.

3.2.3 Model Conclusions

An important design choice in the SCWO/IFCC system presented is pressure matching in the main heat exchanger. As a result, the Brayton cycle runs at much higher pressure than similar cycles currently in use. The requirement of very high pressure operation does not, by itself, make construction of the Brayton turbomachinery impractical. A better picture of the design challenge is given by the pressure ratio, which is an output of the model. In fact, the pressure ratio turns out to be quite modest at 3.4 or lower for the operating regime of interest according to Fig. 3.4. Also due to the high pressures in the Brayton cycle, the pressure difference across the heat recovery steam generator (HRSG) linking the two power cycles is lower than in usual practice—it is

Case	Efficiency (% LHV)
Subcritical PC w/ 90% CO_2 Capture	27.1
Supercritical PC w/ 90% CO_2 Capture	29.3
IGCC w/ 90% CO2 Capture (GE)	33.7
Oxyfuel (CES "Rocket" w/ E-Gas)	41.4
SCWO w/ 100% CO_2 Capture (This Work)	41.6

Table 3.2: Efficiencies of coal-fired designs with CCS [30, 31].

nearly pressure-matched. (See Table A.1.) Similar to the posited main heat exchanger, creep in boiler tubes will be less of a concern than it is for natural gas combined cycle HRSGs.

Based on thermal efficiency and aquifer water flow rates, construction of a coal-fired electric power plant with secure carbon sequestration using SCWO may be feasible. While the amount of water required to dissolve all of the carbon dioxide and create a single-phase injectant is high, it is not beyond current experience. Meanwhile, thermal efficiency is on par with leading coal-with-capture technologies (see Table 3.2) [24, 30, 31]. The SCWO/IFCC system has the added benefit of total combustion product sequestration, including 100% carbon capture, as well as capture of sulfur and metals.

Several aspects of the proposed system must be explored before such a plant could be assembled. Desalination by temperature-driven precipitation has not been developed as an engineered process (possibly since desalinated water from flash or reverse osmosis systems is typically used at ambient temperatures, providing no incentive for a supercritical process). High pressure helium compressors and turbines have been discussed for use with nuclear power, but not for pressures as high as 250 bar. The key to the system, however, is supercritical water processing. As discussed in Ch. 2, SCWO development for hazardous waste destruction has largely focused on relatively low-temperature, homogeneous oxidation. Existing SCW combustors are promising, but they too have been operated with waste destruction in mind. What is needed is a laboratory-scale, flame-based, supercritical water combustor applied to the objective of work extraction.

Chapter 4

Experimental Supercritical Water Combustor

Previous work by other investigators has shown that combustion can occur in supercritical water. However, since hazardous waste treatment was their primary focus, they did not seek to operate their reactors at conditions suited for use in an energy system. The experimental portion of the present project aims to explore the operating space desirable for use in a plant like the one developed in Ch. 3. A new supercritical water combustor was designed and built for this purpose. Complimentary systems to supply reactants and supercritical water were also installed. The combustor is considered first since the other systems were designed to meet its demands.

4.1   Combustor

4.1.1   Requirements

The primary consideration in the design of the experimental combustor is the integration of the combustor with a complete plant. The thermodynamic model of Sec. 3.2 informs the inlet and outlet states of the reformer and combustor pair. It is to be shown that a combustor can be operated at these conditions. From that standpoint, the scale of the device is a free parameter. The size was chosen based on desired

flow characteristics taken from prior experience with laboratory-scale, continuous-flow combustion systems.

The inputs to the combustor are fuel, oxygen, and water at supercritical temperatures and pressures. The fuel for the real combustor would be the synthesis fuel produced in the reformer. Equilibrium calculations from a parallel project investigating the SCW reformer predict that this synfuel will be similar to the output of a gasifier in that it will consist primarily of species that are gases at ambient conditions [32]. A simulated syngas mixture may be used with the experimental combustor in the future, but it will initially use a liquid fuel for ease of storage, pressurization, and flow control. Methanol was chosen because it is miscible with water even at ambient conditions. It also allows for comparison between initial results from the new combustor and those from previous work. Oxygen is used as the oxidizer; any other choice would be a significant departure from the conceptual plant.

Fuel and oxygen flow rates were calculated based on firing rate and equivalence ratio. A firing rate of 10–100 kW was desired based on previous experience with laboratory-scale combustors. The overall fuel oxidation reaction in the plant reformer and combustor should be close to stoichiometric, since both oxygen and fuel have significant cost. Despite the fact that some of the oxygen may go into the reformer, the combustor does not operate fuel rich; the combustor considered by itself is stoichiometric with respect to the synthesis fuel. Hence, the experimental combustor should operate stoichiometrically with whatever fuel is being used. The performance of materials downstream of the burner may depend heavily on the oxidizing or reducing nature of their environment, so the system may be operated just off of stoichiometric to prevent oscillation between slightly rich and slightly lean conditions. Still, the equivalence ratio is taken as unity for experimental design purposes.

To choose a range of inlet water flow rates, the desired outlet conditions must be considered. Because the output stream from the combustor in a real plant will drive a heat engine via heat exchange, the outlet temperature should be as high as possible—within material limits—for good heat engine efficiency. Materials limitations in a heat exchanger will limit the outlet temperature to 2000 K or lower. For the design of this combustor, a range from 1600 to 2000 K should be accessible for experimental

flexibility. If the only streams entering a perfectly-insulated combustor were fuel and oxygen (both with fixed fractions of diluent species), the outlet temperature would equal the adiabatic flame temperature (T_{ad}).[1] This temperature is dependent upon the chosen equivalence ratio. However, in a supercritical water system, there is an additional flow of diluent that is decoupled from the reactant flows, namely water. This additional input allows for independent control of the equivalence ratio and adiabatic flame temperature. Having already specified the firing rate and equivalence ratio, the choice of adiabatic flame temperature determines the water flow rate.

For fast, turbulent mixing and a high volumetric firing rate, Reynolds numbers in the 10^4 to 10^5 range are desired. With relative flow rates established by the choice of equivalence ratio and adiabatic flame temperature, the Reynolds number is a function of firing rate and inner diameter. Figure 4.1 is a map of possible flow conditions for an adiabatic flame temperature of 1800 K. The plot shows the variation in Reynolds number (based on inner diameter) with diameter and firing rate. The solid curves are for firing rates of 10, 50, and 100 kW. The dashed curves are contours of constant mean flow speed, ranging from 0.05 to 1 m/s. Due to the high density of supercritical water, the flow speeds are quite low compared to gas phase combustors. The vertical lines are at diameters of 1, 2, and 3 in. Since a large bore could be narrowed with the insertion of a liner, a larger vessel would have the largest operating space. However, strength and weight considerations prevent the choice of a large bore.

Since the wall thickness of a cylinder must increase linearly with the inner diameter (for constant safety factor), the area of the cross section varies with the square of the diameter. Before choosing an inner diameter, wall thickness was chosen with reference to the eventual diameter. The yield stress of Inconel 625 is ∼70 ksi. It is derated to 75% of the room temperature strength at 700 K. Using a maximum working pressure of 5000 psi (345 bar), a wall thickness equal to the inner diameter gives a safety factor of 5.4.[2] This choice of relative wall thickness is good for safety, providing margin against

---

[1]In this system, the adiabatic flame temperature is taken as the mixed-mean temperature (T_{mm}) at a suitable station past the burner. This location must be far enough downstream that reaction can complete within the advection time to reach it.

[2]Consider a closed, cylindrical vessel having length much longer than its outer diameter. The maximum von Mises stress in a cross section far from the ends of the cylinder occurs at the inside wall. With internal pressure P_i, zero external pressure, and wall thickness equal to the inner diameter,
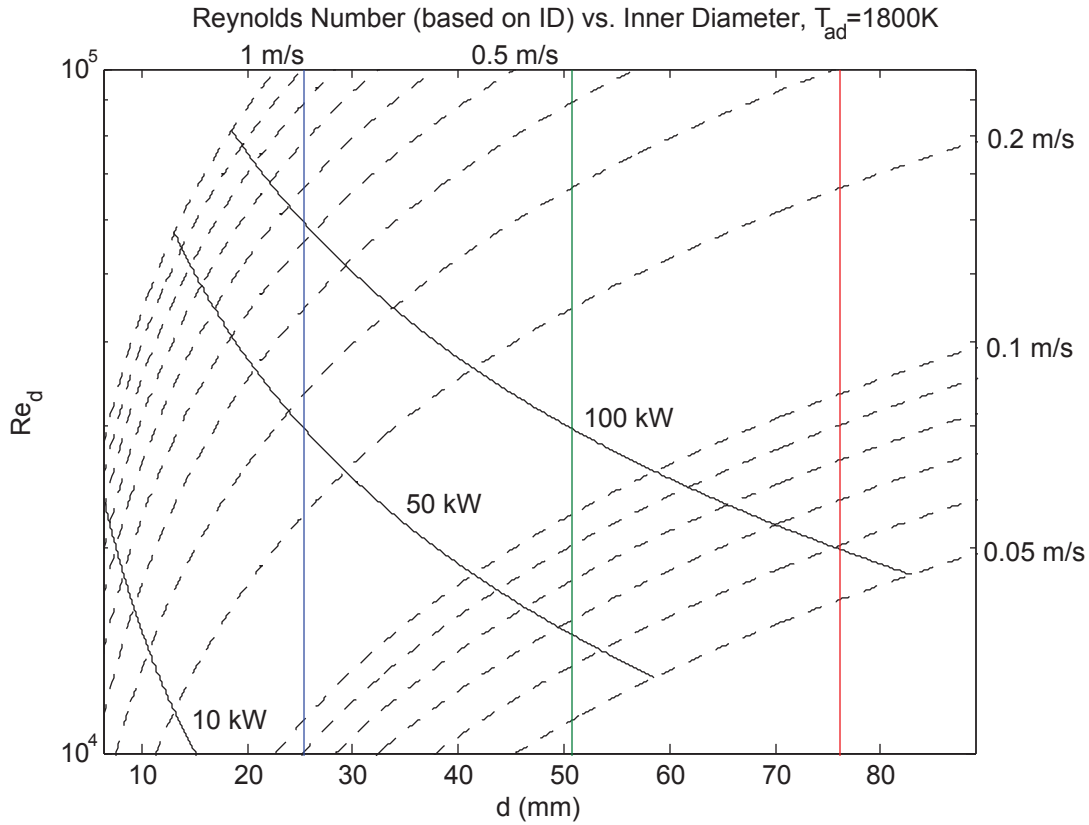
Figure 4.1: Plot of relationship between combustor diameter, Reynolds number, mean flow speed, and firing rate for T_{ad}=1800 K. The solid lines are contours of constant firing rate at 10, 50, and 100 kW. The dashed lines are contours of constant mean flow speed from 0.05 to 1 m/s. The blue, green, and red lines are at 1, 2, and 3 in. inner diameter.

possible pressure spikes due to ignition, as well as allowing for the usual material property uncertainties and stress concentrations around machined features. However, as the diameter increases, such thick walls quickly result in heavy equipment due to the power-law volume scaling. For example, a 3 in. vessel would have over twice the weight of a 2 in. vessel. While a larger bore could prove useful for future work, the added weight and material cost are significant disadvantages. For this reason, a 2 in. bore was selected. This size is still large enough for the use of burners and diagnostic

---

the maximum von Mises stress reduces to $\sigma_{vM,\,max}=9\sqrt{3}P_i/8$.

tools of convenient sizes. The map of Fig. 4.1 shows that it is also sufficiently large to access the desired space of Reynolds numbers and firing rates.

4.1.2   Description

A section view of the combustor vessel is shown in Fig. 4.2. The vessel has three main pieces, termed the combustor, the elbow, and the dilution cooler. (The term combustor is used to refer to one part as well as to the assembly. These uses are distinguished by context.) The sections are connected with Grayloc-style flanges (shown in blue), which eliminates the need for welding traditional flanges to the 2.25 in. thick vessel walls. They also allow the two flanges to be placed near each other without interference. Many ports are provided, each of which can be used for fluid injection, insertion of a thermocouple, or connection of a pressure transducer. All ports except the outlet are cone-and-thread fittings (High-Pressure Equipment Company "medium pressure" type, rated to 20,000 psi) to ensure proper sealing at elevated temperatures. The outlet port is 1/2 in. NPT. Flow is from bottom to top, then to the right (in this view).

The reactant inlet section is at the bottom of the combustor. A larger view of this area is shown in Fig. 4.3. (The cross-section plane of this figure is perpendicular to that of Fig. 4.2.) This section is composed of several parts—including the fuel and oxygen nozzles—and is bolted to the combustor from below. This design permits relatively easy interchange of burner nozzles. On the sides and bottom are inlet ports for the fuel/water solution and oxygen. There is also an inlet for neat water; this port is not visible in either cross-section since it is located 45 degrees out-of-plane. The stream entering this port is called "burner water" due to its location. These streams flow through three coaxial passages formed by the outer vessel and two nozzles, with oxygen in the core, fuel in the inner annulus, and burner water in the outer annulus. Nozzles of varying diameter may be used to change the relationships between mass flow rates, fluid velocities, and Reynolds numbers at the burner. Near the center of the combustor are sapphire windows for observation of the flame. The presence of two opposed windows allows for shadowgraph and Schlieren imaging in addition to
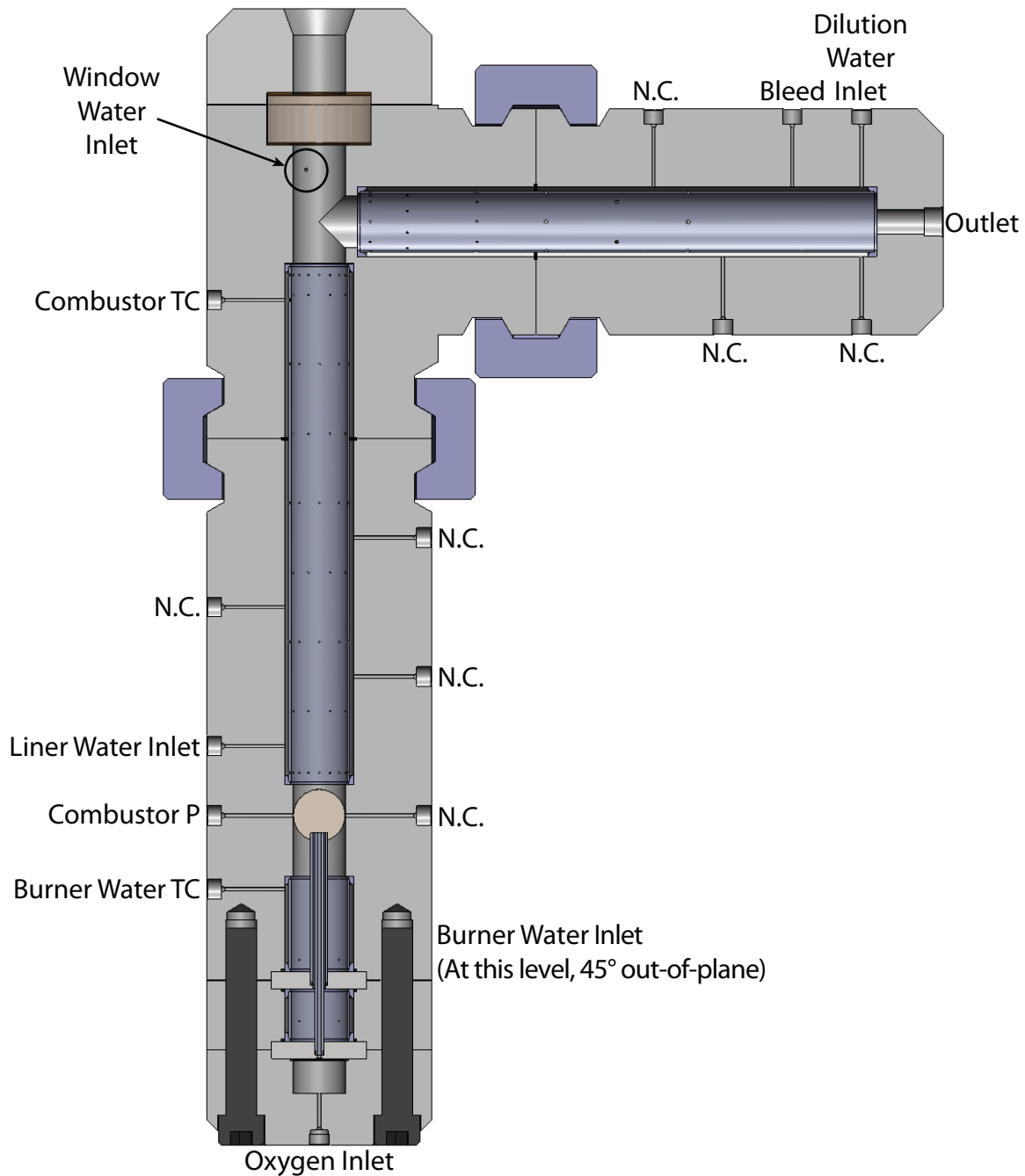
Figure 4.2: Section view of the combustor vessel with ports labeled according to current use. TC=thermocouple, P=pressure transducer, N.C.=no connection (these ports are plugged).

direct photography. The original nozzles end just above the bottom of the window to permit the observation of flame attachment. Shorter nozzles could be substituted to observe flames with lengths longer than the window aperture. One function of the burner water stream is to carry hot, reacting flows downstream so that they do not enter the window cross-bores, potentially causing damage.

Above the windows there is a liner (shown in a darker color than the main body in Fig. 4.2). This perforated metal liner functions like that in a gas turbine combustor, allowing relatively cool fluid (supercritical water in this case) to enter from an outer annular passage, shielding the liner and the pressure wall from the hot combustion products in the core flow. The pattern of 3/64 in. holes for this purpose is shown. This liner extends beyond the combustor, through the flanged joint, and into the elbow. The stream entering the vessel through the annulus and liner is aptly called "liner water".

The elbow section holds a third sapphire window to provide an axial view of the flame below. This allows direct observation of whether or not a luminous flame is touching the walls of the vessel—an undesirable condition. This window is identical to the two lower windows. There is an inlet for injection of 700 K water to prevent the impingement of very hot (1800 K or more) combustion products on the window. (This inlet port is not in the section plane; its intersection with the main passage is circled.)

The final section of the high-pressure stack is the dilution cooler. This section houses another perforated liner and fluid inlets. Here, high-pressure, ambient-temperature water is mixed with the combustion products to form an intermediate temperature mixture. This is the first of two dilution cooling steps to lower the temperature of the effluent to protect equipment downstream.

4.2   Feed Systems

In the concept plant presented in Sec. 3.1, there are several components upstream of the SCWO oxidation system that prepare the water, fuel, and oxygen for injection into the reformer and combustor. Although this work aims to study only the combustor, analogous systems must be installed in the laboratory. Because supercritical water

Burner Water Inlet
(At this level,
45° out-of-plane)

Fuel TC

Fuel Inlet

Oxygen TC

Oxygen Inlet
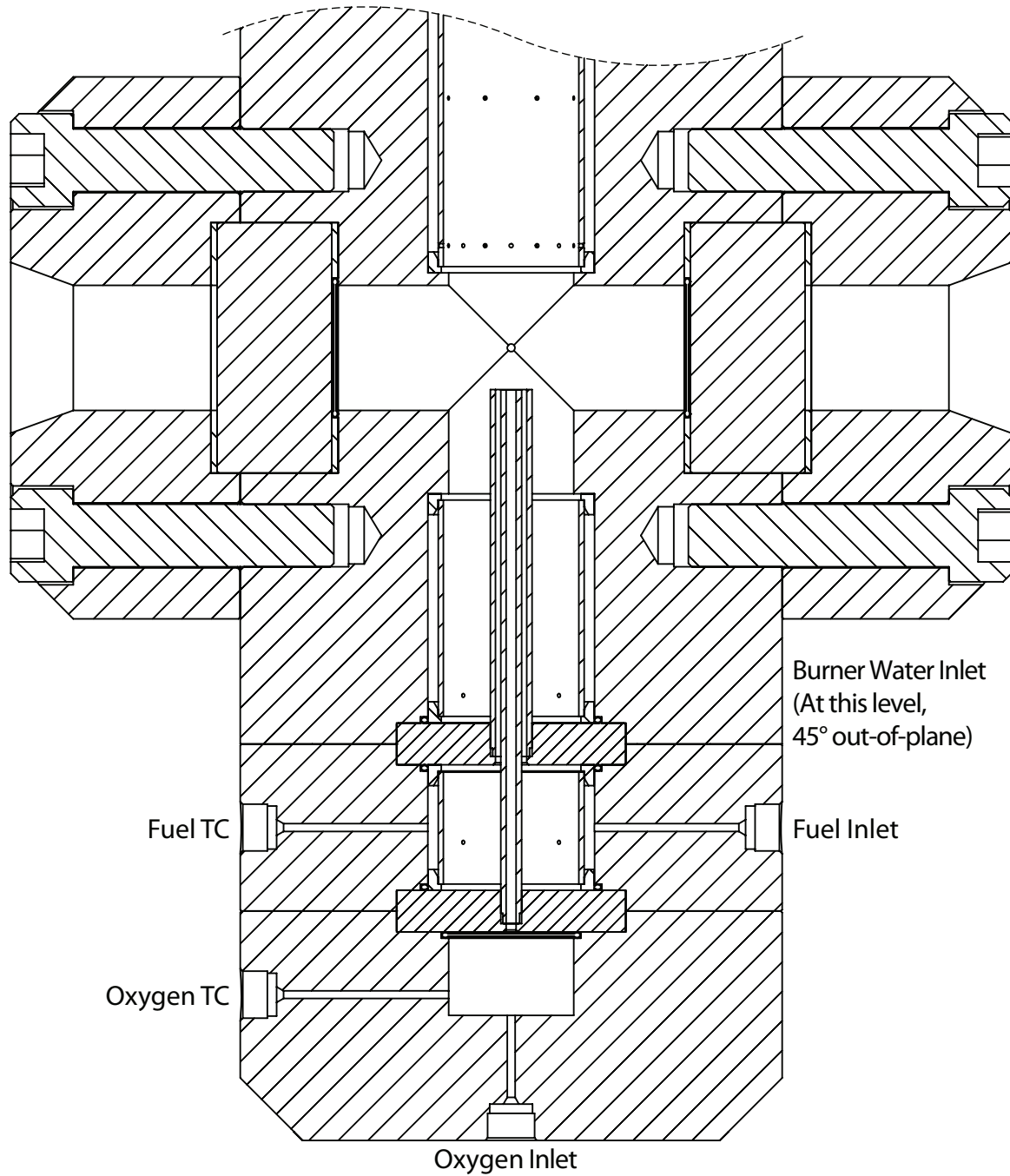
Figure 4.3: Section drawing of the lower portion of the combustor vessel with ports labeled. The section plane is perpendicular to that of Fig. 4.2. Scale 1:2.

conditions require temperatures and pressures both far from ambient conditions, a sizable amount of equipment is required to bring reagents to the supercritical state of water and return the effluent to ambient conditions in a controlled way. Specifically, there must be equipment for the following tasks: reactant storage, pressurization, flow rate control, heating, reaction, pressure reduction, and effluent storage or discharge [19].

Figure 4.4 is a block diagram of the complete experimental setup. The components are divided into six systems: oxygen, fuel, high-pressure (HP) water, low-pressure (LP) water, heaters, and the combustor itself. The oxygen, fuel, and HP water systems deliver controlled amounts of pressurized reagents to the combustor through the heaters. Heating is the last step before the combustor so that no equipment other than tube, tube fittings, and the combustor must be rated for supercritical conditions. Cooling is the step immediately after combustion for the same reason. Primary cooling is accomplished by the addition of ambient-temperature water in the dilution cooler section of the combustor. After depressurization, the effluent—no longer supercritical—separates into gas and liquid phases, which are then cooled. The gas is exhausted and the liquid is sent to a tank. Because the effluent is water prior to any fuel injection, the liquid can be filtered and recycled through the system during heat-up. The five peripheral systems—those other than the combustor—are discussed in detail in the following sections.

4.2.1 High-Pressure Water

The high-pressure water system supplies all water to the combustor. Since most of the fluid flowing through the combustor is water, it also controls the pressure. While previous SCW systems have used back pressure regulators (BPRs) located downstream of the reactors to control the pressure, this system uses a second BPR upstream of the combustor to allow for independent control of multiple water flow rates driven by a single pump.

The system is shown schematically in Fig. 4.5. Filtered water from the low-pressure water system flows to a positive-displacement pump. The pump is a 5000 psi triplex plunger pump marketed for pressure washing applications (General Pump T5050).
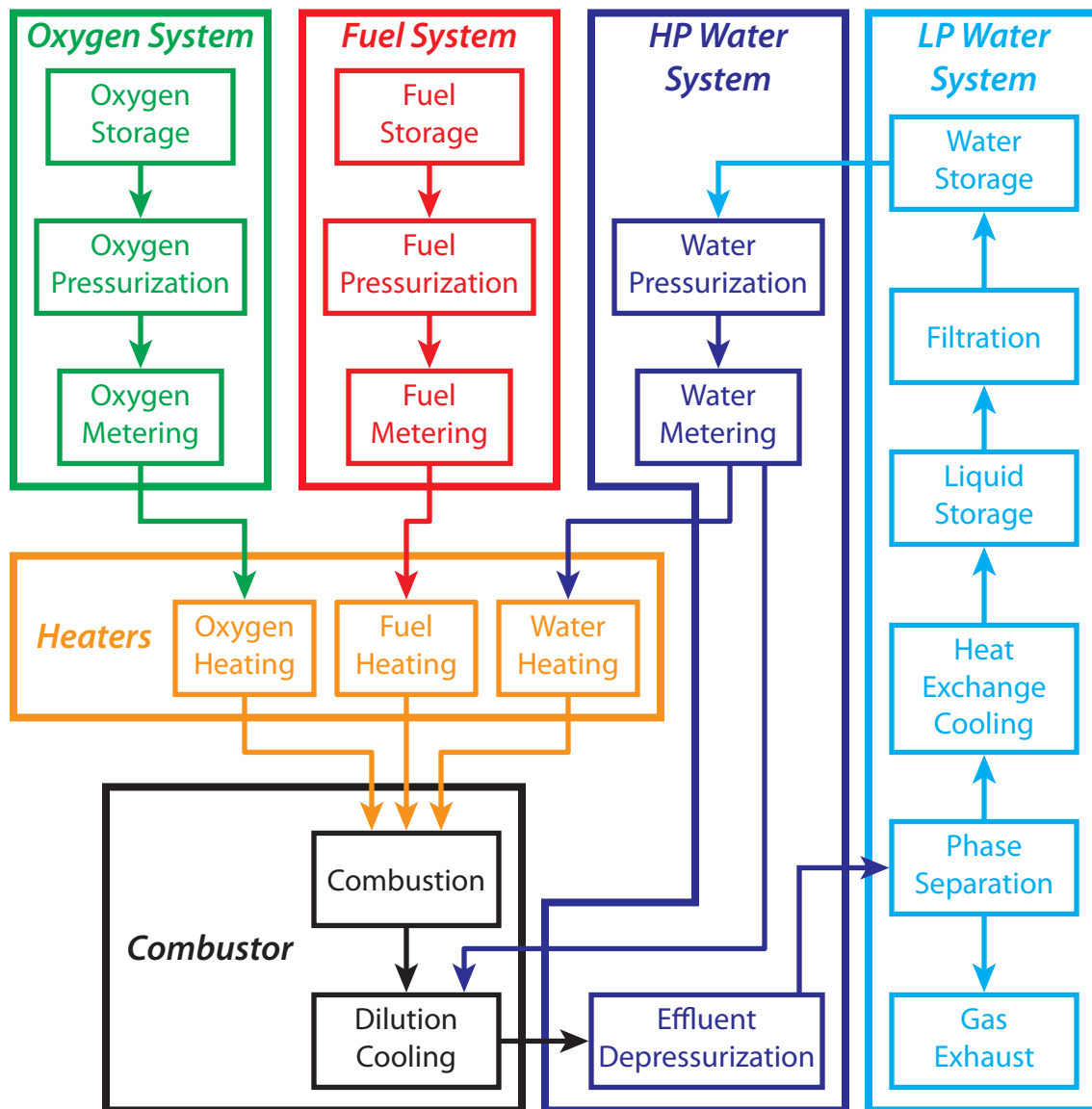
Figure 4.4: Block diagram of the experimental apparatus. The functions are divided into six systems. Oxygen, fuel, and high-pressure water systems deliver controlled flow rates of each pressurized reagent to the heaters. The heaters raise the temperature of these streams to near or above the critical temperature upstream of the combustor. The low-pressure water system conditions effluent water for reuse during heat-up.
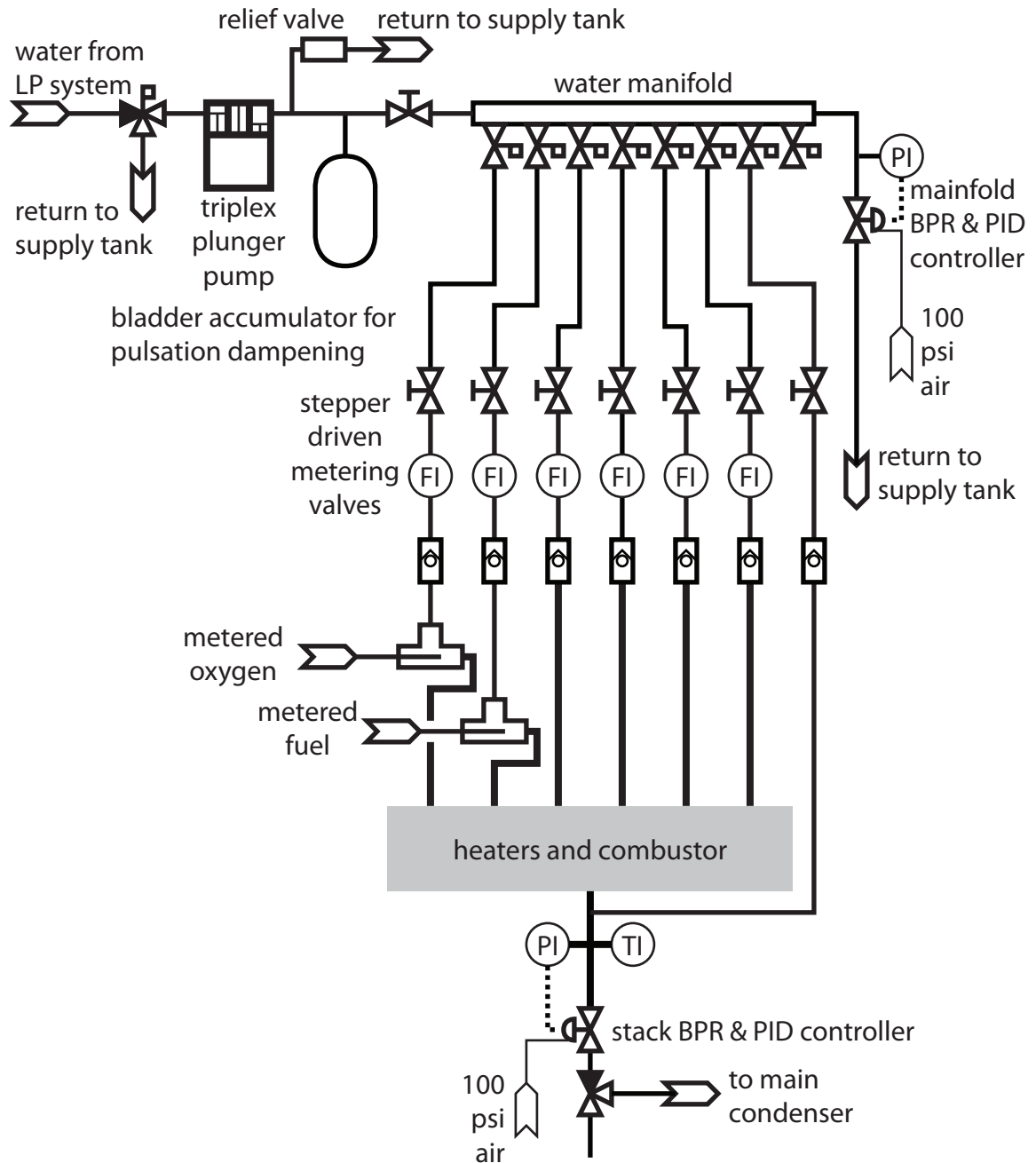
Figure 4.5: Schematic of the high-pressure water system.

Coupled to a variable-speed AC motor, its flow rate can be varied continuously from 1.4 to 5 gpm. A three-way valve just ahead of the pump allows the bleeding of air from the line to prime the pump. A relief valve at the pump outlet set to 5000 psi prevents overpressure and damage in case of flow blockage downstream. A 1-quart bladder accumulator dampens the pressure fluctuations caused by the pump. The capacitance of the accumulator combined with the resistance of a needle valve forms a tunable low-pass filter. Next, the water flows to a manifold, where the flow is distributed to seven lines. Six lines lead to the combustor: water for mixing with oxygen, water for mixing with fuel, burner water, liner water, window water, and finally dilution water for effluent cooling via dilution. A seventh line bypasses the combustor and is used for a second stage dilution cooling. Each of these outlets is equipped with a plug valve that may be used to isolate the line for testing or if it is not needed for a particular experiment. Another outlet connects to a back-pressure regulator (Tescom 54-2162Z28A), termed the manifold BPR. A pressure transducer (GP:50 342-E-RV-3 DA/FJ) and PID controller (Tescom ER3000SI-1) adjust the flow rate through the regulator so that the upstream pressure is close to the desired, set point value. Water exiting the BPR is returned directly to the supply tank in the LP system. The manifold BPR allows for control of manifold pressure independent of the flow rate though the lines leading to the combustor, provided that the pump supplies more water to the manifold than is demanded for the combustor.

Each line from the manifold flows through a needle valve for flow rate control. The valves were sized according to the calculated flow rates for each line. These valves operated by stepper motors for remote operation. To determine the flow rates, the lines connect to spur-gear flow meters. These operate as positive-displacement meters, but are intended for use with fluids more viscous than water. Lower viscosity fluids may slip past the gear teeth without turning the gears at the expected rate. Due to this possibility, the meters were tested with water at flow rates lower than what will be needed for operation of the experiment. The meters were verified to have linear output characteristics (a constant number of pulses per volume passed) over the range required when used with water. After the flow meters, the flows pass through check valves to prevent back flow, and are then sent through the heaters before injection into

the combustor. The connections from the heaters to the combustor are simple tubes and fittings covered with insulation. No control or instrumentation devices are present at this location because they would have to be rated for supercritical temperatures.

The single outlet from the combustor combines with the bypass dilution water to further reduce the temperature. The outflow then connects to a second BPR, known as the combustor BPR. This arrangement is similar to that of the manifold BPR, except that the pressure transducer (GP:50 342-E-RV-3 DA/FO) and BPR (Tescom 26-1762-28-314A) are rated for elevated temperatures. The controller is identical to the one for the manifold BPR, but is tuned independently. The flow exiting the BPR is sent to the condensers in the LP system for further cooling and phase separation. A three-way valve just after the BPR allows the flow to be diverted for testing purposes, primarily calibration of the spur-gear flow meters and qualitative verification of the flow.

This pumping and control strategy was inspired by that of Wellig at ETH [19]. In that system, only one BPR was used, downstream of the reactor. Multiple pumps were used, but still some lines were supplied by a common pump. Since the pump was positive-displacement, an adjustment of any metering valve affected the flow rates in all of the lines fed by the shared pump. This coupling of flow rates was more of a nuisance than a problem. Wellig coped by adjusting all of the valves and the pumping rate in concert until the desired flow rates were reached simultaneously in all of the lines.

Because of the desirable characteristics of good pressure control and manageable flow control in the ETH system, it was taken as inspiration for the present system. The primary improvement is the addition of the manifold BPR, which allows for independent flow rate control in each water line. With pressure control upstream (at the manifold) as well as downstream (after the combustor) of the metering valves, the adjustment of a valve alters the flow rate through only one line. (In practice, the opening or closing of a valve results in a temporary change in all of the flow rates while both BPRs adjust to return to the set-point pressures.)

4.2.2   Low-Pressure Water

The low-pressure water system filters incoming water, and cools and filters water returning from the combustor. The schematic is shown in Fig. 4.6. The water used in the experiment comes from the municipal water supply. It passes through a particulate filter and deionizer before going to the supply tank. This 400 gal. tank holds enough water for four hours of operation at a 50 kW firing rate. A submersible pump in the supply tank feeds a 5 gal. head tank. This tank ensures a steady supply to the high-pressure water pump.

Water and steam returning from the combustor BPR enters the shell side of a shell-and-tube heat exchanger. A P-trap arrangement keeps the condenser mostly full of liquid water for optimal effectiveness. A gas outlet from the top of the main condenser is connected to a residual condenser. The purpose of this second condenser is to cool the exhaust to near the available cooling water temperature. This step condenses more water from the exhaust gas in the system to reduce the amount of potential condensation in the exhaust line exiting the building. The tube sides of both condensers are supplied with 30 gpm of process cooling water at around 16°C. Condensate runs to the drain tank, which, like the supply tank, has a capacity of 400 gal.

The outlet of the drain tank can be sent through a pump to one of two places. If the water in the drain tank does not contain reaction products, it can be recycled through the deionizer and back to the supply tank. If it has been used, it is sent to the municipal sewer.

4.2.3   Fuel

Since the volume of fuel required is much less than the volume of water required, the fuel system uses a batch pressurization method that is nearly pulsation free. The central component is a bladder accumulator. These are normally used for capacitance in hydraulic systems—the pulsation dampener in the HP water system being a typical example. Here, it is a convenient off-the-shelf fluid system element in which one pressurized fluid can be used to pressurize another. It consists of a flexible, elastomer
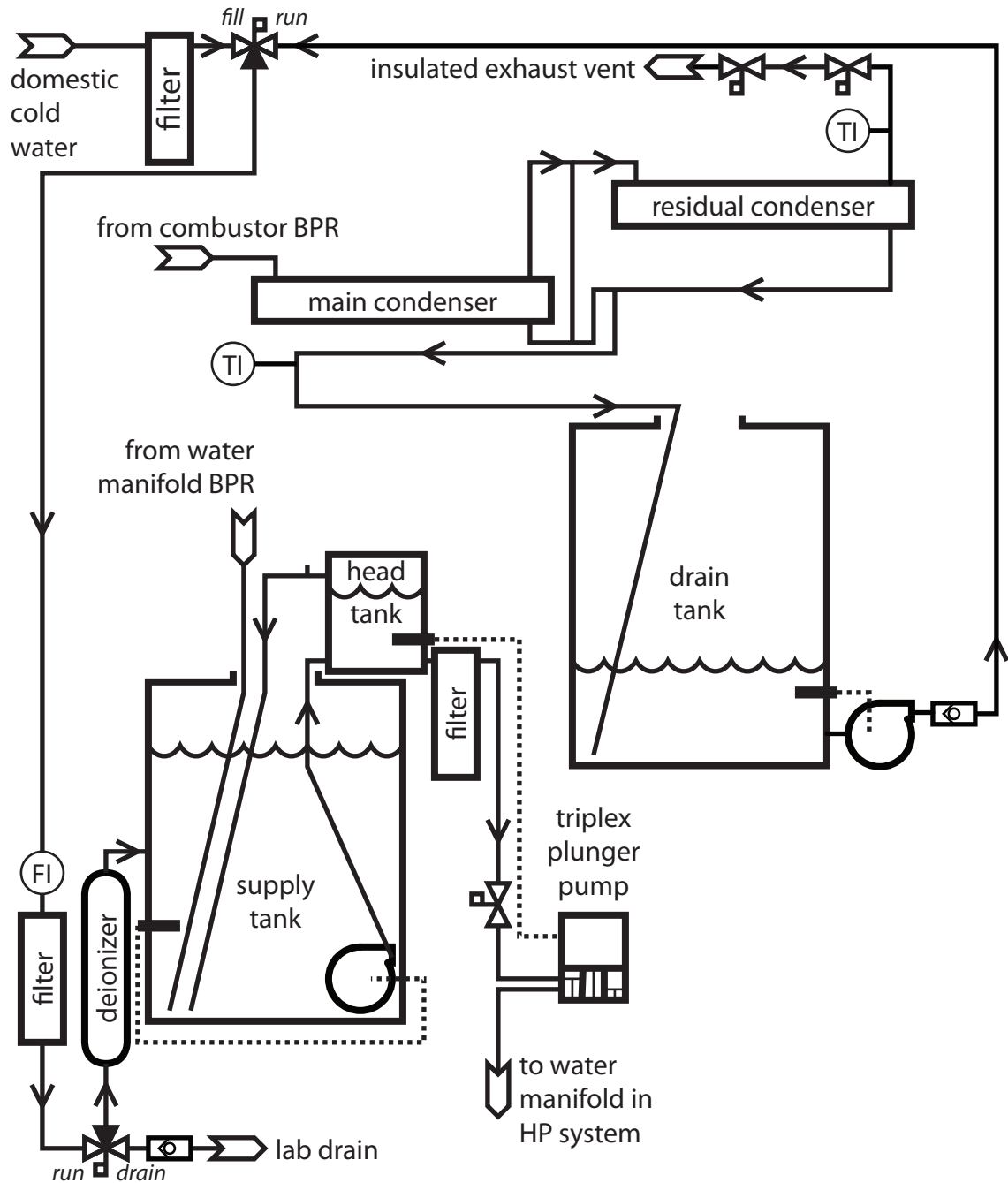
Figure 4.6: Schematic of the low-pressure water system.

bladder inside a steel shell rated to 6000 psi. The space between the bladder and the shell is filled with the fluid to be pressurized (in this case, fuel). The inside of the bladder is pressurized with nitrogen and expands, pressurizing the fluid to an equal pressure. Nitrogen is used rather than air to avoid the possibility of creating a combustible mixture inside the vessel if either fluid leaks past or permeates the bladder.

The fuel system is shown schematically in Fig. 4.7. Prior to operating the combustor, the accumulator is filled by pumping fuel from a drum in a fuel storage room through a filter. The gas side of the bladder is open to atmosphere via a bleed valve during filling. Once filled, the gas side is connected to a high-pressure nitrogen supply, and the valve on the liquid side is turned towards the combustor. Standard nitrogen cylinders cannot be used alone for the nitrogen supply since they are charged to 2200 psi—less than the operating pressure of the combustor. 6000 psi cylinders are available, but they are more expensive, and less than half of each bottle could be used to pressurize fuel. Instead, a two-stage piston booster pump (Haskel AGT-30/75) is used to increase the pressure of nitrogen from a six-pack of standard-pressure cylinders. The pump is driven with compressed air at 150 psi, the flow of which is controlled remotely with a solenoid valve. The booster is also governed by an air-pilot switch. This is needed since the stall pressure of the booster (a function of the gas supply and drive air supply pressures and pump geometry) is above the maximum pressure rating of downstream components. The air-pilot switch stops the pump when the pressure at its outlet surpasses a set point, which in this case has been adjusted to 5000 psi. The switch automatically starts and stops the booster as needed to maintain downstream pressure. The outlet of the booster flows through a 1/2 in. tube acting as a small accumulator, then though a single-stage regulator. The set-point of the regulator controls the pressure in the bladder accumulator.

The fluid outlet of the accumulator is connected to a normally-closed direct-acting solenoid valve (Circle Seal Controls). This valve provides a method of positive shut-off in case of an emergency. It is also used in normal operation to completely stop the flow of fuel when flow is unwanted. The rest of the fuel system is the same as the HP water system. With upstream pressure in the bladder controlled by the nitrogen regulator
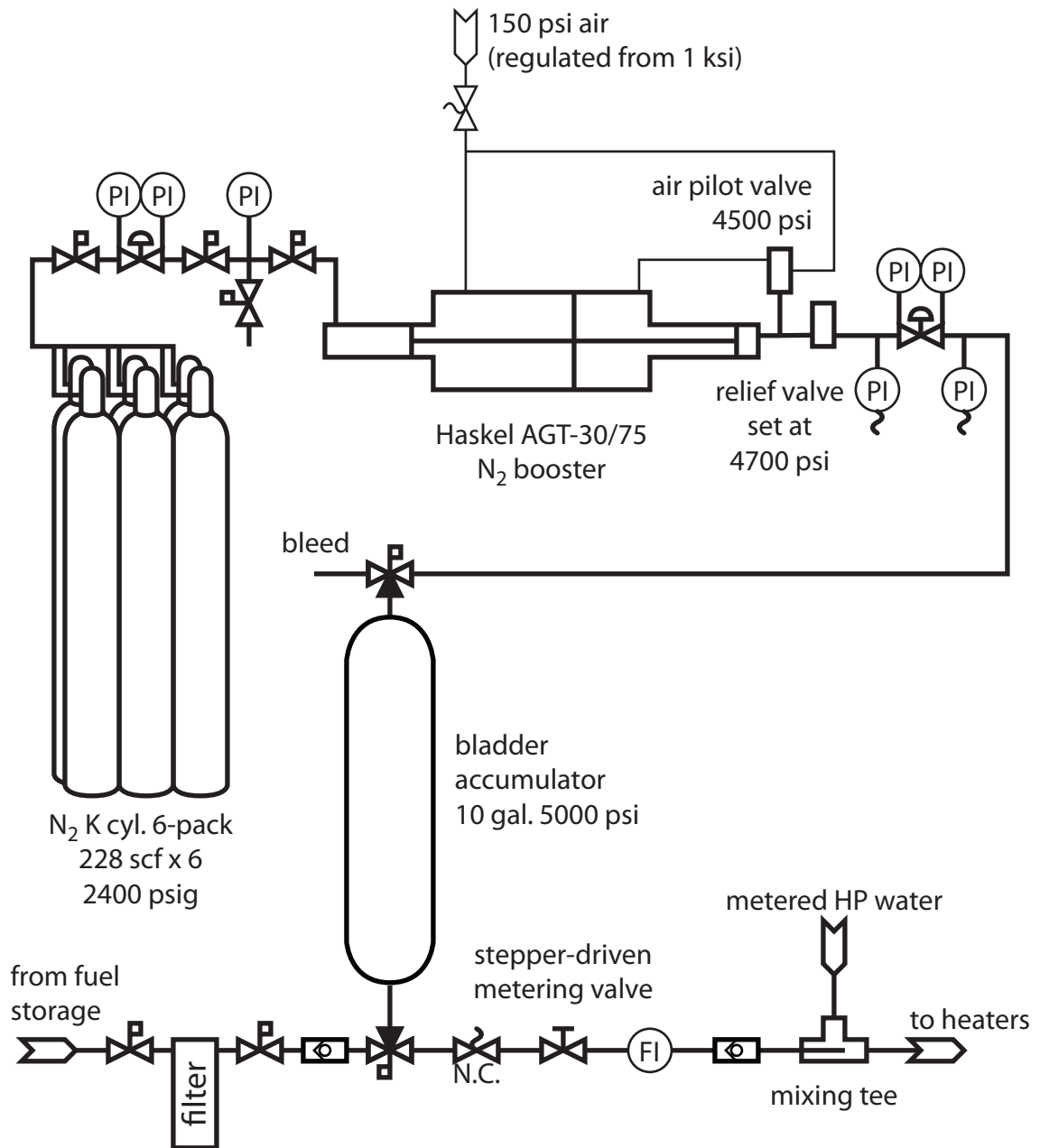
Figure 4.7: Schematic of the liquid fuel system.

and downstream pressure controlled by the combustor BPR, the flow rate is adjusted with a stepper-motor-driven metering valve. A spur-gear flow meter calibrated with fuel measures the flow rate, and a check valve prevents back-flow. After the check valve, the fuel mixes with the fuel water stream in a mixing tee. In this tee, the fuel is introduced to the water flow as a central, turbulent jet to promote rapid mixing. The end of the fuel tube in the tee has a small orifice so that the Reynolds number of the jet will be high enough to create turbulence even at the lowest fuel flow rates desired. The flow passes through a heater before flowing to the combustor.

4.2.4   Oxygen

While liquid species are easier to pressurize and meter, oxygen was chosen as the oxidizer since it would be used in a full-scale plant. One six-pack of cylinders contains enough oxygen for four hours of operation at 50 kW. The six-pack is kept in a separate room for gas cylinders so that a large amount of oxygen is not adjacent to other equipment. The oxygen is regulated to 700 psi and piped to the lab. The supply line is fitted with two direct-acting solenoid valves. One is a normally-closed valve to provide positive shut-off of the oxygen supply in case of an emergency. The other is a normally-open valve on a bleed line. The long supply line to the lab has an internal volume of 360 mL, meaning that a significant volume of oxygen is accessible even if the normally-closed valve is shut. The bleed valve is usually kept energized (closed), but will be opened in case of emergency to vent the supply line. A normally-open valve was chosen so that this will happen automatically in the event of power failure.

Once it reaches the lab, the oxygen is pressurized by a booster pump (Haskel AGT-32/62) similar to the one used for nitrogen in the fuel system. It is also fitted with an air-pilot switch and relief valve. As the booster is not a steady-flow device, it supplies oxygen to a 20 in.^{3} plenum (Haskel). The plenum is intended to provide a nearly-constant input pressure to the regulator while the booster is cycling. The outlet of the regulator is connected to a stepper-motor-driven metering valve. Next is a counterflow, coaxial cooling jacket. This ensures that the gas enters the flow rate measurement setup at a constant temperature. A common method for metering the
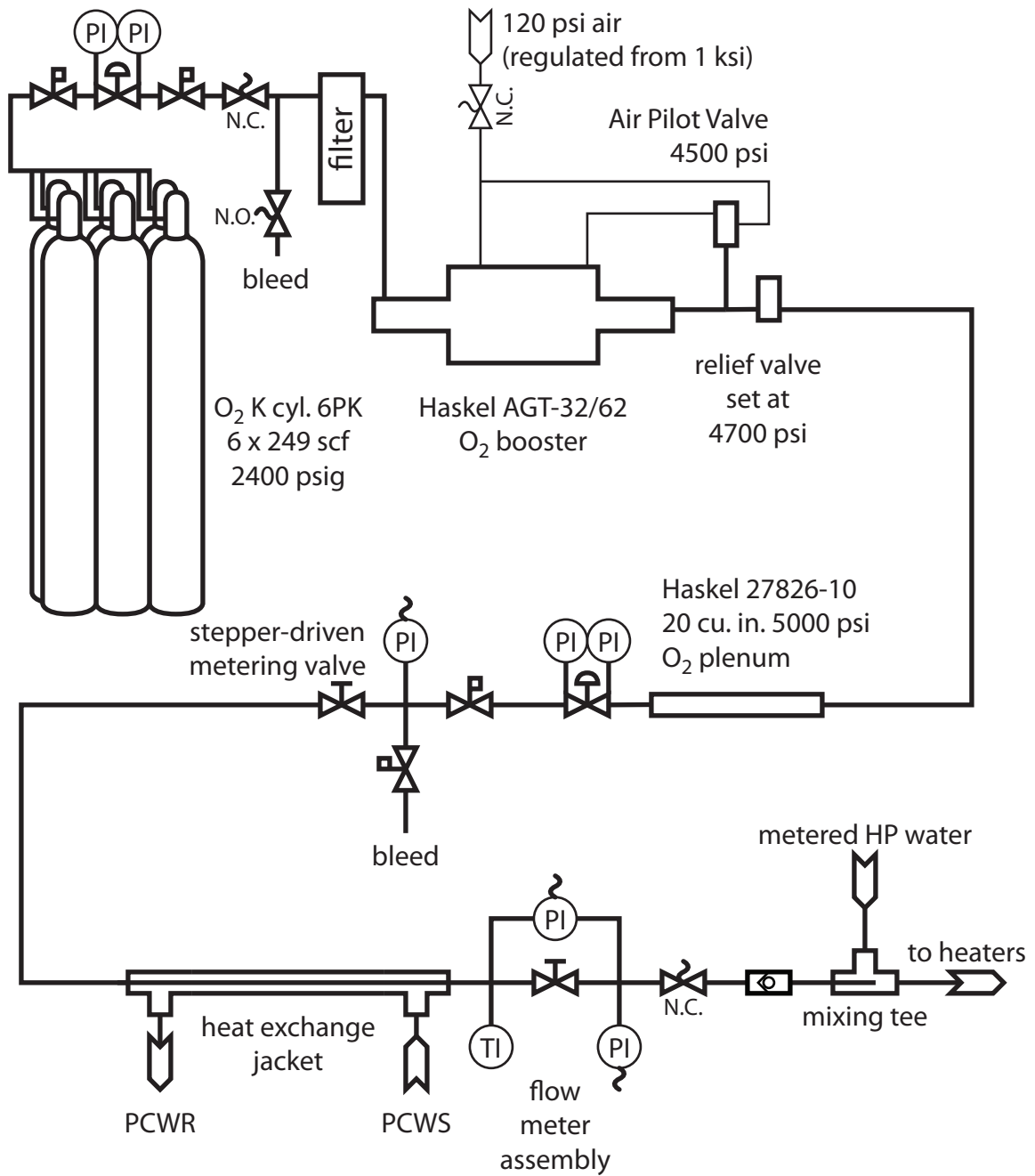
Figure 4.8: Schematic of the oxygen system.

flow of a gas is to use a choked orifice. However, since this apparatus requires gas supplied to the combustor at 250 bar, the upstream pressure required to created a choked flow would be 500 bar. This method was ruled out since oxygen should not be used above 5000 psi (345 bar). Another common method of measuring gas flow rates is a laminar flow element (LFE) in parallel with a differential pressure transducer. The absolute pressure and flow rates required for this experiment are not conducive to use of any off-the-shelf LFEs, so a needle valve (Swagelok SS-31RS4-SC11) is used to create a pressure drop. This valve is not stepper controlled; it is set to an appropriate flow coefficient before calibration and subsequently not adjusted. A 0–30 psid differential pressure transducer with a static pressure rating of 10,000 psia is used (GP:50 315-C-PT CJ-GL-HM). A thermocouple is installed upstream of this combination so that a correction may be made for varying gas density with temperature. This correction should be small due to the use of the heat exchange jacket, but it is included since the process cooling water temperature varies daily.

The differential transducer outputs a 4–20 mA signal. The signal at 0 psid is not always 4 mA, but varies with the absolute pressure. A calibration was performed to correct for this zero-shift with pressure. The calibration takes the form of a linear fit for signal versus static pressure. The behavior of the signal versus static pressure justifies a linear fit in the operating region of interest (3500–3750 psia), though it is quite non-linear outside this range. As a result the calculated oxygen mass flow rate is only valid once this part of the oxygen system is raised to the operating pressure.

Once the system was calibrated to account for the effect of static pressure on the sensor element, it was calibrated to find oxygen flow rate. A constant C_v of the metering valve and a square-root dependance on pressure drop were assumed.[3] Since the pressure drop across the valve is small relative to the absolute pressure (maximum 30 psid compared to 3600 psia), constant density was assumed. A linear fit was performed on the flow rate versus the square root of signal. For this procedure the combustor BPR was dried out and relocated to the output of the solenoid valve. A dry test meter (American Meter DTM-300A) connected to the output of the BPR was used as a flow rate reference. Both of these calibrations were performed using

---

[3]Unlike the linear relationship between flow rate and pressure drop for an LFE.

nitrogen. A correction was applied for the difference in molecular mass. No correction has been applied for the difference in viscosity since it would be smaller than the present accuracy of the measurement system; despite the presence of the plenum, the unsteady output from the booster causes flow rate variations that are difficult to average.

Downstream of the flow measurement setup, the flow passes through a direct-acting solenoid valve of the same type found in the fuel system. It serves the same purpose as in the fuel system, namely, positive shut-off in an emergency. However, it is not used for routine oxygen shut-off since a large flow rate resulting from re-opening with unequal pressures across it can result in a differential pressure large enough to damage the flow measurement transducer. The oxygen then goes through a mixing tee similar to that in the fuel system (only without the small orifice to force the formation of a turbulent jet). The water and oxygen stream goes through the heaters and to the combustor.

Oxygen Safety

All assembled components in the oxygen system were ordered SC-11 cleaned. All tube and tube fittings used were new and were rinsed in sequence with acetone, ethanol, Alconox, and deionized water, then blown dry with bottled nitrogen. The system is pressurized as slowly as practicable. Manual valves are opened by cracking them slightly and allowing pressures to equalize before opening them fully.

4.3   Heaters

Heating of fluids upstream of the combustor is accomplished with custom heaters. Each of two identical units contains six 6-kW electric-resistance cartridge heaters (Chromalox Maxi-Zone) and twelve 1/4 in. Inconel 625 fluid tubes. These components are housed in a cast aluminum block that conducts thermal energy from the electric cartridges to the fluid tubes.

The combined 72 kW heating capacity was chosen so the combustor could be operated with a 50 kW firing rate and 1600 K adiabatic flame temperature. The

heater cartridges' maximum power ratings are specified in terms of power per unit surface area. Their diameter is 0.990 in., but they are available in arbitrary lengths. It was decided that, in a balance between having a few long cartridges or many short cartridges, twelve 40-in. cartridges would be convenient. However, an aspect ratio of 40 made it less practical to drill holes to accept the cartridges. The alternative was to cast the aluminum filler around the heaters and fluid tubes.

The heaters are 5 in. OD by 40 in. long, each containing twelve fluid tubes and six heater cartridges. The need to fixture all of these parts during casting makes mold casting impractical. Instead, a steel shell was used. Each end of the shell was fitted with a header plate. The headers have holes for the fluid tubes and thin sleeves for the cartridges. Placing the cartridges in sleeves protects them from direct contact with molten metal during casting, and may allow for removal and replacement, if necessary. With all of the tubes, sleeves, and cartridges inserted, A206 aluminum alloy was poured through holes in the shell. The completed heater units are shown without insulation in Fig. 4.9.

Flow through a single fluid tube would not provide enough residence time to heat most of the streams from ambient to supercritical temperatures. In these cases, multiple fluid tubes are linked externally to provide a sufficiently long heated passage. Convective heat transfer calculations were performed to determine the number of passes required for each stream.

Heater temperatures are regulated by self-tuning PID controllers, one per unit. The heaters must be operated cautiously as the melting point of pure aluminum is 660°C. The cartridges can easily exceed this temperature if powered continuously, so the control system has been programmed to not allow a set point over 600°C. Also, the feedback thermocouples are located in the core of one of the six cartridges in each unit so that the controllers are responding to the highest temperatures present in each assembly.

Figure 4.9: Photograph of the completed heater units before installation. Aluminum filler is visible through four casting holes on the top of each shell. Each unit has twelve 1/4 in. Inconel 625 tubes to carry the fluids being heated, and six 6-kW electric cartridge heaters.

4.4 Control & Data Acquisition Systems

The experiment is controlled from a separate room through a combination of stand-alone controllers and a MATLAB/Simulink/xPCTarget system. Digital outputs on a National Instruments board (PIC-DIO-96) are used to generate square wave pulses to drive the stepper motors. The two heaters are independently controlled by two self-tuning PID controllers. The set points of these controllers are each adjusted with a voltage signal from an analog output card (National Instruments 6229). The BPRs are also controlled with PID controllers. These units are connected to a PC via

RS-485. Their set points and gains are adjusted manually using software provided by the manufacturer. The same program also displays a plot of the pressure, sampled at 40 Hz. All solenoid valves and the two LP water pumps are controlled from a switch panel adjacent to the control computer. The HP water pump motor drive is controlled through a remote keypad mounted on the same panel.

Data acquisition is through the same xPCTarget system. All pressure transducers use current signalling (4–20 mA) for reduced noise. The current loop from each transducer runs through a resistor across an analog input. The water and fuel flow meters output square, 12 V pulses, which are read as digital inputs. Since xPCTarget is a real-time system, the time of each pulse is recorded. The pulse signals are sampled at 1 kHz to prevent aliasing and allow accurate calculation of the flow rates. The computer also has a 16-channel thermocouple card (Measurement Computing PCI-DAS-TC). Because the thermal inertia of the thermocouple probes act as low-pass filters, the temperature readings are sampled at only 1 Hz.

Chapter 5

Initial Operating Experience

Since it was a newly-built system, the experimental setup described in Ch. 4 required extensive testing and some modifications when first put into operation. Much of this debugging was similar to what might occur in any fluid system. However, the experiences with two elements of the system merit discussion: those with seals and windows. While most components were placed upstream of the heaters to avoid contact with supercritical water, seals and windows must be placed in the combustor. With them, the challenge of withstanding that harsh environment must be met. Once problems with seals and windows were addressed, combustion experiments began. As a starting point, the autoignition results of Steeper and Wellig were replicated. These are a first step toward operating at conditions appropriate for a SCWO/IFCC power plant.

5.1   Seals

Leaks from the combustor were the major source of delays to running flame experiments. To understand the problems encountered with the metal c-seals used in the assembly, it is important to understand how they are intended to function. The c-seal is one of several types of metal seals that mimics the behavior of an elastomer o-ring by virtue of its geometry. In typical applications, an o-ring is seated in a groove in one of two mating parts; the thickness of the uncompressed o-ring is greater than the

depth of this groove. Assembly of the mating parts compresses the seal (Fig. 5.1a). This preloading forces the o-ring to deform and fill surface asperities in the glands, closing any leak paths. When the system is pressurized (Fig. 5.1b), the fluid presses the o-ring against the outer wall of the groove (for internally pressurized applications). Since the o-ring is then constrained, further increase of fluid pressure increases the pressure of the o-ring against the glands, due to the effect of Poisson's ratio. Since the seal is energized by the fluid being contained, the quality of the seal increases with the driving force for leakage.

(a) after
compression

(b) compressed,
system pressurized
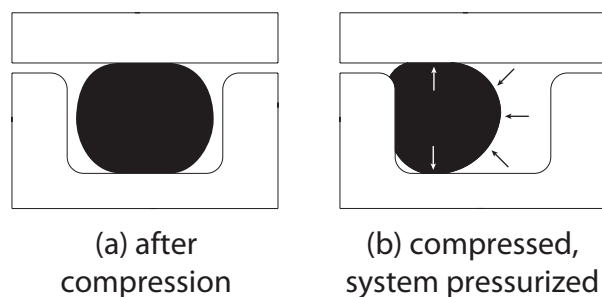
Figure 5.1: Cartoon of an o-ring (a) after installation and (b) when the right side of the system is pressurized. Adapted from [33].

When elastomers cannot withstand the working environment, as with supercritical water, metal seals may be used. If a solid metal o-ring was substituted for an elastomer o-ring of the same dimensions, it would be far too stiff to deform as desired under preload. Often, the yield stress would be exceed in all parts involved, damaging the glands. A solution is to change the cross-section of the seal, so that while made of a stiff material, the overall part will have a stiffness more like that of an elastomer o-ring. As with elastomer o-rings, the height of the uncompressed c-seal is greater than the depth of the groove (Fig. 5.2a). The thickness and shape of the c-seal controls its macroscopic stiffness; they are chosen such that when the seal is compressed to the depth of the groove (Fig. 5.2b), the resulting stress in the seal applies an appropriate force where the seal contacts the glands. Unlike the case with elastomer o-rings, this preload will not be enough to deform the seal to fill asperities. Nevertheless, depending on surface finishes of the c-seal and glands, the resulting seal may be adequate for

some uses, such as liquid service at moderate temperatures. For more demanding applications, such as with gases or supercritical water, the c-seal may be covered with a thin layer of soft metal, such as silver. This layer provides material than can fill asperities without requiring a stress high enough to damage the glands. Finally, when the system is pressurized, the "c" shape of the cross-section allows fluid pressure to directly contribute to the load at the sealing surfaces. With a proper shape and combination of metals, c-seals behave similarly to elastomer o-rings; they deform under preload to close leak paths, and the seal is further energized by fluid pressure.

(a) before
compression

(b) compressed,
system pressurized
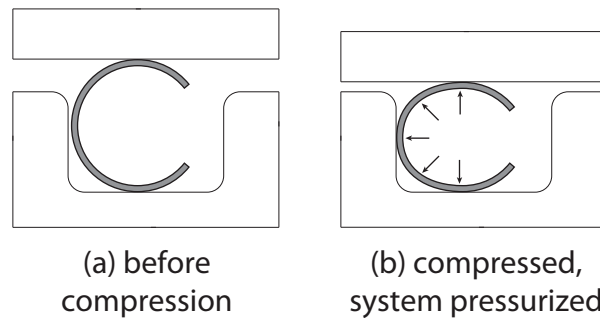
Figure 5.2: Cartoon of a positioned metal c-seal (a) before and (b) after compression.

While the analogy between metal and elastomer rings portrays c-seals as a direct replacement for o-rings in severe environments, a higher standard of engineering must be used in the design and fabrication of the parts surrounding the seal. Closer attention must be given to dimensional tolerances, parallelism, waviness, lay of finish (the direction of tool marks or polishing scratches), and surface roughness of the groove. The size and materials of the c-seals were chosen for this specific application in consultation with the seal manufacturer (Jetseal, Inc.). The material is Inconel 718 with 0.0010–0.0015 in. silver electroplate. Additionally, there is a thin gold underlay to improve adherence of the silver and prevent formation of oxides of silver and nickel (from the Inconel) at high temperatures. Recommendations from Jetseal for seat surface finish were included as specifications on the combustor drawings sent for fabrication.

After installation of the combustor, it was checked for leak tightness at the nominal operating pressure of 250 bar. The nine c-seal locations in the assembly fall into three

classes: four loaded by a traditional bolt circle in the burner inlet section, three where one side of the seal seats against a window, and two in the clamped joints joining the three major sections. Initially, all types experienced leaks. By visual inspection (unaided and with $10\times$ magnification), it was judged that the surface roughness of many of the seal seats did not meet the specification. Not only was it questionably less than 16 μin. Ra, there were visible scratches in the radial direction crossing the sealing line. In response, a series of laps was cut to fit the various groove sizes, and all seats were lapped with 600 and 1200 grit lapping compound. The resulting finishes were free of visible defects under $10\times$ magnification, with an estimated roughness less than 2 μin. This careful dressing of the sealing surfaces improved the sealing of the burner inlet area and windows, but significant leaks remained at the clamped joints. Attention was turned to the functioning of these joints.

The clamps depend on an interference fit between the angled faces on the clamp halves and the vessel sections. When the bolts connecting the clamp halves are tightened, the halves draw together, wedging the vessel sections towards each other. The angled contact surfaces were visibly wavy, possibly preventing the clamps from closing properly and reducing the clamping force generated. Since c-seals cannot tolerate much gland separation, this defect left the possibility of leak paths opening after pressurization. The angled faces of the clamps and vessel were sanded to remove visible waviness. In subsequent assembly, the separation between the clamps is measured to check that they are drawing together by the correct amount in accordance with the specified bolt torque. Even with these alterations, significant leaks remained, even at ambient temperature. With seat finish and preload eliminated as causes, the c-seals themselves came under further scrutiny.

Figure 5.3 is a photograph of an unused seal. The silver plating is not smooth, but has a pitted texture loosely resembling the cratered surface of the Moon. Since the silver is soft, many of the pits are filled in when the seal is installed. The largest (like the one circled) create leaks, as shown in Fig. 5.4. These photographs are of different locations on a seal, but the series illustrates the development of a leak. In each picture, the dark band on the seal is the portion of silver that was pressed flat by contact with the seats. Pits visible within these bands were too large to be smoothed by the

yielding silver. In the center of the top picture there are three pits close together. Here, there was not enough silver to close the leak path. The brown discoloration is evidence that a small amount of leakage occured. The middle photo shows a more substantial leak. There is a clear channel through the silver layer across the sealing line. Once a leak begins, the water passing through the channel erodes the silver, widening the channel and increasing the leak rate. The eventual result is shown in the bottom photo. After about 20 minutes of leakage, the thickness of the silver has been completely removed, exposing the Inconel substrate. While defects like the one in the top photo might result in a slow, tolerable leak, these small leaks eventually grow from drips to continuous streams.
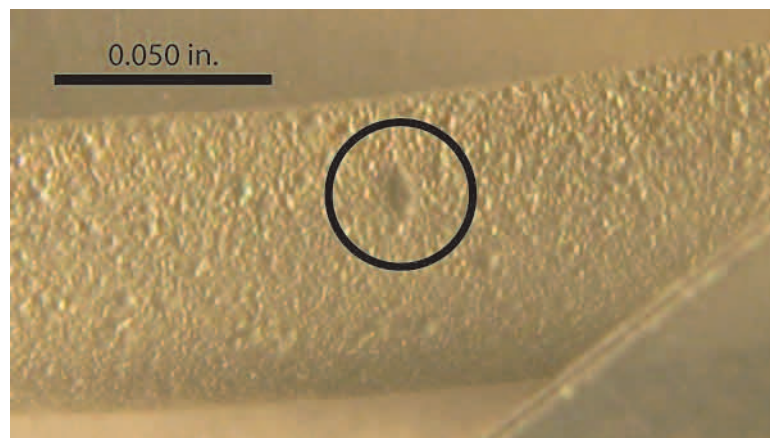
Figure 5.3: Unused seal showing "moon craters" surface finish. The circled defect, given its size and location on the seal, would likely have caused a leak if this seal had been installed.

After trials with multiple fresh c-seals, discussions with the manufacturer revealed that the "moon crater" effect silver plating should not have passed quality control. A second batch of seals was received with silver plating meeting specifications, exhibiting a smoother finish termed "orange peel" by the manufacurer. At the same time, two procedural improvements were made. Before installation, the c-seals are covered with a small amount of vacuum grease. This layer protects the silver plating from scratching during assembly. Also, when the system is pressurized, the pressure is increased as fast as possible from atmospheric to 210 bar. Because of a small volume
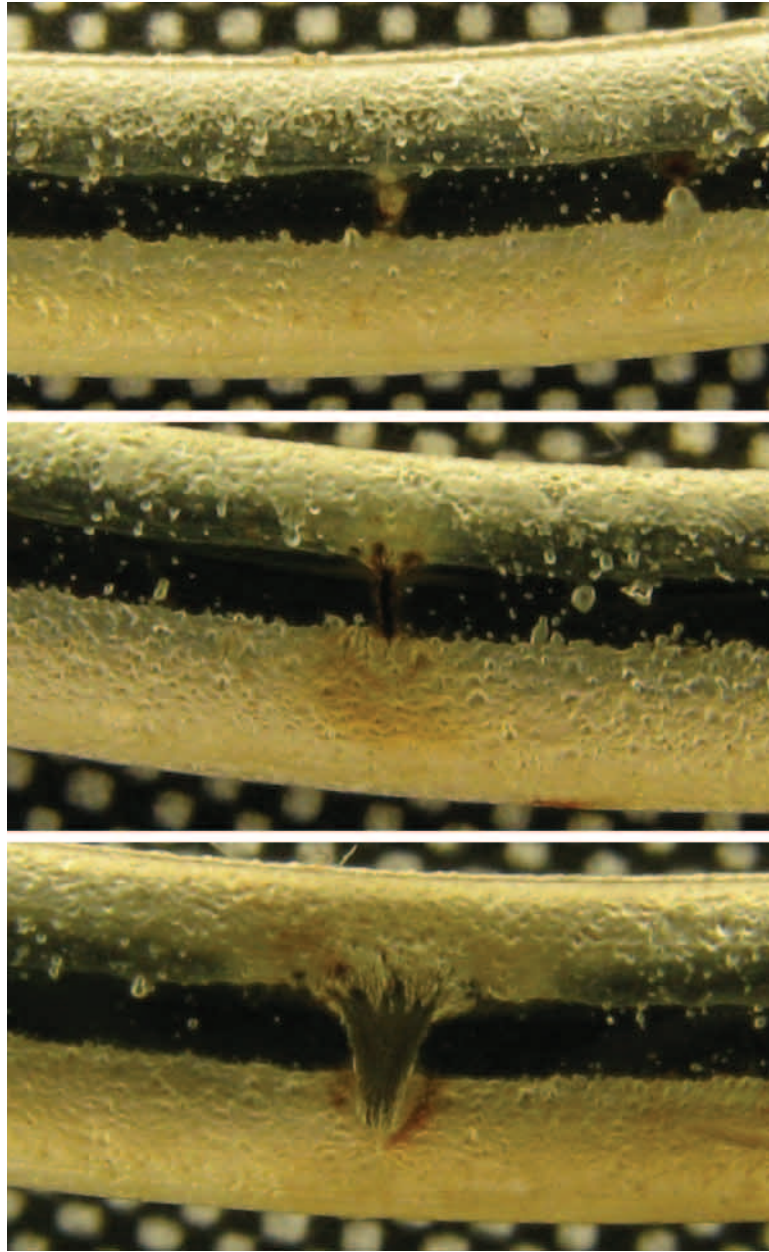
Figure 5.4: Progression of a leak. The background is a 0.005 in. checkerboard for scale.

of trapped gas that cannot readily be bled from the system, this pressure rise takes approximately 2 seconds. It is believed that this procedure seats the seal in place quickly, deforming the silver to fill voids before water has an opportunity to form a leak path. The seal manufacturer recommended a rapid increase to 35 bar, but 210 bar has greatly increased the success rate of forming good seals. With these procedures, smoother silver plating, and lapped seal seats, the success rate is approaching the 90% value quoted by the manufacturer. The four c-seals in the burner inlet section were installed, removed, and reinstalled, and continue to seal after many pressurization cycles including several heating and cooling cycles.

Before the flaw with the original silver plating was discovered, other sealing methods were sought for the clamped joints. While the other joints could be sealed with the faulty c-seals (albeit unreliably), the clamped joints were a continued source of rapidly-forming, large leaks. Operating on the theory that increased pressure at the seats could result in an effective seal, a ring seal was made having a solid cross section with a raised point on each side (Fig. 5.5). This seal had a diameter and height such that it would fit in place of a c-seal. The height of this seal at its inner diameter matched the size of the c-seal gland (0.075 in.), but the raised points were taller than the gland height such that they were crushed during installation. It was thought that having pressure on the seal surfaces high enough to yield stainless steel or Inconel would provide a reliable seal. In fact, one such seal in each of stainless steel and Inconel did seal at room temperature and during heat-up of the pressure vessel. However, both leaked dramatically during cool-down. It is believed that this behavior is due to thermal expansion. During heat-up, the ring—in contact with preheated water—is likely warmer than the surrounding vessel. Hence, thermal expansion keeps a positive load on the sealing surfaces. During cool-down, the opposite thermal gradient is present, contracting the ring faster than the vessel. This action unloads the seal and opens a leak path. Once these seals leaked, they would not re-seal. Either the ring had yielded to a size smaller than the gland, or the gland had been enlarged by the warmer ring during heat-up, or both.

Although a failure, the solid ring seals demonstrated that a seal could be made by applying sufficient stress to mating surfaces. They failed due to a lack of resilience in
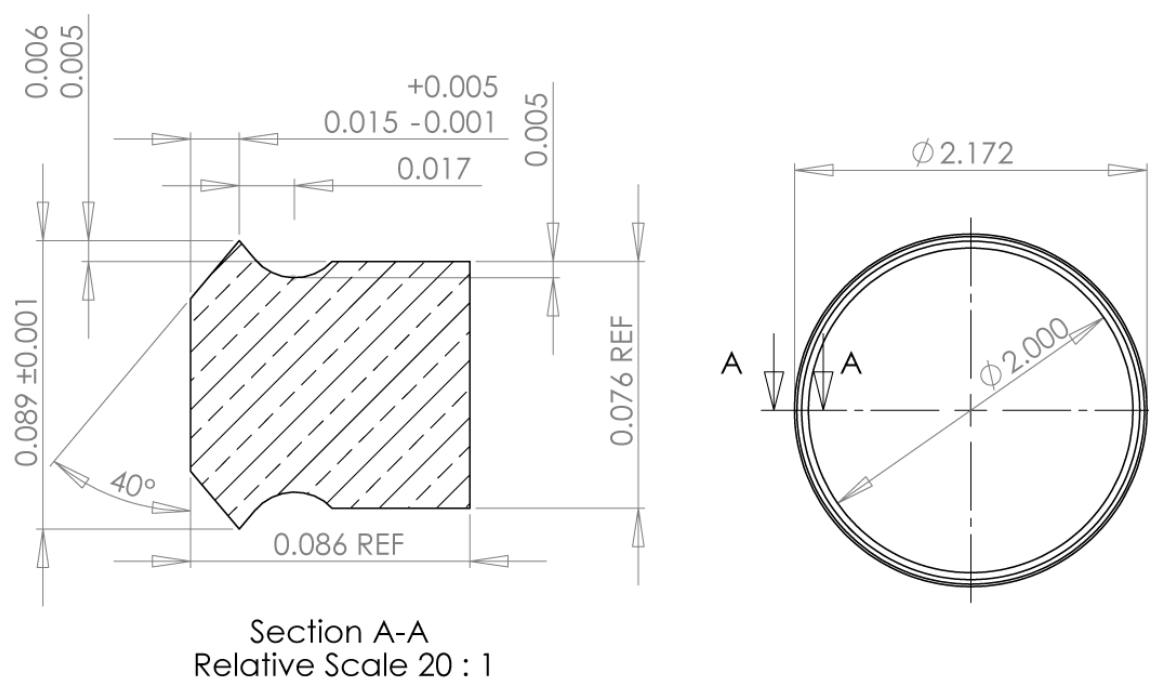
Figure 5.5: Design of pointed seal ring.

the assembly. Although the clamps themselves behave elastically, once the mating surfaces of the two parts of the vessel are touching, there is nothing except fluid pressure to act on the seal. A seal placed between the large, formerly-mating surfaces, rather than in the gland, could remain loaded by the clamps at all times since it would hold the vessel sections apart. However, such a seal would have to be quite thin to not have an adverse affect on the operation of the clamps. This is because the clamps are designed to interfere with the flanges, and too much interference will cause them to not load properly, or will prevent assembly entirely.

After an attempt with aluminum foil, gasket seals were fabricated from 0.008 in. fully-annealed copper sheet. One such seal is shown in Fig. 5.6, ready for installation. The inner diameter is slightly smaller than the outer diameter of the gland, but is larger than the combustor and cooler liners so as not to block the fluid flow in the annulus outside the liner. Three locating tabs that do reach the outer diameter of the liner keep the gasket centered during assembly. The outer diameter of the gasket is large enough that the gaskets are strong enough to be handled easily without damage,

but small enough that a pressure exceeding the yield stress of annealed copper is generated by the clamps. Based on analysis of the clamped joint and impressions on pressure-sensitive film, a pressure of about 30,000 psi is applied to the gasket. Removed gaskets show complete impressions of machining marks from the adjacent Inconel surfaces. This design of copper gasket has proven successful in sealing the vessel during both heat-up and cool-down.

Figure 5.6: Copper gasket before installation.

5.2 Windows

The sapphire windows are a key feature of the combustor. They were included as the primary diagnostic technique since direct observation is the most straightforward method of assessing the flow field, especially when turbulent; the use of velocity probes in the flow would be difficult due to the environment. However, their inclusion comes at a price. Because they are made of a brittle material, the yield criterion must never be exceeded at any location. To this end, the design used a large safety factor of six, soft copper seats to reduce stress concentrations, and a mandated bolt torque to reduce the chance of failure. At ambient temperature, the windows have withstood

the full pressure the system can apply (5000 psi), and fast pressure transients. Even steady-state thermal loads are not a problem; due to differences in the coefficients of thermal expansion of sapphire and the surrounding parts, the load on the windows actually decreases if the assembly is heated isothermally. The real difficulty is with stresses from thermal transients. One method of limiting thermal stresses on windows in a heated apparatus is to keep the thermal gradients away from the windows. This approach is used by Príkopský [20]. Another is to raise and lower the temperature slowly. This approach was taken by Serikawa [34] and is the one used here.

The driver of temperature in the window is the water flowing in the combustor. The greatest temperature gradient and hence the greatest stresses are found at the inside surfaces of the windows. The temperature of the inlet water must not be adjusted too quickly. Since the temperature is controlled by the heaters, and there is ∼2 m of tubing between the heaters and the combustor that smooth fluctuations, the heater set points can be adjusted in reasonable steps without consequence. Still, the heaters must be adjusted upwards in accordance with the overall rate of temperature rise in the windows. As a proxy for the maximum temperature gradient, the temperature was monitored on the outside wall of the vessel and this value compared to the water temperature. During the first few heated runs, the heater temperatures were increased in 50 K increments every 15 minutes or when the temperature difference was less than 50 K, whichever was longer. This protocol was used a few times without incident, until one window shattered with no indication of any other abnormal conditions in the system. Although the chosen rate of temperature rise did not cause a failure the first few times, it was decided to switch to a more conservative strategy and that metal blanks should be used in place of windows for the first combustion experiments.

After performing the two successful combustion runs with blanks in all three locations, another attempt was made to obtain a visible flame. This entailed reinstalling a single window. (Without an optical path all the way through the combustor, the flame would need to be luminous to be visible.) With better knowledge of how to make metal seals function, the window was installed with the bolts at the original torque specification. A slower heat-up protocol was implemented. The two heater controller set points were increased by 2 K after 2 minutes and then by 3 K after

the next 2 minutes. This pattern was repeated, resulting in an approximately 8 hour heating time during which the temperature difference across the window was not more than 40 K. The combustor inlet streams were nearly at the desired temperatures for fuel and oxygen injection when a failure unrelated to the window occurred.

The piston seat in the BPR is made of Vespel, a high-performance polyimide polymer from Dupont. According to Dupont, Vespel is subject to hydrolysis, which may result in the failure of parts after prolonged exposure to water or steam above 373 K. In spite of this warning, Tescom rated the BPR as a whole to a considerably higher temperature. To conserve dilution cooling water (which is used once-through from the supply tank and cannot be replenished during an experiment), the combustor BPR inlet temperature was allowed to rise to 400 K. After $\sim$3 hours at that condition, the Vespel seat degraded such that the BPR could not close sufficiently to maintain the backpressure near 250 bar. When this occurred, the flow rates increased. With the water flow rates increased, the flows no longer had sufficient residence time in the heaters to reach the previously established outlet temperatures, and the temperatures of the inlet stream decreased rapidly. Of particular interest with respect to the window, the burner water temperature decreased, leading the temperature at the inside of the window to drop by 130 K in 38 seconds. The resultant, very large thermal gradient near the inside face of the window is thought to have caused the window to fracture.

While the first window failure was likely the result of excessive preload and transient thermal stress, the root cause of the second failure was not related to any part of the mechanics of the window mount or the heating protocol. It was instead a result of interactions of disparate components of the system. Since the windows are the most vulnerable parts of the system, it was decided that none should be installed until significantly more operational experience is gained with the blanks in place. This measure should allow the discovery of other unforeseen interactions and the implementation of corresponding modifications to hardware or procedure to reduce the likelihood of future window breakage.

5.3   Exothermic Results

Once the sealing problem was resolved sufficiently and blanks inserted in place of windows, initial combustion experiments were conducted. The eventual goal of the combustor is steady-state operation with compact, high-firing-rate flames. As the combustor was designed with autoignition in mind, and has no mechanism for forced ignition, the first step towards that goal is to produce a flame by autoignition. Previous work was used as a guide to select the inlet conditions. Based on the range of autoignition limits reported for analogous work, an initial fuel concentration of 25% w/w methanol was selected [16, 19]. This fraction is relative to the fuel water flow only. Although the burner water will mix with the fuel/water solution as the flow proceeds downstream, it does not affect the concentration where the fuel and oxygen streams first meet at the nozzle.

Figure 5.7 shows the methanol and oxygen mass flow rates and the downstream temperature trace (measured by "Combustor TC" in Fig. 4.2) during the first simultaneous injection of reactants. The temperature rise indicates that exothermic reaction occurred. Note that the temperatures shown are subcritical since the measurement location is $\sim$30 cm downstream of the burner nozzle; significant cooling of the flow occurred by this point since the vessel walls had not been heated to a steady-state condition. If the flow had been adiabatic, the measured temperature would have risen from $\sim$660 K before combustion (equal to the mixed mean inlet temperature) to $\sim$1100 K, assuming complete combustion and uniform mixing with the burner and liner water flows. Without optical access, it cannot yet be said with certainty that a hydrothermal flame was present, but it is certain that fuel and oxygen reacted exothermically when brought together in supercritical water.

To be confident that reaction occurred, another possible cause of the temperature rise was discounted. When reactant injection begins, the total mass flow increases. Since the flow is cooled significantly before reaching the downstream thermocouple, an increase in flow speed could also increase the observed temperature by reducing the time available for heat transfer. After the flow of reactants was stopped (at 181 min.),
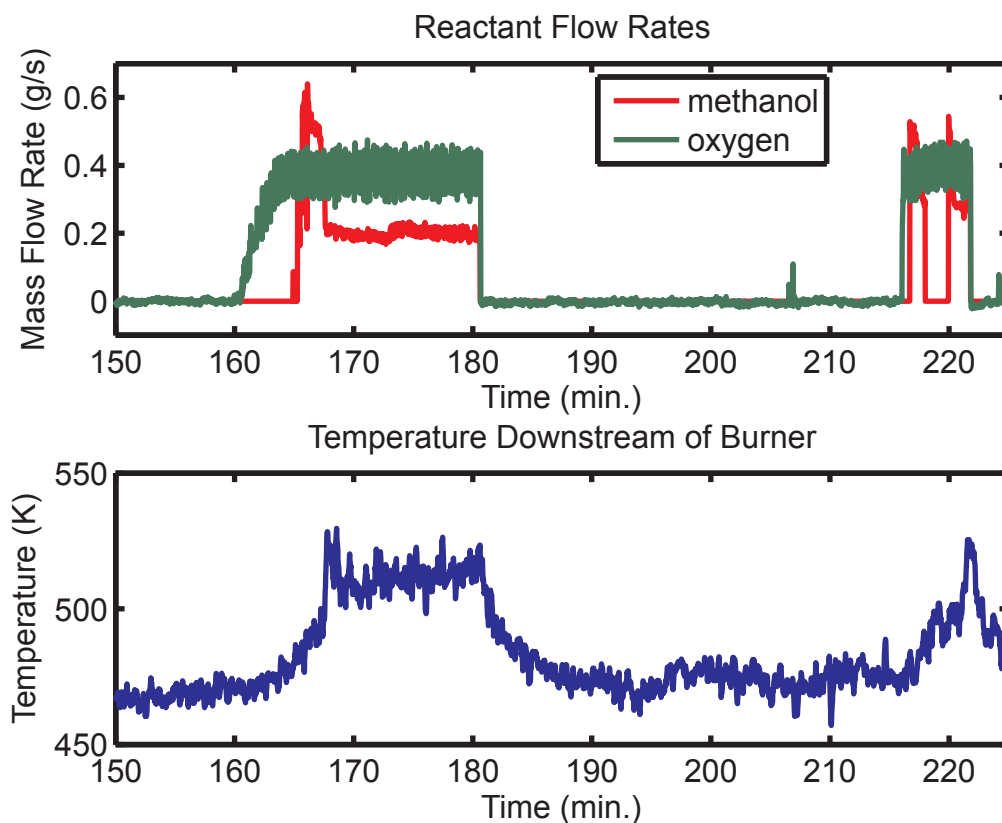
Figure 5.7: Mass flow rates and temperature during the first set of combustion experiments. The zero point of the time scale is arbitrary.

water flow continued until the temperature returned to its value before ignition (460–470 K). Next, the water flow rates through the fuel/water and oxygen/water lines were increased slightly as a surrogate for the added mass flow of fuel and oxygen. The temperature rose, but markedly less than with the reactants; the small peak centered at 200 minutes is the result. Following that test, fuel was injected with oxygen a second and third time to see if the observed temperature rise was repeatable. The temperature trace shows that exothermic reaction occurred again.

The flow rate and downstream temperature plots for the second set of experiments are shown in Fig. 5.8. This time, there were no temperature rises attributable to the flow of methanol and oxygen during the first and third injections, indicating that little

or no reaction occurred. The temperature effect of the second and fourth injections is less pronounced, but present. In particular, the fourth resulted in only a brief spike in temperature because the reactant flows were stopped at about the same time that hot products reached the thermocouple.
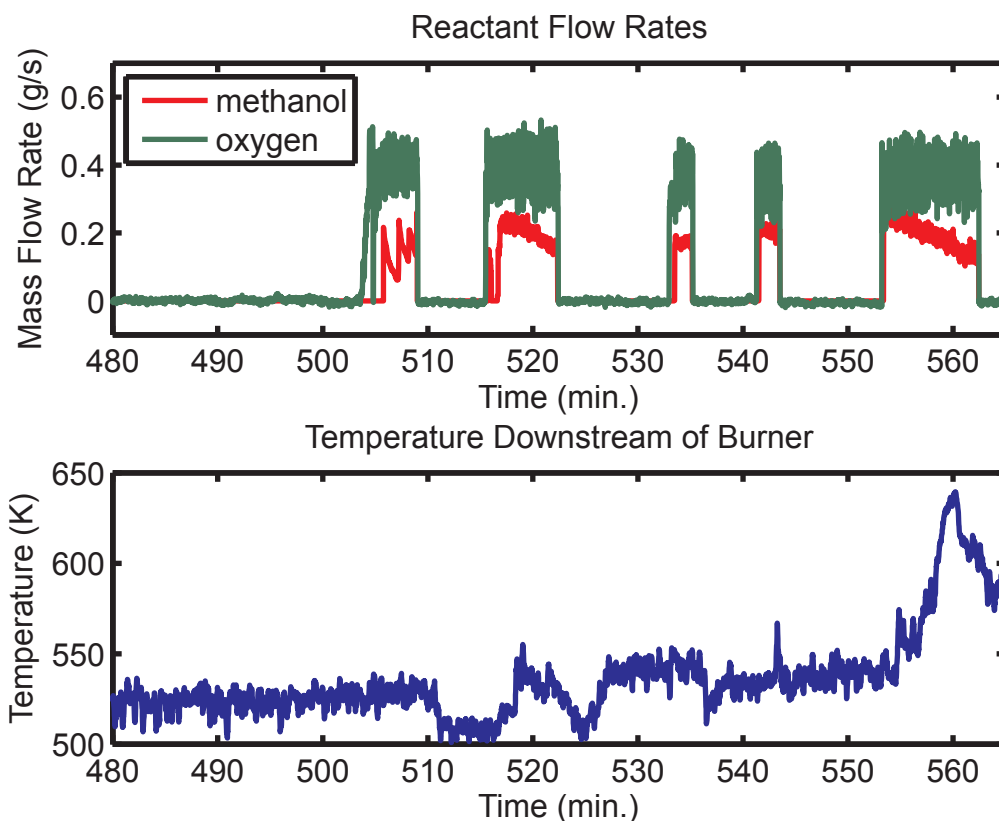
Figure 5.8: Mass flow rates and temperature during the second set of combustion experiments. The zero point of the time scale is arbitrary.

Important parameters not shown in Figs. 5.7–5.8 are the temperature and concentration of the fuel stream. A scatterplot of inlet temperature vs. methanol concentration for the eight injection periods from the first two experiments is shown in Fig. 5.9. The curves are ignition and extinction limits from multiple workers, as indicated in the figure [16, 19, 20]. For the present study, inlet temperatures are not accurately known because the thermocouples in the reactant streams are located well upstream

of the burner (see Figs. 4.2–4.3). For all trials, the burner water was injected at a lower temperature than the fuel/water solution. Due to heat transfer—from the fuel, through the burner tubes, to the water in the outer annulus—the temperature of the fuel at the nozzle is lower than it was at the thermocouple location in the base of the assembly.[1] As a result, a pair of connected points is plotted for each trial; the top point shows the measured temperature of the fuel stream, and the bottom point shows the measured temperature of the burner water at the start of injection. These are upper and lower bounds on the true temperature of the fuel upon reaching the nozzle and contacting oxygen. Closed circles denote cases where autoignition is believed to have occurred, and open circles are for those with no indication of ignition.

Considering the uncertainty in the temperature measurements, the data span a qualitative extrapolation of the ignition curve from Steeper. This curve represents the minimum inlet temperature required for autoignition with varying fuel concentration. (Wellig used a somewhat different definition to generate his higher temperature curve.) During the present experiments, the pressure in the combustor fluctuated up to ± 1 bar at 29 Hz due to the action of the high-pressure piston pump, but averaged 250 bar at all times. The pseudocritical temperature at this pressure is 658 K, marked by the dashed line in the figure. For both cases in which ignition did not occur, the lower temperature bound is below the pseudocritical temperature, such that the fuel may have been below pseudocritical at the nozzle. In all cases with autoignition, the fuel temperature was, with near certainty, above the pseudocritical temperature.

The temperature ranges for all but one of the trials lie entirely above the critical temperature (647 K), but recall that, above the critical pressure, the boundary in property space between the liquid and supercritical phases is a convention without physical basis (Sec. 2.1). At higher pressures, the pseudocritical temperature—while not corresponding to any discontinuities—is the best marker of changes in the behavior of water. At 250 bar, the density falls from 450 kg/m^3 at 653 K to *half* of that value

---

[1]Meanwhile, the oxygen is subject to heat transfer with the fuel. The fuel and oxygen streams are preheated in the same heater unit, and thus have temperatures within a few degrees of each other when entering the combustor. From that location, the temperature of the oxygen follows that of the fuel, since their flow passages form a co-flow heat exchanger. Because of this coupling, and the fact that the behavior of water will emerge as the controlling factor, the temperature of the oxygen is not mentioned further.
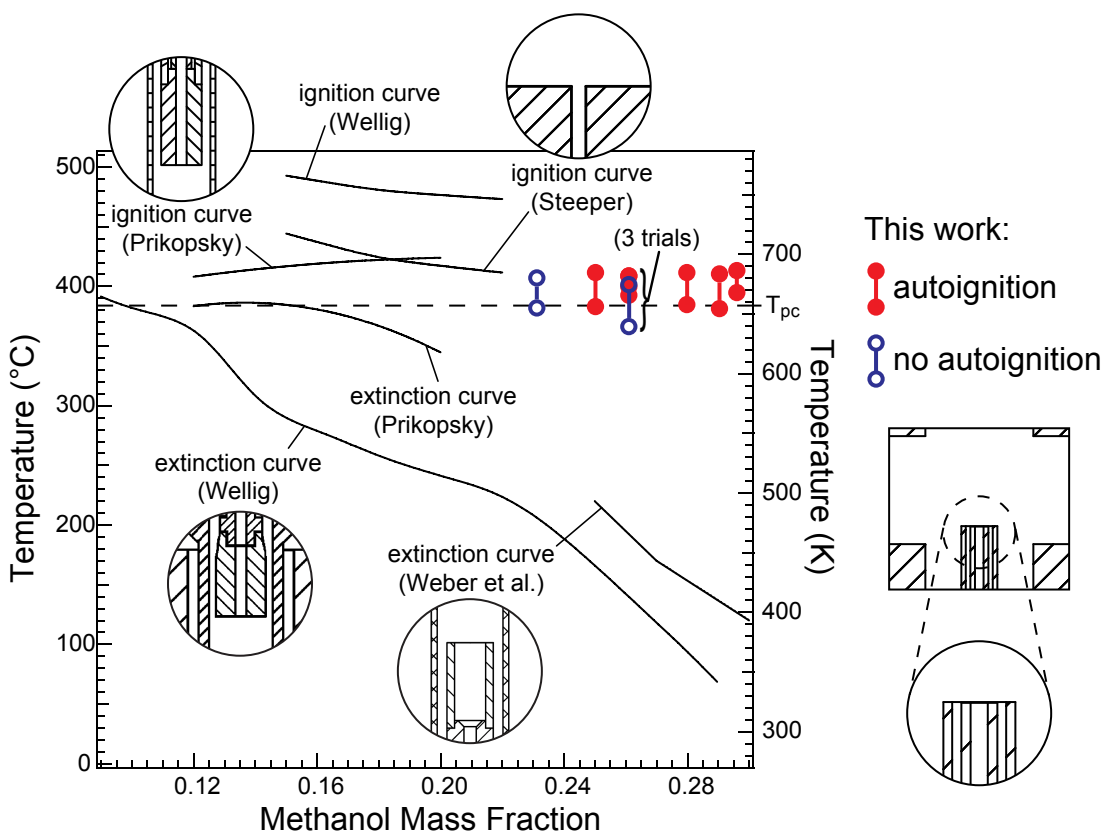
Figure 5.9: Initial autoignition results from this work. All trials were conducted at 250 bar; the pseudocritical temperature at this pressure is 658 K, marked by the dashed line. Solid curves are ignition and extinction limits from prior work. The inset drawings show the burner configurations used in these experiments. The variations in burner geometry account for the differences in autoignition and stability behavior. Adapted from [16, 19, 20].

at 662 K—a span of only 9 K. This precipitous drop in density as temperature rises rapidly increases the ability of water (and methanol/water solutions) to mix with oxygen. The ability of fuel and oxygen to mix is key to the progress of combustion. Hence, it is not surprising that the initial results indicate an autoignition limit near the pseudocritical point.

Chapter 6

Conclusions

A system for pre-equilibrated injection has been described. The SCWO/IFCC system exploits the properties of supercritical water to reform and combust coal at high pressure in aquifer-sourced water, producing a high-pressure CO_2/brine solution ready for injection.

The SCWO/IFCC system and its major components were described. Since salts are not soluble in SCW, the regenerator for preheating incoming aquifer water doubles as a desalinator using precipitation. Coal is reformed in SCW into a supercritical-phase synthesis fuel. Oxygen from an air-separation unit reacts with this synfuel in a supercritical water combustor. A heat engine extracts work from the hot combustor effluent. The partially-cooled effluent is cooled to near-ambient temperatures while flowing through the outflow side of the regenerator/desalinator. Salts are reintroduced, resulting in an injectant that is denser than the native aquifer brine.

A thermodynamic model of the SCWO/IFCC design was developed to evaluate its performance as compared to other coal-fired systems with CCS. With an SCW combustor outlet temperature of 1600 K and the use high-pressure helium Brayton and steam Rankine cycles for work production, efficiencies of 41–42% (LHV basis) may be achieved. This figure provides a favorable comparison against, for example, IGCC with capture and compression. Furthermore, while a typical IGCC with "full capture" only captures and stores ∼90% of product CO_2, the present system prevents atmospheric release of *all* coal-derived effluent species, including those containing

carbon, sulfur, and heavy metals. Future work includes explicit modeling of the
air separation unit instead of using a published work requirement. The inclusion of
a detailed ASU will allow for thermal integration with the combined cycle. Also,
flash desalination should be modeled as it is an already-developed alternative to the
hypothesized precipitation-driven desalination currently assumed.

Several components posited for use in such a plant will require research to implement
at scale:

- Combination regenerator/desalinator unit that removes salts from brine via
  temperature-driven precipitation. Alternatively, the desalination could occur in
  staged flashes, the performance analysis of which is part of a second phase of
  theoretical work in this project [35].

- Supercritical water reformer. Research is on-going in a companion project [32].

- Separation of solids from SCW (mineral matter and insoluble products).

- Supercritical water combustor. Initial results from this work were presented in
  Ch. 5.3.

- High-temperature heat exchanger where the inlet hot fluid is SCW and products
  from coal.

- High-pressure turbomachinery for closed Brayton cycles.

- Chemical behavior of injected CO_2/brine solution in saline aquifers.

While a companion project began investigations of the reformer, the present work
focused on the combustor. A laboratory-scale SCW combustor and associated systems
were constructed, informed by prior work focused on hazardous waste destruction.
The combination of elevated temperature and pressure of SCW presents challenges
with regard to materials. While corrosion and high-temperature strength can be
addressed by choosing a suitable alloy, seals remain problematic since SCW excludes
the use of common seal materials. The sealing strategy has been improved enough
to permit preliminary combustion experiments. Initial results indicate that this

combustor performs similarly to previous SCW combustors engineered for hazardous waste destruction.

Near-term future work with the combustor includes installation of more thermocouples to more precisely measure autoignition data. Continued improvements in sealing strategies will increase the rate at which experiments can be conducted. Transparent flow barriers should be installed between the burner and the sapphire window ports to guard against thermal shock from cold fluid. This will enable the planned operation with optical access with greatly reduced risk of damage to the windows. In the longer term, the full operating space should be explored. The combustor was initially operated at 5 kW; as experience is gained the firing rate will be increased to 35 kW. The oxygen system should be upgraded to reduce flow rate variations as the booster cycles. An increase in booster drive air supply is also needed so that the firing rate can be increased to the design point of 50 kW. With a larger operating space, investigations into autoignition limits, stability, and burner design can be undertaken. As firing rate increases, other aspects of combustor design can be explored, including liner design. Issues relevant to the main heat exchanger may also be examined, including heat transfer, materials, and environmental barrier coatings.

Appendix A

Thermodynamic Model Details

A.1   Model Parameters

These are the system component parameters used in the model calculations discussed in Sec. 3.2.1.

- Environment

  - Temperature: 300 K

  - Pressure: 1.01325 bar (1 atm)

- Fuel

  - Moisture-and-ash free (MAF) coal based on Wyodak-Anderson [25]

  - Ultimate analysis: 75.39% C, 5.36% H, 1.12% N, 18.04% O

  - LHV: 29.87 MJ/kg

- ASU

  - Work requirement (without LOX pump): 220 kWh/tO_2 (792 kJ/kgO_2)

  - Liquid oxygen pump inlet pressure: 170 kPa

- Aquifer

- Temperature: 32.8°C (306.0 K)

- Pressure: 8.96 bar

- Salinity: 20,000 ppm w/w NaCl

- Well drawdown: 3.45 MPa

- Well pipe friction loss: 0.586 MPa

- Water pumps

  - Lift pump polytropic efficiency: 80%

  - SC pump polytropic efficiency: 90%

  - Injection pump polytropic efficiency: 80%

- SCWO system pressure: 250 bar

- Regenerator

  - Oxygen pressure drop: 5%

  - Water pressure drop: 5%

  - Products pressure drop: 5%

  - Effectiveness: 95%

- Main heat exchanger

  - SCWO-loop-side pressure drop: 5%

  - Brayton-side pressure drop: 5%

  - Effectiveness: 95%

- Brayton cycle

  - Compressor polytropic efficiency: 90%

  - Turbine

    * Polytropic efficiency: 89%

∗ Cooled blade rows: 4 (2 stators, 2 rotors)

∗ Blade temperature: 1000 K

- HRSG

  – Brayton-side pressure drop: 5%

  – Rankine-side pressure drop: 5%

  – Effectiveness: 95%

  – Approach + pinch-point temperature difference: 17 K

- Rankine cycle

  – Condenser

    ∗ Condenser pressure: 6.77 kPa

    ∗ Cooling water inlet temperature: 300 K

    ∗ Cooling water temperature rise: 10 K

  – Condensate pump polytropic efficiency: 90%

  – Storage pressure: set to environment pressure of 1.01325 bar (1 atm)

  – Feed pump polytropic efficiency: 90%

  – Turbine polytropic efficiency: 87%

  – Turbine outlet quality: 90%

A.2   Calculated States and Flow Rates

Table A.1 lists the thermodynamic states and flow rates found in the optimized model plant with SCWO system outlet temperature of 1600 K and Brayton inlet pressure of 79.5 bar. Stations are as labeled in Fig. 3.3.

Stream	COAL	W2	W3	W4	INJECTANT	O1	O2
Temperature (K)	300	306	308	666		90	96
Pressure (bar)	1.013	1.013	263.2	250.0		1.700	263.2
Mass flow (kg/s)	40.3	1948	340	340	2079	90.8	90.8
Enthalpy flow (W)	-5.135e7	-3.082e10	-5.366e9	-4.589e9		-3.681e7	-3.452e7
Mass fractions							
O_2						1	1
N_2					2.18e-4		
CO_2					5.35e-2		
H_2O		1	1	1	9.46e-2		

Stream	O3	O4	P1	P2	P3	B1	B2
Temperature (K)	308	666	1600	673	391	399	662
Pressure (bar)	263.2	250.0	250.0	237.5	225.6	79.5	250.0
Mass flow (kg/s)	90.8	90.8	470.6	470.6	470.6	285.7	243.7
Enthalpy flow (W)	-3.718e6	3.325e7	-4.607e9	-5.735e9	-6.549e9	1.492e8	4.600e8
Mass fractions							
O_2	1	1					
N_2			9.63e-4	9.63e-4	9.63e-4		
CO_2			2.36e-1	2.36e-1	2.36e-1		
H_2O			7.62e-1	7.62e-1	7.62e-1		
He						1	1

Stream	B3	B4	R1	R2	R3	R4	R5
Temperature (K)	1533	976	312	312	899	313	312
Pressure (bar)	237.5	83.7	1.013	84.9	80.7	0.071	0.068
Mass flow (kg/s)	243.7	285.7	242.6	242.6	242.6	242.6	242.6
Enthalpy flow (W)	1.588e9	1.005e9	-3.836e9	-3.834e9	-2.977e9	-3.309e9	-3.836e9
Vapor fraction			0	0	1	0.90	0
Mass fractions							
H_2O			1	1	1	1	1
He	1	1					

Table A.1: States and flow rates in the optimized plant model. Operating conditions are the same as for Table 3.1.

Bibliography

[1] Solomon, S., D. Qin, M. Manning, Z. Chen, M. Marquis, K.B. Averyt, M. Tignor and H.L. Miller (eds.). Working Group I Report "The Physical Science Basis". In *IPCC Fourth Assessment Report: Climate Change 2007*. Cambridge University Press, 2007.

[2] James R. Fincke, Raymond P. Anderson, Timothy A. Hyde, and Brent A. Detering. Plasma pyrolysis of methane to hydrogen and carbon black. *Industrial & Engineering Chemistry Research*, 41(6):1425–1435, 2002.

[3] Marco Mazzotti. Mineral carbonation and industrial uses of carbon dioxide. In B. Metz, O. Davidson, H.C. de Coninck, M. Loos, and L.A. Meyer, editors, *IPCC Special Report on Carbon Dioxide Capture and Storage*, pages 319–338. Cambridge University Press, 2005.

[4] Lawrence Livermore National Laboratory. Estimated U.S. carbon dioxide emissions in 2008. Technical report, Department of Energy, 2010.

[5] Sally Benson and P. Cook. Underground geological storage. In B. Metz, O. Davidson, H.C. de Coninck, M. Loos, and L.A. Meyer, editors, *IPCC Special Report on Carbon Dioxide Capture and Storage*, pages 195–276. Cambridge University Press, 2005.

[6] M. Burton and S.L. Bryant. Eliminating buoyant migration of sequestered CO_2 through surface dissolution: Implementation costs and technical challenges. In *Society of Petroleum Engineers Annual Technical Conference and Exhibition*, 2007.

[7] S. Bachu and J.J. Adams. Sequestration of CO_2 in geological media in response to climate change: capacity of deep saline aquifers to sequester CO_2 in solution. *Energy Conversion and Management*, 44(20):3151–3175, 2003.

[8] T.J. Feeley, L. Green, J.R. Murphy, J. Hoffmann, and B.A. Carney. Department of energy/office of fossil energy's power plant water management r&d program. Technical report, Department of Energy/Office of Fossil Energy, 2005.

[9] J.W. Tester, H.R. Holgate, F.J. Armellini, P.A. Webley, W.R. Killilea, G.T. Hong, and H.E. Barner. Supercritical water oxidation technology: Process development and fundamental research. In D. William Tedder and Frederick G. Pohland, editors, *Emerging Technologies in Hazardous Waste Management III*, volume 518 of *ACS Symposium Series*, pages 33–76. American Chemical Society, Washington, DC, 1993.

[10] The International Association for the Properties of Water and Steam. Release on the Static Dielectric Constant of Ordinary Water Substance for Temperatures from 238 K to 873 K and Pressures up to 1000 MPa, September 1997. Erlangen, Germany.

[11] The International Association for the Properties of Water and Steam. Release on the Ionization Constant of H_2O, August 2007. Lucerne, Switzerland.

[12] M.A. Frisch. Supercritical water oxidation. In H.M. Freeman, editor, *Standard Handbook of Hazardous Waste Treatment and Disposal*, pages 8.167–8.190. McGraw-Hill, New York, second edition, 1998.

[13] P.A. Marrone and G.T. Hong. Corrosion Control Methods in Supercritical Water Oxidation and Gasification Processes. *NACE Corrosion Conference & Expo 2008*. paper no. 08422.

[14] E.U. Franck. Dense fluids—new aspects and results. *Physica B+C*, 139–140:21–30, 1986.

[15] W. Schilling and E.U. Franck. Combustion and diffusion flames at high pressures to 2000 bar. *Berichte der Bunsen-Gesellschaft für Physikalische Chemie*, 92:631–636, 1988.

[16] R. R. Steeper. Methane and methanol oxidation in supercritical water: Chemical kinetics and hydrothermal flame studies. Technical Report SAND96-8208, Sandia National Laboratories, Livermore, CA 94551, 1996.

[17] S.F. Rice, R.R. Steeper, C.A. LaJeunesse, R.G. Hanush, J.D. Aiken. Design strategies for optically-accessible, high-temperature, high-pressure reactor cells. Technical Report SAND99-8260, Sandia National Laboratories, Livermore, CA 94551, 2000.

[18] Hans Lucas La Roche. *Wandgekühlter Hydrothermal-Brenner (WHB) für die überkritische Nassoxidation*. PhD thesis, Swiss Federal Institute of Technology (ETH) Zurich, 1996. Diss. ETH No. 11585.

[19] Beat Wellig. *Transpiring-wall reactor for supercritical water oxidation*. PhD thesis, Swiss Federal Institute of Technology (ETH) Zurich, 2003. Diss. ETH No. 15038.

[20] Karol Príkopský. *Characterization of continuous diffusion flames in supercritical water*. PhD thesis, Swiss Federal Institute of Technology (ETH) Zurich, 2007. Diss. ETH No. 17374.

[21] P.C. Dell'Orco, L. Li, and E.F. Gloyna. The separation of particulates from supercritical water oxidation processes. *Separation Science and Technology*, 28(1–3):625–642, 1993.

[22] J.M. Kendall. Gas turbine power conversion systems for modular HTGRs. Technical Report IAEA-TECDOC-1238, International Atomic Energy Agency, Vienna, 2001.

[23] J.H. Horlock. *Advanced Gas Turbine Cycles*. Pergamon, Amsterdam, first edition, 2003.

[24] K. Thambimuthu, M. Soltanieh, and J.C. Abanades. Capture of CO_2. In B. Metz, O. Davidson, H.C. de Coninck, M. Loos, and L.A. Meyer, editors, *IPCC Special Report on Carbon Dioxide Capture and Storage*, pages 105–178. Cambridge University Press, 2005.

[25] Argonne National Laboratory. Argonne premium coal samples. http://www.anl.gov/PCS/report/part2.html, 2008. Accessed January 28, 2008.

[26] William C. Reynolds. *Thermodynamic Properties in SI*. Department of Mechanical Engineering, Stanford University, 1979.

[27] S.J.T. Hangx. Behavior of the CO_2-H_2O system and preliminary mineralisation model and experiments. Technical report, CATO Workpackage WP 4.1, Deliverable WP 4.1-3-05, 2005.

[28] John H. Perepezko. The hotter the engine, the better. *Science*, 326:1068–1069, November 2009. DOI: 10.1126/science.1179327.

[29] Russ Burman. Properties and application of molybdenum. In *Refractory metals and their industrial applications: a symposium sponsored by ASTM Committee B-10 on Reactive and Refractory Metals and Alloys, New Orleans, La., 23-24 Sept. 1982; Robert E. Smallwood, ed.*, pages 3–17, 1984.

[30] National Energy Technology Laboratory. Cost and Performance Baseline for Fossil Energy Plants Volume 1: Bituminous Coal and Natural Gas to Electricity. Technical Report DOE/NETL-2010/1397, National Energy Technology Laboratory, Morgantown, WV, November 2010.

[31] Edward L. Parsons and Walter W. Shelton. Advanced Fossil Power Systems Comparison Study. Technical report, National Energy Technology Laboratory, Morgantown, WV, December 2002.

[32] Reginald E. Mitchell, Christopher Edwards, Scott Fendorf, Ben Kocar, Adam Berger, Eli Goldstein, J.R. Heberle, BumJick Kim, Andrew Lee, Paul Mobley, and

Rebecca Pass. Coal Energy Conversion with Aquifer-Based Carbon Sequestration: An Approach to Electric Power Generation with Zero Matter Release to the Atmosphere. Technical report, Global Climate and Energy Project, Stanford University, 2011.

[33] Parker Hannifin Corporation. Parker O-Ring Handbook. Technical Report ORD 5700, Parker Hannifin Corporation, 2360 Palumbo Drive, Lexington, KY 40509, 2007.

[34] R.M. Serikawa, T. Usui, T. Nishimura, H. Sato, S. Hamada, and H. Sekino. Hydrothermal flames in supercritical water oxidation: investigation in a pilot scale continuous reactor. *Fuel*, 81:1147–1159, 2002.

[35] Paul D. Mobley, Rebecca Zarin Pass, and Chris F. Edwards. Exergy analysis of coal energy conversion with carbon sequestration via combustion in supercritical saline aquifer water. In *Proceedings of ASME 2011 5th International Conference on Energy Sustainability & 9th Fuel Cell Science, Engineering and Technology Conference*, August 2011. Paper No. ESFuelCell2011-54458.